# Structural Optimization and Sensitivity Analysis using Finite Element Force Method

Amandeep Singh

A thesis

in

The Department

of

Mechanical and Industrial Engineering

Presented in Partial Fulfillment of the Requirements
for the Degree of Master of Applied Science (Mechanical Engineering) at
Concordia University
Montreal, Quebec, Canada

August 2006

*Your file Votre référence*
*ISBN: 978-0-494-28944-0*
*Our file Notre référence*
*ISBN: 978-0-494-28944-0*

# ABSTRACT

Structural Optimization and Sensitivity Analysis using Finite Element Force Method

Amandeep Singh

The objective of the present research is to develop a computer aided environment for optimization of structures by integrating the structural and design sensitivity analysis using the finite element force method, and mathematical programming techniques. A reliable tool for sensitivity analysis is perquisite for performing interactive structural design, synthesis and optimization. The sensitivity analysis is used to provide the gradient information to the gradient-based optimization algorithm. The developed structural optimization methodology using the force method is used to optimize discrete structures subjected to stress, displacement and frequencies constraints, and results are compared with those generated from displacement method and those in literature. The improved accuracy and efficiency of the developed optimization algorithm using analytical sensitivity analysis is also demonstrated by comparing the results with those obtained from the numerical sensitivity analysis

Later, the developed optimization methodology is extended to the design of the stiffened panels subjected to uniform uniaxial compression loading. The buckling characteristic of stiffened panels subjected to uniform in-plane loading is of considerable importance, while designing for the aerospace, naval and civil engineering applications. The finite element model for the linear buckling analysis of the eccentrically stiffened panels based on the force method is developed, and is validated by extensive numerical analysis. The explicit expressions of the sensitivity of the buckling load with respect to dimensions of

plate and stiffener are formulated, and integrated with the optimization algorithm and finite element analysis. The developed optimization algorithm is used to design different types of stiffened panels.

# ACKNOWLEDGEMENT

I would like to express my gratefulness and thanks to Dr. Ramin Sedaghati for supervising me through all stages of this thesis. His research guidance, teaching, consistent encouragement and moral support were invaluable to me. I have benefited immensely from the trust he placed in me at all times. Special thanks due to Dr. Rajamohan Ganesan who paved the way for understanding the basics of stress analysis and finite element analysis with his coursework.

I also had the pleasure of meeting and working with a group of wonderful people who had contributed to my enjoyment of research. I would like to thanks all my colleagues and friends at Concordia University who made my stay a wonderful experience.

I am heartly grateful to my parents, Narinderjit Singh and Rachpal Kaur, and my beloved brother, Raminderdeep Singh, for their encouragement and support which have always been key factor behind every success in my life. I would like to thank them for their love and sacrifices. Last but not least, I would like to thank my friend who helped me and made me feel comfortable during my stay in Montreal.

# TABLE OF CONTENTS

# LIST OF FIGURES

# LIST OF TABLES

# NOMENCLATURE

| | |
|---|---|
| $A_{st}, A_{sk}$ | Area of cross section of the stringer and skin, respectively |
| $\{A\}$ | Vector representing the cross sectional area of elements. |
| $b_s$ | Width of the panel |
| $b_w$ | Height of the stiffener |
| $b_f$ | Length of Flange |
| $[B]$ | Equilibrium matrix |
| $[B_e]$ | Element equilibrium matrix |
| $[C]$ | Compatibility matrix |
| $[D]$ | Compliance matrix |
| E | Modulus of Elasticity |
| $f$ | Objective function |
| $\{\mathrm{F}\}$ | Vector of internal forces |
| $\{F_T\}$ | Vector of surface traction |
| $\{F_B\}$ | Vector of body forces |
| $g$ | Vector of inequality constraints |
| $[G]$ | Flexibility matrix |
| $[G_e]$ | Element flexibility matrix |
| $h$ | Vector of equality constraints |
| $[H]$ | Hessian Matrix |
| $I_y$ | Moment of area about $y$ axis |
| $J$ | Polar moment of inertia |
| $k$ | Buckling parameter |
| $[K]$ | Stiffness matrix |
| $[K_g]$ | Geometric stiffness matrix |
| $l$ | Length of the element |
| L | Length of the element |

| | |
|---|---|
| $L$ | Lagrangian function |
| $L_P$ | Length of the panel |
| $[L]$ | Differential operator |
| $\{L\}$ | Length of each member |
| $M$ | Mass of the structure |
| $[M]$ | Mass matrix |
| $[M_f]$ | IFM mass matrix |
| $M_x, M_y$ | Moment along $x$ and $y$ direction respectively |
| $M_{xy}$ | Twisting moment |
| $N_c$ | Critical buckling load |
| $[N]$ | Displacement interpolation matrix |
| $n_e, n_{ie}, n_d$ | Numbers of equality, inequality and side constraints |
| $n_{sc}, n_{dc}, n_{fc}$ | Number of stress, displacement and frequency constraints |
| $n, m$ | Number of force and displacement degrees of freedoms |
| $p$ | Iteration Number |
| $\{\mathrm{P}\}$ | Vector of external load |
| $\{Q_T\}$ | Nodal load vector due to surface tractions |
| $\{Q_B\}$ | Nodal load vector due to body forces |
| $\{\delta\mathrm{R}\}$ | Vector of initial deformations |
| $r$ | Number of compatibility conditions |
| $S$ | Modulus of rigidity |
| $SH$ | Shear Modulus |
| $\{s\}$ | Search direction |
| $[S]$ | System Matrix of IFM |
| $[S_b]$ | IFM stability Matrix |
| $t_s$ | Thickness of the panel |
| $t_w$ | Thickness of the stiffener |

| | |
|---|---|
| $t_f$ | Thickness of the flange |
| $[T]$ | Coordinate transformation matrix |
| $\{U\}$ | Vector of displacements |
| $U_c$ | Complimentary Energy |
| $\{U_e\}$ | Vector of nodal displacements |
| $v$ | Poisson ratio |
| $\{V_R\}$ | Right eigen vector |
| $\{V_L\}$ | Left eigen vector |
| $w$ | Transverse deflection |
| $W_I$ | Internal work |
| $W_E$ | External work |
| $W_I^C$ | Complimentary internal work |
| $W_I^C$ | Complimentary external work |
| X,Y,Z | Global coordinate system |
| $x, y, z$ | Element or local coordinate system |
| $\{X\}$ | Vector of design variables |
| $[Y]$ | Stress Interpolation matrix |
| $[Z]$ | Strain displacement relation |
| $\{\sigma\}$ | Stress vector |
| $\{\varepsilon\}$ | Strain vector |
| $\{\beta\}$ | Deformation vector |
| $\{\beta_0\}$ | Initial deformation vector |
| $\theta_x$ | $x$ direction rotation |
| $\theta_x$ | $y$ direction rotation |
| $\Phi$ | Airy stress function |
| $\sigma_x, \sigma_y$ | Stress along $x$ and $y$ direction respectively |
| $\tau_{xy}$ | Shear stress |

| | |
|---|---|
| $\varepsilon_x, \varepsilon_y$ | Strain along $x$ and $y$ direction respectively |
| $\lambda_{xy}$ | Shear strain |
| $\lambda$ | Lagrangian multiplier |
| $\mu$ | Buckling Load factor parameter need to be change |
| $\omega$ | Frequency |
| $\alpha_p$ | Step length |
| $\rho$ | Density |
| $\nabla$ | Gradient |

**Acronyms**

| | |
|---|---|
| DDR | Deformation displacement relation |
| DM | Displacement Method |
| IFM | Integrated Force Method |
| SQP | Sequential Quadratic Programming |
| SVD | Standard Value Decomposition |
| FE | Finite Element |
| NLP | Non Linear Programming |
| IFM(AG) | IFM with analytical gradient |
| IFM(AG) | IFM with numerical gradient |
| IFM1 | IFM without considering the torsional rigidity of stiffener |
| IFM2 | IFM considering the torsional rigidity of stiffener |

# Chapter 1
# INTRODUCTION

## 1.1 Problem Statement

The scientific research in the field of structural optimization has increased rapidly during recent decades. The increasing interest in this field has been boosted by the advent of reliable general analysis method like Finite Element (FE) method, method of design sensitivity analysis and methods of programming, along with exponentially increasing speed and capacity of digitals computers. This environment integrates design processes by allowing the design engineer to create a geometric model, to build a finite element model, to parameterize the geometric model, to perform FE analysis, to visualize FE results, to characterize performance measures, and to carry out design sensitivity analysis and optimization. Most of the commercials structural optimization codes are based on the Displacement Method (DM) and very few investigations have been done on structural optimization using the force method. The main objective of the present research is to develop, to implement and to integrate the structural and design sensitivity analysis using the FE force method, and mathematical programming techniques into specific purpose computer aided environment.

## 1.2 State of Art

The structural optimization has been topic of interest for many years. The early work of Maxwell [1] and the subsequent development by Michell [2] provided a basic theory for the optimal layout of minimum weight of trusses under single load condition and subject

to stress constraints. Michel's work provided a basis for generating an optimal orthogonal layout given the positions, in a two-dimensional space, of the load application and support conditions. In 1940's and the early 1950's significant work was done on the component optimization as represented by such works as Shanley's "Weight –Strength Analysis of Aircraft Structures" [3].

Development of linear programming techniques by Dantzig [4] together with the advent of digital computer, led to the application of mathematical programming techniques to the plastic design of beam and frame structures as described by Heyman [5]. Schmit [6] was the first who combined the mathematical programming techniques with the finite element method to solve the nonlinear, inequality constrained problems of designing elastic structure under multiplicity of loading conditions. The mathematical programming problem involves finding the values of a set of design variables that yields the smallest value of a specified objective function, subject to a set of equality and inequality constraints. This leads to the modern structural optimization concept known as structural synthesis.

Mathematical programming algorithms require the evaluation of the objective, constraint functions and their gradients, and in turn these require a complete structural analysis each time the design variables are modified. Because in most practical cases, the constraints are defined implicitly in terms of design variables, the approximate technique, such as finite difference technique was generally used to evaluate the gradients that require one additional analysis of the structure for each gradient. In general, the number of iterations

necessary to solve a programming problem is rather large, and in turns demands a very large number of analyses on the structure being optimized. Flurry and Sander [7] pointed out that the number of structural analysis increases with the number of design variables. Frind and Wright [8], and Pappas [9] concluded that the mathematical programming methods were not suited to the structural optimization problem because of the heavy computational burden and the large number of structural re-analysis required.

Nevertheless, by 1970 it had become apparent that the available optimization capabilities based on combining the FE analysis with the mathematical programming techniques required inordinately long run time to solve structural design problem of only modest practical size. However, the outlook for the mathematical programming approach did not deter researcher from attempting to improve the situation. Schmit[10] recognized that obstacle to the implementation of efficient programming based structural synthesis method were associated with large numbers of design variables, large number of inequality constraints, and many inequality constraints that are computationally burdensome implicit function of the design variables.

These problems were then alleviated by introduction of approximation concepts such as the coordinated use of design variable linking, temporary constraint deletion, and the construction of high quality explicit approximation for retained constraints using Taylor series expansion. Design variables linking reduce the number of independent design variables by making groups of elements linearly dependent upon a single generalized design variable. Linking also maintains geometric consistency and allows time saving

reduction in the number of design variables. Constraint deletion procedure can be used to temporarily ignore behavior constraints, which would have no influence in upcoming design step. Schmit [11] reduced the number of analysis cycle by creating approximation functions to the objective and constraints using tailor series expansion. The approximations are then updated using precise analysis of the proposed optimum and the process is repeated until convergence to the precise optimum has been achieved. Further, the efficient techniques to calculate the sensitivity derivatives were also developed and new field in the structural optimization known as sensitivity analysis was emerged.

Mathematical programming algorithms such as the Sequential Quadratic Programming (SQP) method, sequential linear programming, sequential unconstraint optimization, the generalized reduced gradient method, the method of moving asymptotes, and the modified method of feasible direction are commonly used for structural optimization problems. SQP methods are regarded as the standard general purpose mathematical programming algorithms for solving non –linear programming optimization problems and considered to be the most suitable method for solving structural optimization problems. Such methods make use of local curvature information derived from linearization of the original function, by using their derivative with respect to design variables at points obtained in the process of optimization.

## 1.3 Finite Element Force Method and Structural Optimization

Equilibrium and compatibility equations are two main constituents for solving the structural problems. Accuracy of numerical solution depends highly on the degree to

which these equations are satisfied. Equilibrium is the force balance concept and was put into mathematical equations by Cauchy [12-13]. Determinate structures can be easily solved by using equilibrium equations, but compatibility equations are required to obtain sufficiency in case of indeterminate structures. Compatibility equations in terms of strains for deformable solids were formulated by St. Venant [12] which was then expressed in terms of stresses by Beltrami and Michelle [13].

Clebch [14] wrote the equilibrium equations in terms of displacements and observed that the number of equations and displacement unknowns are the same. This formulation led to the displacement method (DM), but it was not very successful in that time as there was no practical way to solve these large numbers of simultaneous equations. Maxwell [14, 15] proposed another formulation to satisfy the compatibility equation by the concept of redundant members. A statically indeterminate structure is initially reduced to one that is determinate by removing redundant forces. The remaining determinate structure is solved for applied forces in order to obtain the internal forces and relative displacements at the cuts for all the load systems. The compatibility equation is then satisfied by setting up the equilibrium equations between redundant and external forces that closes the gaps, and these are solved to calculate the redundant reactions.

Before 1960, the redundant force method was more popular because it was elegant for manual calculation as compared to the DM. With the advent of computer age, the DM starts dominating in structural analysis due to its amenability to computer programming. The DM is well documented in many books [14, 16]. Several efforts have been done to

improve the process of selection of redundancies [17]; however, all these procedures either result in matrices with certain undesired properties, or lack the physical interpretation.

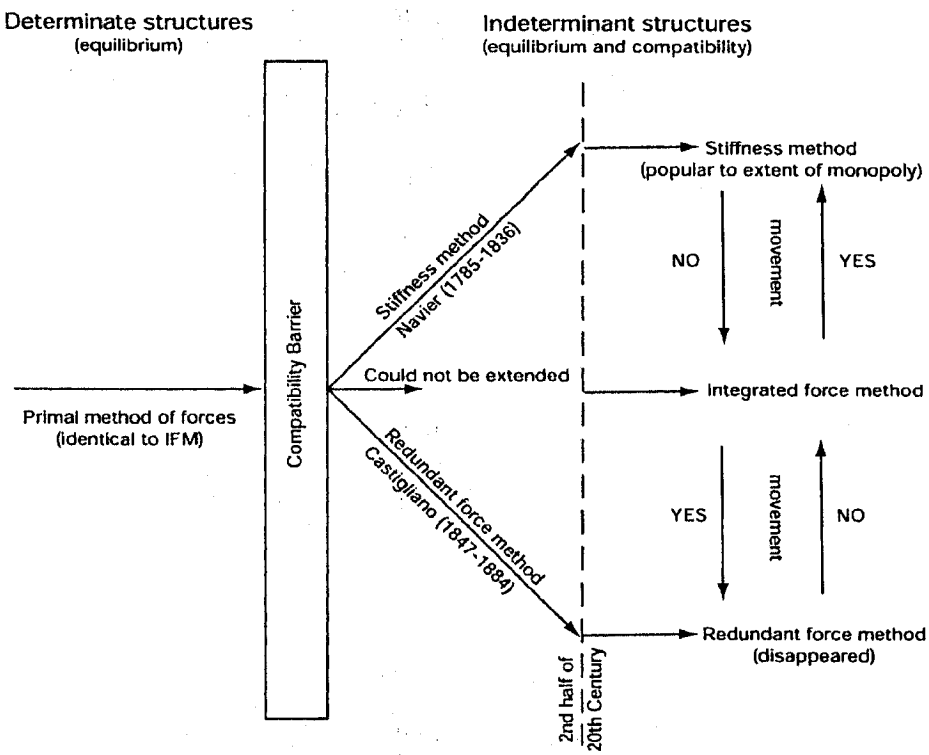


**Figure 1-1** Structural analysis method and their status

In the recent years, efforts have been done to revitalize the force method. A new automated force method formulation known as the Integrated Force Method (IFM) has been developed by Patnaik [18-25]. The independent forces are treated as unknown variables which are obtained by solving the system of equations consisting of equilibrium and compatibility conditions. The procedures for generating the compatibility conditions have been developed which yield sparse and banded matrices [22-24], and are easily

amenable to computer application. A finite element library for the two [20] and three [21] dimensional analysis have been developed and performance of different types of elements have been analyzed. This method overcomes many drawbacks of redundant force method like generation of compatibility by selecting redundant elements. IFM has been successfully applied for static [17-20] and free vibration analysis [25]. The equations of the IFM can be specialized to obtain the stiffness method [18] and the redundant force method [19] as shown in Figure 1-1.

The application of the IFM to structural optimization was first proposed by Patnaik [26]. Patnaik developed the closed form sensitivity analysis equations for truss structures, and designed the truss structures subjected to stress and displacement constraints [26]. Furthermore, Sedaghati and Esmailzadeh [27] combined the IFM with mathematical programming techniques in order to design the truss and frame structures subjected to stress and displacement constraints. They compared the optimization results obtained from the IFM with those obtained from the DM and concluded that the IFM is extremely efficient to analyze and optimize the beam and truss structures, subjected to stress and displacement constraints. Further, Sedaghati et. al. [28] optimized the truss and frame structures under single and multiple frequency constraints. They concluded that in structural problems with multiple frequency constraints, the analysis procedure (force or displacement method) significantly affect the finial optimum design. All these structural optimization investigation were limited to small scale problem because of large computational expense involved in calculation of gradient of behavior constraint by the finite difference method.

Patnaik has extended the application of the IFM in various other applications of structural optimization, such as calculation of analytical initial design [29], to identify singularities in optimization [30], and modified fully utilized design [31]. An initial design for the optimization is either assumed or obtained from the experience of designer, but the initial design can be calculated analytically by using the IFM [29]. A good initial design accelerates the convergence of optimization algorithm. The IFM has also been used as an analysis tool to identify singularities in optimization [30]. Singularities occur because of the redundant nature of stress and displacement constraints, and can increase the number of optimization iterations or can break down the process prematurely without an optimum solution. Recently, a modified fully utilized design method has been developed for the design of structures with both stress and displacement constraints [31]. The traditional fully stresses design method for stress constraints using the DM, when extended for stress and displacement constraints, can generate an over design. The modified fully utilized design method has been verified through successful solutions of number of design examples and produce results comparable with non linear mathematical programming technique.

## 1.4 Sensitivity Analysis and Force Method

Sensitivity analysis is the most important and time-consuming part of a gradient-based optimization procedure. Although, sensitivity analysis is mostly mentioned in the context of structural optimization, it has evolved into a research topic of its own. Design sensitivity analysis deals with change of structural system response with respect to design variables. The structural system response or performance measure may be displacement,

stress, natural frequency and critical buckling load etc. The finite element sensitivity analysis represents an essential ingredient for the efficient and accurate convergence of the gradient-based optimization methods. Mathematical programming generates a set of design variables that require performance values from structural analysis and sensitivity information from design sensitivity analysis to find an optimum design. The accuracy of sensitivity may highly influence the optimization solution, the required number of optimization cycles and the convergence.

Design sensitivity information provides a quantitative estimate of desirable design change, even if a systematic design optimization method is not used. Based on the design sensitivity results, a designer can decide on the direction and amount of design change needed to improve the performance measure. Design sensitivity information can also be used during a post processing of the interactive design process to improve the design.

Several techniques have been developed which can be mainly distinguished by their formulation and implementation aspects. The methods for the sensitivity analysis can be mainly divided into approximation, discrete and continuum approach [32]. The first approach is based on finite difference method, which can be easily implemented. In this method the perturbed structural system for each design parameter has to be analyzed to obtain the difference between the initial and the perturbed structural performance. Such procedure can be prohibitively computationally expensive especially for large problems with many design parameters. Moreover in certain cases performance of such methods depends on the step size. The computational expense and uncertainty of step size make

the finite difference approach less attractive. In the discrete method, design sensitivity is obtained by taking design derivatives of the discrete governing equations. The derivative of the stiffness and mass matrices is needed for this purpose which can be obtained analytically or by the finite difference method. In the continuum approach derivatives are obtained by differentiating the continuum equations that govern the structural behavior.

Most of the sensitivity analysis work is based on the finite element DM, but insignificant work has been done on developing sensitivity analysis formulation based on the force method. Patnaik and Gallagher [33] developed the discrete sensitivity analysis equations for the truss structure using the force method and compared the results with numerical gradient. They concluded that gradient calculation using the IFM is computationally inexpensive, since only flexibility matrix depends on the design variables. Further, the feasibility of using approximate gradient of the stress and displacement constraint using IFM have been investigated for different optimization methods [34]. It was shown that the approximate gradient can produce the correct optimum results and reduce the computational time significantly. Sensitivity analysis using the force method is a field required to be extended further and effort has been done in this research to develop the sensitivity analysis of discrete and continuous structures using the IFM.

## 1.5 Integrated Force Method versus Displacement Method

Force method has long been considered as an alternative to the DM. It was originally developed in structural analysis by the introduction of the concept of redundant forces. It has been almost neglected not because it is less accurate as compared to the DM, but

because it is difficult to automate redundant selection process in this method. Furthermore, in two and three-dimensional problems, concept of 'redundancy' loses its meaning, and also it can not be easily extended to the dynamic and stability problems. On the other hand, the DM because of its good amenability to automation has become the method of choice for the solution of structural mechanics problem, and it has been grown well with several general purpose FE codes available.

Although the DM produces acceptable displacement and frequency results, but it is not much accurate for stress calculation. Stress which forms the basis for most failure criteria is not necessarily accurate even when the maximum displacement has apparently converged. Typical displacement based finite element techniques require much higher mesh density for obtaining accurate stresses than for obtaining accurate displacements. Stresses are calculated from the differential of approximate displacement and it is known that error in differential of a function is more than function itself, which may induce inaccuracy in stress calculations. Moreover, inter element strain compatibility is not satisfied in the DM, and the compatibility condition is satisfied by the continuity of the displacements. In general, stresses obtained by the DM along the element interface boundary satisfy neither equilibrium nor compatibility conditions. Because of these limitations in the DM, stress computation is typically avoided at the cardinal nodal points or along element interfaces. The deficiency has been researched and improved with some success. A new formulation of stiffness method called hybrid stress method [35] has been developed for the calculation of more accurate stresses. However, in hybrid method, the inversion of the flexibility matrix is necessary in order to generate the element stiffness

matrix which may become a computational burden, especially if higher order approximation of stress fields is required.

The IFM makes automation as convenient as it is with the DM and yet retains the known potential for the superior stress field accuracy for the FE model that is associated with the force method solution technique. The IFM provides a convenient way to enforce constraints on the FE model of a continuum namely strain compatibility at the inter element boundaries. In IFM all the independent forces are treated as unknown variables those can be calculated on the basis of simultaneous imposition of equations of equilibrium and compatibility conditions. The basic equation of the IFM can be stated as:

$$\left[\frac{\text{Equilbrium Equation}}{\text{Compatability Conditions}}\right]\{\text{Stress}\}=\left\{\frac{\text{Mechanical Load}}{\text{Intial Deformation}}\right\} \qquad (1\text{-}1)$$

The equilibrium equations represent the balance of internal forces and mechanical load. Compliance of forces and initial deformation is achieved through compatibility condition. Equilibrium equations represent the necessary conditions and sufficiency is achieved through the compatibility conditions. Eq. (1-1) is sufficient for the calculation of stresses, and displacements can be back calculated from stresses. The comparison of basic equations of the IFM and the DM formulations is shown in Figure 1-2. It can be seen that strain compatibility conditions are missing in the DM formulation, and DM only satisfies the displacement continuity.

IFM equilibrium equations are independent of material characteristics and structural design parameters and in the compatibility conditions only flexibility matrix depends on design variables. Also, the load vector is independent of material characteristic and

design variables of the structure. The right hand side load vector in DM which includes both mechanical load vector and equivalent load vector is a function of design variables and mechanical load of the structures. The DM equivalent loads are non zeros even for compatible initial deformation that do not induce stresses in the system.

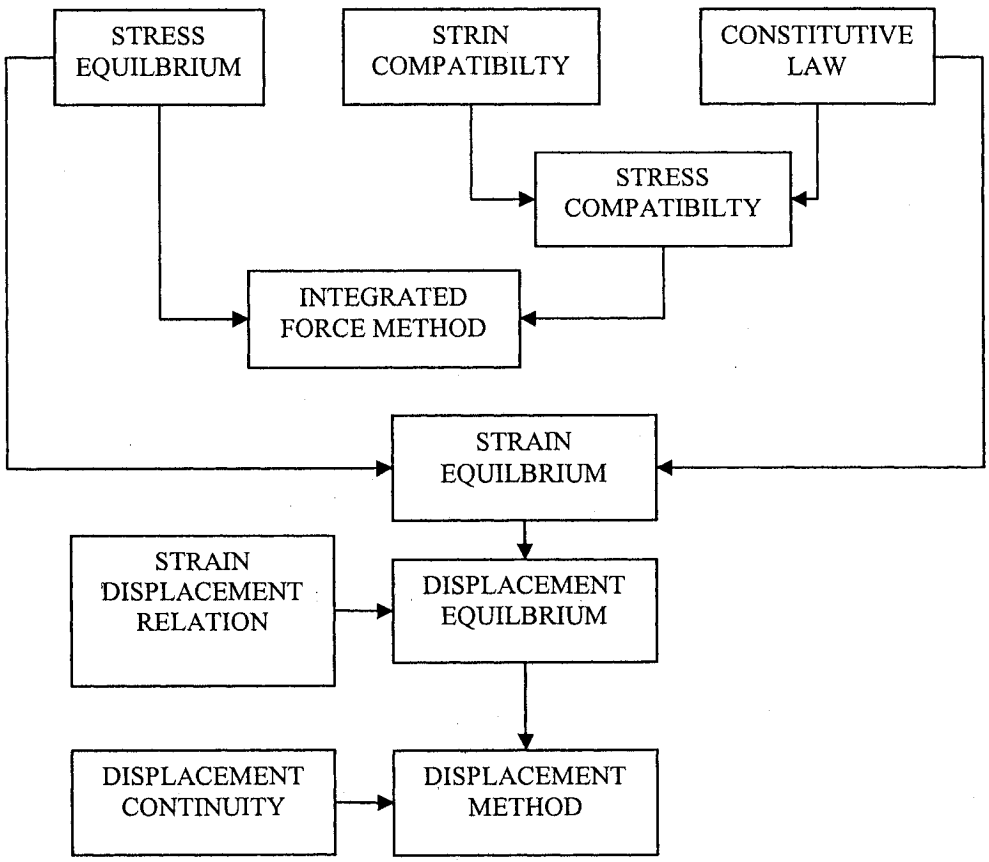


**Figure 1-2** Basic equations of IFM and displacement method.

IFM is also very efficient for stress calculation because stresses are calculated directly as compared to the DM, which requires series of transformations and back substitutions (from local to global system to generate displacement and then from global to local system to calculate forces). It is known that the solution of the DM is sensitive to the

choice of the displacement field; on the other hand IFM is not sensitive to the choice of the stress field. The overall solution accuracy in the IFM depends highly on satisfaction of the system equilibrium and global compatibility. In other words, the element quality or the type of interpolation polynomial plays an insignificant role in overall accuracy of the results.

## 1.6 Design Optimization of Stiffened Panel

Many industrial structures such as those used for aerospace, marine and offshore application are, generally, made up of stiffened panels. The stability of these members is of great interest since it generally controls the optimum design of these kinds of structures. Therefore the correct evaluation of the buckling load is of paramount importance for the economical design of the structure. The study of the stability of the stiffened panel has along history. Troitsky [36] discussed the earlier development in this field. Bryan [37] was first to apply energy criteria to study the stability of stiffened plates under uniform compression. Timoshenko and Gere [38] presented the numerical tables for buckling load of rectangular plates stiffened by longitudinal and transverse ribs. The effect of the eccentricity of the stiffener was introduced as the effective moment of inertia of the stiffener by Seide [39]. The case of multiple stiffeners was discussed by Cox and Riddel [40] using strain energy formulation. Dawe [41] applied the finite element DM to the solution of stiffened panel problems. Plates with arbitrarily oriented stiffeners have been solved by Shastry [42]. Mizusawa [43] was the first to study the stability of skew stiffened plate with various bending and torsional stuffiness's of the stiffeners. Razzaque and Mathers [44] analyzed the stiffened plates and shells.

Among all the numerical methods, the FE method is found to be powerful technique to model the stiffened panel. The extensive research has been done on this topic and many elements has been developed so far using the DM. However to correctly evaluate the buckling stress in the stiffened panel, a very fine FE model or a higher order finite elements are required. This increases the computational time for the problem and sometimes it become impossible to design the stiffened panel using the FE method.

Although significant research has been done to analyze and optimize the stiffened panel using the finite element DM, however no work has been reported using the FE force method, which is more accurate for evaluation of stresses. In this study a design optimization methodology based on the FE force method as analyzer and sequential quadratic programming technique as optimizer is developed to minimize the mass of the stiffened panels while guarding against buckling. Moreover, the analytical sensitivity of the buckling constraints with respect to design variables is formulated and integrated with the optimization algorithm.

## 1.7 Current Work and Expected Contribution

The objectives of the present thesis are (1) to conduct fundamental study in the IFM, (2) to formulate general expression for discrete sensitivity analysis for stress, displacement, frequency and stability constraints using the IFM (3) to investigate structural optimization using the IFM, (4) and to develop the methodology for FE analysis, sensitivity analysis and optimization of stiffened panels using the IFM.

In the literature, most of the work related to the IFM is focused on the analysis part, and a very few investigation has been done related to structural optimization. The comprehensive study of small and large scale structural optimization problems using IFM is the main aim of this research work. A reliable tool for design sensitivity analysis is a prerequisite for performing interactive structural design, synthesis and optimization. General expression for design sensitivity analysis of stress, displacement and frequency constraints with respect to size design variables are formulated for discrete and continuous structures. The analytical discrete approach is used to evaluate the design sensitivity, and analytical expressions for various matrices in IFM are calculated. A number of benchmark structural optimization problems regarding truss and frame structures subjected to stress, displacement and frequency constraints are solved using the IFM with analytical gradient IFM(AG), the IFM with numerical gradient IFM(NG) and the DM. Various performance criteria's such as computational time, solution accuracy, convergence, etc are compared for all these approaches. The main objective of this study is to compare the relative performance of the force and displacement method in the structural optimization of discrete structures under different types of constraints. It is also demonstrated by several examples that analytical sensitivity analysis is computationally inexpensive and completely eliminates the inaccuracy in problem.

Last part of the research is focused on using the IFM for the design and optimization of stiffened panels subjected to buckling constraints. The FE model using the IFM is developed for the buckling analysis of eccentrically stiffened panels. The panel and stiffener are treated as separate members where the compatibility between these two

types of members is maintained. The force FE equations for panel and stiffener elements are formulated. The finite element modeling is validated by performing the force finite element analysis of different sizes of stiffened panels. The convergence study has been also performed in order to estimate the mesh size required for the solution accuracy. The effect of torsional stiffness of the stiffener on the buckling load of stiffened panels is also investigated. Further, the strategy for the optimization of panel having large number of similar stiffener subjected to uniform compressive loading, has been developed. The explicit expressions of the sensitivity of the buckling load with respect to dimensions of plate and stiffener are formulated. An optimization algorithm is developed integrating the IFM, sensitivity analysis and SQP to obtain the optimum values of dimensions of stiffened panel while guarding against buckling failure.

## 1.8 Thesis Organization

The present thesis contains six chapters. The present chapter introduces the objective of thesis and motivation for the work. A state-of-the-art review of developments in the area of numerical structural optimization and FE force method is presented. The concept of sensitivity analysis is introduced and its state-of-art with respect to force method is presented. A historical review of the design optimization of stiffened panel is presented. A brief comparison is made between the IFM and the DM formulation. Finally, the current work and expected contributions are clearly stated.

Chapter 2 presents the introduction to basic governing equations of the IFM. The various aspects of the IFM like generation of equilibrium and flexibility matrix, stress

interpolation, displacement interpolation and different methods to generate compatibility matrix are presented in detail. The IFM finite elements library is developed and general procedure to formulate a new element using IFM is presented. Finally, extensive numerical analysis is performed to validate the IFM formulation, and to demonstrate its accuracy over the DM.

Chapter 3 presents the structural optimization using the IFM. The mathematically optimization statements are formulated for size optimization of discrete structures subjected to stress, displacement, frequency and system stability constraints. The comparison is made between different approaches to evaluate the design sensitivity. An efficient approach to find the sensitivity analysis of structural response such as stress, displacement and frequency for truss and frame type structures is formulated. The sensitivity analysis is combined with optimization algorithm to provide the information about the gradient of the constraints required in SQP technique.

Chapter 4 contains a large array of numerical benchmark tests and examples to investigate the application of the proposed formulations and methodologies in structural optimization. The structural optimization problems ranging from small to large sizes are investigated, and comparison is made with the DM. The structures are subjected to different types of constraints: (1) stress constraints only (2) stress and displacement constraints (3) single frequency constraints and (4) multiple frequency constraints. Finally, the relative merits and demerits of the IFM in structural optimization under different types of behavior constraints are discussed.

Chapter 5 presents the design and optimization of stiffened panels using the IFM. A FE formulation based on the IFM has been formulated for the buckling analysis of the stiffened panels. In order to validate the FE formulation, first the buckling analysis of simply supported square plate subjected to unidirectional compression is performed, and results are compared with those obtained from the analytical solution and the DM. Further, the stiffened panels of various sizes are analyzed and convergence study with varying number of elements is performed. The finite element sensitivity analysis of buckling load with respect to design variables is developed, and integrated with optimization algorithm. Finally the developed optimization code is used to optimize different shapes of stiffened panels.

The present work is summarized in the conclusion in the Chapter 6 where possible future extensions are also discussed.

# Chapter 2
# INTEGRATED FORCE METHOD

## 2.1 Introduction

In the IFM, all independent forces are treated as unknown variables that can be calculated on the basis of simultaneous imposition of equations of equilibrium and conditions of compatibility. The IFM overcomes the general drawback of the redundant force method i.e. automatic generation of the compatibility condition. It has also been successfully extended to the free vibration and buckling analysis of the structures. In this chapter, the basic equations of the IFM for the static and free vibration analysis are presented. A general procedure to generate the finite elements in the IFM is described and a library of the finite elements is developed. Finally, the IFM is tested on the analysis problems for which analytical solutions are available, and comparison is made with the DM.

## 2.2 Basics Equations of Integrated Force Method

If a continuous object is discretized using finite elements, resulting in $n$ force degrees of freedom and $m$ displacement degrees of freedom, then it will have $m$ equilibrium equations and $r = (n - m)$ compatibility equations.

Equilibrium equations are based on the force balance concept and can be written as:

$$[B]\{F\} = \{P\} \tag{2-1}$$

where $\{F\}$ and $\{P\}$ are unknown independent forces and nodal load vectors, respectively, and $[B]$ is the $(m \times n)$ rectangular equilibrium matrix, having numbers of

columns greater than number of rows. It is very sparse, unsymmetrical matrix with full row rank.

Indeterminate structure can not be solved only by equilibrium equations; compatibility is required to obtain the sufficiency. The structure will have $r=(n-m)$ compatibility equations and these are:

$$[C][G]\{F\}=\{\partial R\} \tag{2-2}$$

where $[C]$ is the $(r\times n)$ compatibility matrix and $[G]$ is the $(n\times n)$ symmetrical flexibility matrix. The flexibility matrix is the block diagonal matrix, where each block represents a flexibility matrix for individual element. $\{\delta R\}$ is the *r*-component effective initial deformation vector and can be written in term of initial deformations vector $\{\beta_0\}$ as:

$$\{\partial R\}=-[C]\{\beta_0\} \tag{2-3}$$

The detail about the generation of each of these matrices will be discussed in next sections. The compatibility matrix is basically constraint on the deformations of the element and flexibility matrix converts deformation constraints into forces constraints, in order to assemble it with equilibrium matrix. The equilibrium and compatibility equations are coupled to obtain the governing equations of the IFM as:

$$[S]\{F\}=\{P^*\} \tag{2-4}$$

where

$$[S]=\begin{bmatrix}[B]\\ \hline [C][G]\end{bmatrix}\quad,\quad \{P^*\}=\begin{Bmatrix}P\\ \hline 0\end{Bmatrix} \tag{2-5}$$

The internal forces $\{F\}$ can be directly calculated by solving Eq. (2-4). Subsequently, stresses can be calculated by substituting forces into the stress interpolation relation.

The vector of unknown nodal displacement $\{U_e\}$ is obtained by back substitution as:

$$\{U_e\} = [J][G]\{F\} \tag{2-6}$$

where $[J]$ is the $(m \times n)$ deformation matrix that represents the top $m$ rows of the transpose of the matrix $[S]^{-1}$.

In IFM analysis, continuous structure under consideration is discretized into the finite elements. The stress and displacement fields are interpolated, and then used to generate the equilibrium and flexibility matrices for the element. The detail description of the equilibrium, flexibility and compatibility equations will be discussed in next sections.

## 2.3 Equilibrium Equations

The equilibrium equations written in terms of forces at the grid points of a FE model represent the vectorial summation of $n$ internal forces $\{F\}$ and $m$ external loads $\{P\}$. The element equilibrium matrix for the bar and beam element can be easily obtained by force balance concept, but for the continuous structure very few equilibrium matrix are reported in the literature [14, 15]. In the IFM, a general procedure is developed to generate the equilibrium matrix. The stress and displacement field is required to be interpolated, to generate the equilibrium matrix in the IFM. The stress and displacement field within the element are interpolated in terms of two sets of independent variables. The displacement interpolation is the same as that in the DM, and the displacement field $\{U\}$ interpolated in term of nodal displacement $\{U_e\}$ as:

$$\{U\} = [N]\{U_e\} \tag{2-7}$$

where $[N]$ contains the displacement interpolation or shape functions. Stress field $\{\sigma\}$ is interpolated in terms of independent internal forces $\{F\}$, which are unknown in the force formulation. Stress field is thus interpolated as:

$$\{\sigma\} = [Y]\{F\} \tag{2-8}$$

where $[Y]$ is the stress interpolation matrix .

The general equation to generate the equilibrium matrix is generated from the principal of virtual work. The principal of virtual work can be stated that internal virtual work $\partial W_I$ is equal to external virtual work $\partial W_E$ :

$$\partial W_I = \partial W_E \tag{2-9}$$

The internal virtual work per unit volume is the product of the real stress $\{\sigma\}$ and the virtual strain $\{\partial\varepsilon\}$, and is given by:

$$\partial W_I = \int_V \{\partial\varepsilon\}^T \{\sigma\} dV \tag{2-10}$$

The strain vector within the element can be obtained by differentiating the displacement vector in Eq. (2-7), and can be written as:

$$\{\varepsilon\} = [Z]\{U_e\} \tag{2-11}$$

where $[Z] = [L][N]$, and $[L]$ is the matrix of differential operator. Thus, given the virtual nodal displacements $\{\partial U_e\}$, virtual strains in the element are:

$$\{\partial\varepsilon\} = [Z]\{\partial U_e\} \tag{2-12}$$

Substituting Eqs. (2-8) and (2-12) into Eq. (2-10) yields the finial expression for the internal virtual work as:

$$\partial W_I = \{\partial U_e\}^T \int_V [Z]^T [Y][F] dV \tag{2-13}$$

The external virtual work is the combination of work done by surface traction and body forces. The external virtual work due to surface traction $\{F_T\}$ can be written as:

$$\int_s \{\partial U\}^T \{F_T\} ds_t = \int_s (([N]\{\partial U_e\})^T \{F_T\} ds_t = \{\partial U_e\}^T \int_s [N]^T \{F_T\} ds_t \tag{2-14}$$

Contribution to the external work done by body forces $\{F_B\}$ is:

$$\int_v \{\partial U\}^T \{F_B\} dV = \int_V (([N]\{\partial U_e\})^T \{F_B\} dV = \{\partial U_e\}^T \int_v [N]^T \{F_B\} dv \tag{2-15}$$

Adding Eqs. (2-14) and (2-15) yields the total external virtual work as:

$$\partial W_E = \{\partial U_e\}^T \int_s [N]^T \{F_T\} ds + \{\partial U_e\}^T \int_v [N]^T \{F_B\} dv \tag{2-16}$$

According to the principal of virtual work expressed in Eq. (2-9), we may write:

$$\{\partial U_e\} \int_v [Z]^T [Y][F] dv = \{\partial U_e\}^T \int_S [N]^T \{F_T\} ds_t + \{\partial U_e\}^T \int_V [N]^T \{F_B\} dv \tag{2-17}$$

$$\int_v [Z]^T [Y][F] dv = \int_s [N]^T \{F_T\} ds + \int_v [N]^T \{F_B\} dv \tag{2-18}$$

Eq. (2-18) can be written in the following compact form as:

$$[B_e]\{F\} = \{Q_T\} + \{Q_B\} \tag{2-19}$$

where $\{Q_T\}$ and $\{Q_B\}$ are the equivalent nodal force vectors due to surface traction and body force, respectively. $[B_e]$ is the element equilibrium matrix which balance the internal forces $\{F\}$ with nodal forces on the element due to externally applied forces and can be written as:

$$[B_e] = \int_v [Z]^T [Y] dv \tag{2-20}$$

The equilibrium matrix is obtained by integrating the product of stress and displacement interpolation matrices over the entire domain. For simple elements, closed form integration can be obtained; otherwise numerical integration like Gauss Quadrature is preferred. The equilibrium matrix is $(m \times n)$ rectangular matrix having rows corresponding to element displacement degrees of freedom and columns corresponding to element force degrees of freedom. It is also independent of material properties and the design parameters of the structure. The finial system equilibrium matrix of the structure is obtained by assembling element equilibrium matrices and assembling procedure is similar to that in the DM.

## 2.4 Flexibility Equations

The flexibility matrix requires expressing the compatibility in terms of forces, which can then be coupled to equilibrium equation, which are already available in term of forces. It represents the relation between deformation and internal forces. The generation of flexibility matrix in finite element analysis is well established in the literature. The IFM flexibility matrix is generated from the principal of complementary strain energy and castigliano's theorem. The change in complementary strain energy $U_c$ of the element with small change in external loading can be expressed as:

$$\delta U_c = \frac{1}{2} \int_v \{\delta\sigma\}^T \{\varepsilon\} dv \tag{2-21}$$

Strain can be expressed in terms of stress by the stress-strain relation as:

$$\{\varepsilon\} = [D]\{\sigma\} \tag{2-22}$$

where $[D]$ is the compliance matrix. Now substituting Eq. (2-22) in Eq. (2-21) yields:

$$\delta U_c = \frac{1}{2}\int_v \{\delta\sigma\}^T [D]\{\sigma\} dv \tag{2-23}$$

Substituting Eq. (2-8) in Eq. (2-23) yields:

$$\delta U_c = \frac{1}{2}\int_v \{\delta F\}^T [Y]^T [D][Y]\{F\} dv \tag{2-24}$$

The deformations $\{\beta\}$ are obtained from the castigliano's theorem, which states that deformations are the rate of change of complimentary strain energy with respect to forces:

$$\{\beta\} = \frac{\partial U_c}{\partial\{F\}} = \frac{1}{2}\int_v [Y]^T [D][Y] dv\{F\} = [G]\{F\} \tag{2-25}$$

where $[G]$ is the flexibility matrix, and its general expression can be written as:

$$[G] = \frac{1}{2}\int_v [Y]^T [D][Y] dv \tag{2-26}$$

Thus, the flexibility matrix $[G]$ can be obtained by substituting stress interpolation matrix and compliance matrix into Eq. (2-26), and then integrating. Similar to the equilibrium matrix, global flexibility matrix is obtained by assembling the flexibility matrix of each element.

## 2.5 Compatibility Equations

The deficiency in the compatibility condition has prevented the development of direct stress determination method in structural analysis and elasticity. Earlier in the force method, compatibility was achieved through the concept of redundant forces, with virtual cuts and subsequent closing of gaps. Condition of compatibility, formulated in pre computer era were found to be inconvenient and inefficient for automated computation of

large scale problems, thus hinder the growth of the force method in this computer era. Strain or deformation balance represents the physical concept behind the compatibility condition. Saint-Venant formulated the strain balance equation in elasticity, by eliminating displacements from strain displacement relation. The two steps of Saint-Venant formulation in elasticity are:

1) Formulation of strain displacement relation:

$$\varepsilon_x = \frac{\partial u}{\partial x},\ \varepsilon_y = \frac{\partial v}{\partial x},\ \gamma_{xy} = \frac{\partial u}{\partial y} + \frac{\partial v}{\partial x} \tag{2-27}$$

2) Elimination of displacement to obtain the compatibility conditions:

$$\frac{\partial^2 \varepsilon_x}{\partial y^2} + \frac{\partial^2 \varepsilon_y}{\partial x^2} - \frac{\partial^2 \gamma_{xy}}{\partial x \partial y} = 0 \tag{2-28}$$

The compatibility conditions for FE analysis are obtained as an extension of Saint-Venant's formulation in elasticity [22-24]. The strain-displacement relation is replaced by the displacement deformation relation (DDR), and then displacements are eliminated from the DDR.

The DDR in the finite element analysis is derived from the principle of complimentary virtual work [15]. The principle of complimentary virtual work state that:

$$\partial W_E^C = \partial W_I^C \tag{2-29}$$

where $\partial W_E^C$ and $\partial W_I^C$ are external and internal complimentary virtual work done, respectively. The external complimentary virtual work done due to the external virtual load $\{\partial P\}$ and real displacements $\{U_e\}$ is:

$$\partial W_E^C = \{\partial P\}^T \{U_e\} \tag{2-30}$$

Substituting Eq. (2-1) into Eq. (2-30) yields:

$$\partial W_E^C = \{\partial F\}^T [B]^T \{U_e\} \tag{2-31}$$

The internal complimentary virtual work done due to internal virtual forces $\{\partial F\}$ and corresponding real deformations $\{\beta\}$ is:

$$\partial W_I^C = \{\partial F\}^T \{\beta\} \tag{2-32}$$

Now with substitution of Eqs. (2-31) and (2-32) into Eq. (2-29), we have:

$$\{\partial F\}^T [B]^T \{U_e\} = \{\partial F\}^T \{\beta\} \tag{2-33}$$

or

$$\{\beta\} = [B]^T \{U_e\} \tag{2-34}$$

The Eq. (2-34) represents the DDR in which $n$ deformations $\{\beta\}$ are expressed in terms of $m$ nodal displacements $\{U_e\}$ by the transpose of equilibrium matrix. Therefore, there are $r = (n-m)$ constraints on the deformation which represents the compatibility equations. The compatibility equations are obtained after eliminating the $m$ displacements from $n$ DDR is:

$$[C]\{\beta\} = \{0\} \tag{2-35}$$

The deformations $\{\beta\}$ in Eq. (2-35) represent total deformations, consisting of initial deformations $\{\beta_o\}$ and elastic deformations $\{\beta_e\}$, as $\{\beta\} = \{\beta_e\} + \{\beta_0\}$. The compatibility conditions in terms of the elastic deformations $\{\beta_e\}$ can be written as:

$$[C]\{\beta_e\} = \{\delta R\} \tag{2-36}$$

where

$$\{\delta R\} = -[C]\{\beta_0\} \tag{2-37}$$

Now substitute Eq. (2-25) into Eq. (2-36) yields:

$$[C][G]\{F\} = \{\delta R\} \tag{2-38}$$

The rectangular and banded compatibility matrix $[C]$ of dimension $(r \times n)$ has a full row rank of $r$. It is independent of sizing design parameters, material properties, and external loads.

The elimination of deformation from the DDR is amenable to computer automation and can be performed in two ways, direct elimination and indirect elimination. The procedures to generate the compatibility matrix using direct and indirect techniques are discussed in detail here.

*Direct Elimination*

The compatibility matrix can be obtained by direct elimination of the displacements from the global DDR. The direct elimination can be performed by standard value decomposition technique (SVD) [27].

The nodal displacement can be expressed in term of deformation from the Eq. (2-34) as:

$$\{U\}_e = \left[[B][B]^T\right]^{-1}[B]\{\beta\} = \left[[B]^T\right]^{pinv}\{\beta\} \tag{2-39}$$

The matrix $\left[[B]^T\right]^{pinv}$ denotes the Moorse-Penrose pseudo inverse of $[B]^T$. Substituting displacement $\{U\}_e$ from Eq. (2-39) into Eq. (2-34) yields:

$$\{\beta\} = [B]^T\left[[B]^T\right]^{pinv}\{\beta\} \tag{2-40}$$

$$[\Pi]\{\beta\} = 0 \tag{2-41}$$

where $$[\Pi] = \left|I_{n\times n} - [B]^T\left[[B]^T\right]^{pinv}\right| \tag{2-42}$$

Eq. (2-41) is similar to the compatibility equation given by Eq. (2-35), however the rank of $(n \times n)$ matrix $[\Pi]$ is $r$, which means that rows of $[\Pi]$ are dependent on each other. The SVD technique is used to extract the $(r \times n)$ compatibility matrix from $[\Pi]$. The detail of SVD technique can be found in the reference [48]. By applying the SVD method to $[\Pi]$, we obtain:

$$[\Pi] = [R][\Sigma][\Gamma]^T \tag{2-43}$$

where $[R]$ and $[\Gamma]$ are the $(n \times n)$ orthogonal matrices and

$$\Sigma = \begin{bmatrix} \Lambda & 0 \\ 0 & 0 \end{bmatrix}_{(n \times n)} \tag{2-44}$$

with $\Lambda = diag\{\Lambda_1, \Lambda_2 ..... \Lambda_r\}$, and $\Lambda_1 \geq \Lambda_2 \geq ..... \geq \Lambda_r \geq 0$. It follows that:

$$[\Pi] = [R] \begin{bmatrix} C \\ 0 \end{bmatrix} \tag{2-45}$$

Therefore the $(r \times n)$ compatibility matrix $[C]$ can be represented by:

$$[C] = \Lambda [\Gamma_1 \ \Gamma_2 ..... \Gamma_i ..... \Gamma_r]^T \tag{2-46}$$

where the vector $\{\Gamma_i\}$ denotes the $i$th column of the matrix $[\Gamma]$.

It should be noted that the compatibility matrix introduced in Eq (2-46) may not be banded. The direct technique is efficient for relatively small size problems; however it is numerically expensive for large size problems.

*Indirect method*

The direct elimination technique to generate the compatibility matrix is easy to implement, but it is numerically expensive for large scale structural problems. The indirect elimination technique [22-24] is more systematic and efficient, and suitable for

large scale problems. In this approach, the compatibility conditions are divided into three distinct categories: 1) the interface compatibility conditions, 2) the cluster, or field compatibility conditions, and 3) the external compatibility conditions. The general procedures to generate each of these compatibility conditions are the same and the main steps are:

1) Separate a local region from the structural model on the basis of interface, cluster or external bandwidth consideration.

2) Establish the DDR for the local region. The elimination of displacement from the DDR yields the compatibility conditions for that region. Repeat this process for every local region until we obtain the required number of compatibility conditions.

Each compatibility condition is generated separately, and then assembled with global compatibility conditions. The physical concept behind each of these compatibility conditions and procedure to generate them are discussed in next sections.

### 2.5.1 Interface Compatibility Conditions

The interface is the common boundary shared by two or more elements. The deformation in the two elements should be compatible along the interface between them, which defines compatibility conditions of the interface. To better understand the interface compatibility condition, let us consider the 2-D structure shown in Figure 2-1. The structure is discretized by triangle and quadrilateral elements. The number of force degrees of freedom for triangular and quadrilateral elements are three and five, respectively. Structure has 16 nodes and each node has two displacement degrees of freedoms. The common boundary along nodes 2 and 5 is the interface between elements

1 and 2, and the boundary connecting node 5 and 6 is the interface between elements 2 and 6. The compatibility condition at the interface of element 1 and 2 means that deformation between elements 1 and 2 must be compatible along the common boundary shared by them.

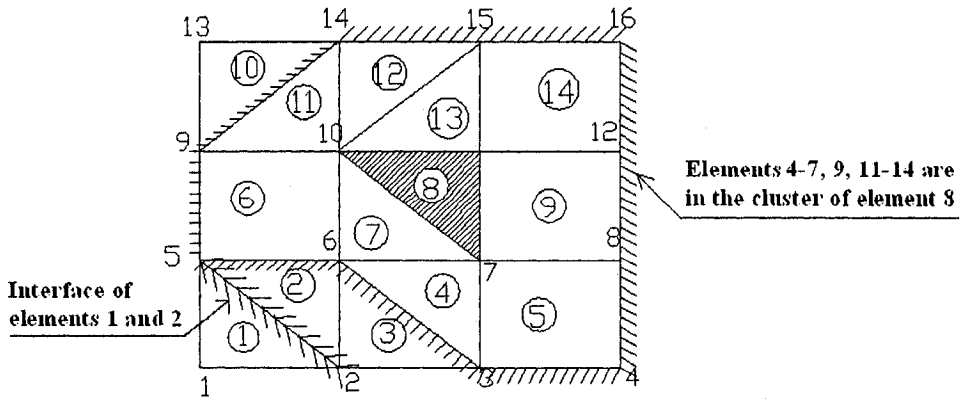


**Figure 2.1** Interface and Cluster Compatibility

The numbers of compatibility condition at the interface depend on the element type and their numbers at the interface. In other words, the numbers of compatibility condition at the interface of elements 1 and 2 are different from those at interface of elements 2 and 6. The compatibility condition is generated by extracting the DDR for each interface from the global DDR, and then eliminating the displacements from the DDR. The number of global DDR of the structure is reduced after the generation of each compatible condition. The reduced set designated has $m$ rows and $(n_1 = n - n_{c1})$ columns, where $n_{c1}$ represents the number of compatibility equations generated in previous step. It is obtained by dropping one of the deformations from the DDR that had participated in compatibility equation generated in previous step. Dropping a deformation that has participated in the compatibility condition immediately after its generation avoids the possibility of its further participation in other compatibility conditions, thus maintaining the uniqueness of

the compatibility condition. The degree of indeterminacy of the structure will reduce by one with drop of any deformation from the global DDR and structure behavior will approach towards that of the determinant structure.

### 2.5.2 Cluster Compatibility Conditions

In the FE model, a cluster is defined as a series of adjoining elements. The cluster compatibility describe that the deformation of all the elements in cluster must be compatible with each other. For example, the element 8 of the structure shown in the Figure 2-1 have elements 4-7, 9, and 11- 14 in its cluster. The deformations of each element in cluster of element 8 must be compatible with each other. The DDR of the cluster of element 8 is extracted from the global DDR, and then displacements are eliminated from the DDR to generate the constraints on the deformations. The global DDR relation is updated immediately after generation of each compatibility condition by dropping any deformation that has participated in compatibility. The procedure is repeated for every element and compatibility is generated for each cluster. Similar to the interface compatibility, the number of compatibility conditions in the cluster depends on the type of elements and their numbers.

### 2.5.3 External Compatibility

The FE model of the structure is restrained at the nodes to suppress the free degrees of freedom of the structure. If such restraints on the boundary exceed the number of rigid body motion of the structure, then it is externally indeterminate. The degree of externally indeterminacy $R_{ext}$ of the structure can be calculated as:

$$R_{ext} = T_S - T_R \tag{2-47}$$

where $T_S$ is the number of displacement components suppressed on the boundary and $T_R$ is the number of boundary conditions required only for the kinematics stability of the structure. The local restrain region is separated from the whole structure, and the compatibility condition for this region is generated similar to as done for interface and cluster compatibility.

To further reduce the computational time to generate compatibility, the concept of node determinacy can be used. Node is determined, if the numbers of displacement degrees of freedoms $ND_i$ is equal to the number of force components presents in the equilibrium equations written at that node $NF_i$. The node determinacy factor can be written as:

$$\text{Node determinacy } NR_i = NF_i - ND_i \tag{2-48}$$

If node is determined i.e. $NR_i = 0$, then forces present at that node are determined and thus, do not participate in compatibility conditions. Consequently for determined node, forces or deformation along with displacement can be dropped simultaneously from the DDR. It is equivalent to the elimination of appropriate columns and rows in the DDR. The node determinacy can reduce the number of DDR; however number of compatibility conditions remains the same. This increases the computational efficiency of the compatibility generation procedure.

## 2.6 Stress Field Interpolation

The proper interpolation of stresses within the element is necessary to obtain the accurate results, since it appears in both the equilibrium and the flexibility matrices. The general guidelines of stress interpolation, in context to the hybrid method application were discussed by Pian [45-46] and Spliker [47]. Stress fields are interpolated without any reference to the shape and number of kinematics degrees of freedom of the considered element. It was suggested that approximated stress field should satisfy equilibrium equations, free from any zero energy modes and should be invariant with respect to coordinate transformation. Spliker [47] have shown that necessary and sufficient condition for the element to be invariant with respect to coordinate transformation is that it should possess complete polynomial. As discussed in hybrid method [45-47], number of stress parameters must be greater than or equal to the number of element displacement degree of freedom minus number of rigid body modes. However a large plausible stress field can be defined which sometimes result in element possessing zero energy modes and also increase the computational cost, so there is always tendency to have minimum number of stress parameters.

In the IFM, the correct rank of element equilibrium matrix ensures the absence of spurious zero energy modes [20-21]. It is seen that if the element equilibrium matrix has the correct rank then there are only zero energy modes associated with the rigid body modes of the element. Thus in order to eliminate spurious zero energy modes, the stress field must be constructed such that the resulting equilibrium matrix has the correct rank.

An Airy's stress function as complete polynomial is usually used to interpolate stresses in the IFM. Airy's stress function is given by:

$$\Phi(x,y) = \sum_{j=0}^{q} C_j x^{q-j} y^j \tag{2-49}$$

where $C_j$, for $j = 1.....q$, are constants, and $x$ and $y$ are Cartesian coordinates. The stresses are obtained from Airy's stress function by the proper differentiation of it. Stress in $x$ direction $\sigma_x$ can be obtained from Eq. (2-49) as:

$$\sigma_x = \frac{\partial^2 \Phi}{\partial y^2} = \sum_{j=0}^{q-2} C_{j+2}(j+1)(j+2) x^{q-2-j} y^j \tag{2-50}$$

Similarly $y$ direction stress $\sigma_y$ can be obtained as:

$$\sigma_y = \frac{\partial^2 \Phi}{\partial x^2} = \sum_{j=0}^{q-2} C_j (q-j)(q-j-1) x^{q-2-j} y^j \tag{2-51}$$

and shear $\tau_{xy}$ stress can be written as,

$$\tau_{xy} = -\frac{\partial \Phi}{\partial x \partial y} = -\sum_{j=0}^{q-2} C_j (j+1)(q-j-1) x^{q-2-j} y^j \tag{2-52}$$

Stresses are interpolated in terms of constants $C_j$, and these constants subsequently can be replaced by independent internal forces $\{F\}$ within the element. For example by taking $q = 3$ in Eq. (2-49), Airy's stress function can be written as:

$$\Phi(x,y) = C_0 x^3 + C_1 x^2 y + C_2 x y^2 + C_3 y^3 \tag{2-53}$$

Stresses obtained from Eqs. (2-50), (2-51) and (2-52) are then described as:

$$\sigma_x = 6C_3 y + 2C_2 x \tag{2-54}$$

$$\sigma_y = 6C_0 x + 2C_1 y \tag{2-55}$$

$$\tau_{xy} = -2C_1 x - 2C_2 y \tag{2-56}$$

Now assuming

$$6C_3 = F_1, 2C_2 = F_2, 6C_0 = F_3, 2C_1 = F_4 \tag{2-57}$$

$\sigma_x, \sigma_y$ and $\tau_{xy}$ in Eqs. (2-54), (2-55) and (2-56) can be written as:

$$\sigma_x = F_1 y + F_2 x \tag{2-58}$$

$$\sigma_y = F_3 x + F_4 y \tag{2-59}$$

$$\tau_{xy} = -F_4 x - F_2 y \tag{2-60}$$

Therefore the stress field is expressed in terms of four independent forces $F_1$, $F_2$, $F_3$ and $F_4$. Stress field of high approximation can be obtained by taking the polynomials of higher order. The stress field obtained from above approach satisfies the equations of equilibrium at any point inside the domain of the element and the resulting element matrix is invariant with respect to coordinate transformations.

As discussed earlier, there is always tendency to reduce the number of independent forces in stress field representation while preserving all the desirable properties of resulting element matrices. Patnaik [20] proposes the imposition of the compatibility conditions on the stress field to reduce the number of unknown forces. The compatibility condition can be written as:

$$\nabla^2 (\sigma_x + \sigma_y) = 0 \tag{2-61}$$

The number of independent forces required to interpolate the stresses are reduced by Eq. (2-61), which subsequently reduces the computational time for the analysis.

## 2.7 Frequency and Buckling Analysis

The IFM methodology can also be easily extended to frequency and buckling analysis [18, 25]. The basic frequency equation in the DM is:

$$[M]\{\ddot{U}_e\}+[K]\{U_e\}=0 \tag{2-62}$$

where $[M]$ and $[K]$ are the mass and stiffness matrices of the structures, respectively. The static equations of the DM can also be written as [16]:

$$[K]\{U_e\}=\{P\} \tag{2-63}$$

Now considering Eqs. (2-1), (2-6) and (2-63), one may represent Eq. (2-62) in the following form:

$$\left[\frac{[M][J][G]}{[0]}\right]\{\ddot{F}\}+[S]\{F\}=0 \tag{2-64}$$

$$[M_f]\{\ddot{F}\}+[B]\{F\}=0 \tag{2-65}$$

where IFM mass matrix $[M_f]$ is described as :

$$[M_f]=\left[\frac{[M][J][G]}{[0]}\right] \tag{2-66}$$

In free vibration, it is assumed that forces are harmonic and can be written in terms of force mode shapes $\{F_m\}$ as:

$$\{F\}=\{F_m\}Sin\,\omega t \tag{2-67}$$

Substituting Eq. (2-67) into Eq. (2-65) yields the frequency equation of the IFM as:

$$([S]-\omega^2[M_f])\{F_m\}=0 \tag{2-68}$$

Even though Eq. (2-68) represents $(n\times n)$ system of equations, the numbers of frequencies are only $m$ corresponding to the number of equilibrium equations. To

increase the computational efficiency of the analysis, Patnaik [25] proposed a method to reduce the $(n \times n)$ system of equations to $(m \times m)$ system of equations by taking advantage of null matrices. The forces are divided into set of redundant forces $\{F_r\}$ and basic determinant forces $\{F_d\}$ in the structure, and Eq. (2-68) is written accordingly as:

$$\begin{bmatrix} S_{dd} & S_{dr} \\ S_{rd} & S_{rr} \end{bmatrix} \begin{Bmatrix} F_d \\ F_r \end{Bmatrix} - \omega^2 \begin{bmatrix} M_d & M_r \\ & 0 \end{bmatrix} \begin{Bmatrix} F_d \\ F_r \end{Bmatrix} = 0 \tag{2-69}$$

Eq. (2-69) can be further expanded as:

$$[S_{dd}]\{F_d\} + [S_{dr}]\{F_r\} - \omega^2 ([M_d]\{F_d\} + [M_r]\{F_r\}) = 0 \tag{2-70}$$

$$[S_{rd}]\{F_d\} + [S_{rr}]\{F_r\} = 0 \tag{2-71}$$

Elimination of $\{F_r\}$ from these $(n \times n)$ systems of equations given in Eqs. (2-70) and (2-71), results in the following $(m \times m)$ system of equations:

$$([S_{dd}] - [S_{dr}][S_{rr}^{-1}][S_{rd}])\{F_d\} - \omega^2 ([M_d] - [M_r][S_{rr}^{-1}][S_{rd}])\{F_d\} = 0 \tag{2-72}$$

$$\{F_r\} = [S_{rr}^{-1}][S_{rd}]\{F_d\} \tag{2-73}$$

The solution of the reduced eigen value problem expressed by Eq. (2-72) provides $m$ eigen values, then both Eqs. (2-75) and (2-76) are used to find the associated force eigen vectors. Although this formulation increase efficiency of the frequency analysis significantly, but the process of selection of redundant complicates the procedure.

Similarly linear bucking analysis in the IFM can be written as:

$$[[S] - \lambda [S_b]]\{F\} = \{0\} \tag{2-74}$$

where $[S_b]=\begin{bmatrix}[K_g][J][G]\\ \hline 0\end{bmatrix}$ is the stability matrix of the IFM, $[K_g]$ is the geometric stiffness matrix and $\lambda$ is the load factor parameter.

## 2.8 Finite Element Library

The implementation of all equations to generate the finite elements in the IFM is presented in this section, to give some insight into finite element formulation procedure. The stress and displacement field within the element is required to be interpolated in order to generate element matrices. These approximations are performed independently: the displacement components within the element are approximated in terms of element nodal displacements, while the components of stress tensor are approximated in terms of set of independent forces. The equilibrium and flexibility matrices are then generated from the stress and displacement interpolation. The DDR of the element is generated in terms of equilibrium matrix, and then compatibility matrix is generated by the elimination of displacements from the DDR. The FE formulation of some basic finite elements is presented in the next sections.

### 2.8.1 Truss Element

Truss element as shown in the Figure 2-2 has one axial nodal displacement degree of freedom at each node.

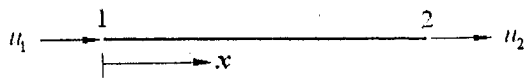


**Figure 2-2** Two node truss element

A linear variation of displacement in term of axial nodal displacements $u_1$ and $u_2$ is assumed:

$$u = N_1 u_1 + N_2 u_2 \tag{2-75}$$

where

$$N_1 = 1 - \frac{x}{\mathrm{L}}, \quad N_2 = \frac{x}{\mathrm{L}} \tag{2-76}$$

From Eqs. (2-11) and (2-75) the strain displacement matrix is:

$$[Z] = \left[\frac{-1}{\mathrm{L}} \quad \frac{1}{\mathrm{L}}\right] \tag{2-77}$$

The stress field within the element is interpolated in term of axial force as:

$$\sigma_x = \frac{F_1}{A} \tag{2-78}$$

The uniform internal force in the bar is $F_1$, associated stress is $\sigma_x$ and the cross sectional area of the truss is $A$. From Eqs. (2-8) and (2-78) the stress interpolation matrix is:

$$[Y] = \left[\frac{1}{A}\right] \tag{2-79}$$

Substituting Eqs. (2-77) and (2-79) into Eq. (2-20) yields the equilibrium matrix as:

$$[B_e]_T = \begin{bmatrix} -1 \\ 1 \end{bmatrix} \tag{2-80}$$

Substituting Eq. (2-79) into Eq. (2-26) yields the flexibility matrix as:

$$[G_e]_T = \left[\frac{\mathrm{L}}{AE}\right] \tag{2-81}$$

Flexibility matrix is of size $(1 \times 1)$ because the truss element contains only one force degree of freedom.

## 2.8.2 Beam Element

Beam Element has one transverse and one rotational degree of freedom at each node as shown in Figure 2-3. The transverse and rotational displacements of the element are related by Kirchhoff's assumption.

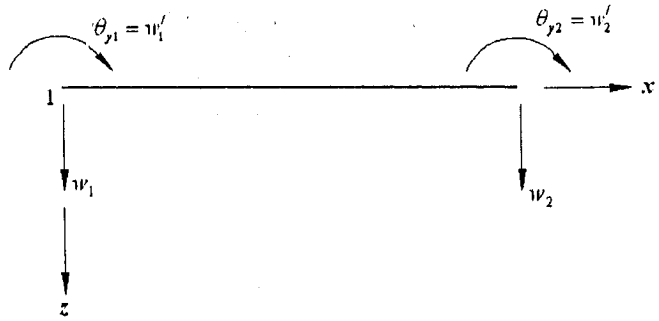


**Figure 2-3** Two node beam element

The transverse nodal displacement is interpolated in terms of transverse displacements $w_1$ and $w_2$, and rotational displacements $\theta_{y1}$ and $\theta_{y2}$ as:

$$w = N_1 w_1 + N_2 \theta_{y1} + N_3 w_2 + N_4 \theta_{y2} \tag{2-82}$$

where

$$N_1 = 1 - \frac{3x^2}{L^2} + \frac{2x^3}{L^3}, \quad N_2 = x - \frac{2x^2}{L} + \frac{x^3}{L^2}$$
$$N_3 = \frac{3x^2}{L^2} - \frac{2x^3}{L^3}, \quad N_4 = -\frac{x^2}{L} + \frac{x^3}{L^2} \tag{2-83}$$

Now considering Eqs. (2-11), (2-82) and (2-83), the strain-displacement matrix can be obtained as:

$$[Z] = -z\left[\frac{-6}{L^2} + \frac{12x}{L^3} \quad \frac{-4}{L} + \frac{6x}{L^2} \quad \frac{6}{L^2} - \frac{12x}{L^3} \quad -\frac{2}{L} + \frac{6x}{L^2}\right] \tag{2-84}$$

where z is the distance from the centroidal axis of the beam element.

Moment Field is interpolated linearly along the $x$ axis as:

$$M_y = F_1 + F_2 x \tag{2-85}$$

where $M_y$ is the $y$ direction moment field, and $F_1$ and $F_2$ are independent force degrees of freedom. The stresses in the element can be related to moment as:

$$\sigma_x = \frac{12z}{t^3} M_y \tag{2-86}$$

Now using Eqs. (2-8), (2-85) and (2-86), the stress interpolation matrix can be stated as:

$$[Y] = \frac{12z}{t^3}[1 \quad x] \tag{2-87}$$

where $t$ is the thickness of the beam. Substituting Eqs. (2-84) and (2-87) into Eq. (2-20) yields the equilibrium matrix as:

$$[B_e]_B = \begin{bmatrix} 0 & 1 \\ -1 & 0 \\ 0 & -1 \\ 1 & \mathrm{L} \end{bmatrix} \tag{2-88}$$

Also substituting Eq. (2-87) into Eq. (2-26) yields the flexibility matrix as:

$$[G_e]_B = \begin{bmatrix} \frac{\mathrm{L}}{I} & \frac{\mathrm{L}^2}{2I} \\ \frac{\mathrm{L}^2}{2I} & \frac{\mathrm{L}^3}{3I} \end{bmatrix} \tag{2-89}$$

where $I$ denotes the area moment of inertia of cross section of the element about $y$-axis.

### 2.8.3 Frame Element

Frame element includes both the axial and the bending deformations. Element has three displacement degrees of freedom at each node, one corresponding to axial deformation and two corresponding to bending displacements. Equilibrium and flexibility matrices of

the truss and beam elements are superimposed to obtain the equilibrium and flexibility matrices of the frame element.

The equilibrium matrix obtained after superimposing Eqs. (2-80) and (2-88) is:

$$[B_e]_F = \begin{bmatrix} -1 & 0 & 0 \\ 0 & 0 & 1 \\ 0 & -1 & 0 \\ 1 & 0 & 0 \\ 0 & 0 & -1 \\ 0 & 1 & L \end{bmatrix} \tag{2-90}$$

Frame structures generally consist of numbers of members oriented at different angles with respect to each other. The transformation of the equilibrium matrix is required to assemble the element equilibrium matrix in the global formulation. Equilibrium matrix for the frame element having local axis inclined at angle $\theta$ with respect to global axis is given by:

$$[B_e]_{FG} = [T]^T [B_e]_F \tag{2-91}$$

where $[T]$ is transformation matrix and is given by:

$$[T] = \begin{bmatrix} c & s & 0 & 0 & 0 & 0 \\ -s & c & 0 & 0 & 0 & 0 \\ 0 & 0 & 1 & 0 & 0 & 0 \\ 0 & 0 & 0 & c & s & 0 \\ 0 & 0 & 0 & -s & c & 0 \\ 0 & 0 & 0 & 0 & 0 & 1 \end{bmatrix} \quad \text{where } c = \cos\theta \text{ and } s = \sin\theta \tag{2-92}$$

Flexibility matrix is obtained after superimposing of Eqs. (2-81) and (2-89) and can be written as:

$$[G_e]_F = \frac{1}{E}\begin{bmatrix} \frac{L}{A} & 0 & 0 \\ 0 & \frac{L}{I} & \frac{L^2}{2I} \\ 0 & \frac{L^2}{2I} & \frac{L^3}{3I} \end{bmatrix} \tag{2-93}$$

### 2.8.4 4-Node Quadrilateral Membrane Element

The 4-node quadrilateral membrane element is basic element for two dimensional finite element analyses. It has four corner nodes and each node has two displacement degrees of freedom, therefore element has total eight degrees of freedom. Node numbering and dimension of the element are shown in Figure 2-4.

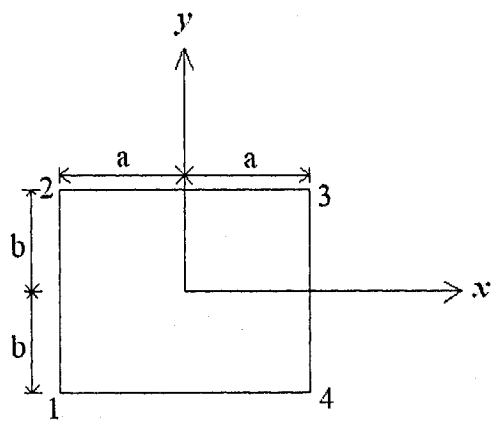


**Figure 2-4** 4-Node quadrilateral membrane element

The displacement field is interpolated in terms of nodal displacements as:

$$\begin{aligned} u &= N_1 u_1 + N_2 u_2 + N_3 u_3 + N_4 u_4 \\ v &= N_1 v_1 + N_2 v_2 + N_3 v_3 + N_4 v_4 \end{aligned} \tag{2-94}$$

where $u_i$ and $v_i$ are horizontal and vertical nodal displacement at $i$th node, respectively and interpolation functions are described as:

$$N_1 = \frac{1}{4ab}(a-x)(b-y),\ N_2 = \frac{1}{4ab}(a-x)(b+y)$$
$$N_3 = \frac{1}{4ab}(a+x)(b+y),\ N_4 = \frac{1}{4ab}(a+x)(b-y) \tag{2-95}$$

The strain field within the element obtained from the strain displacement relation as:

$$\begin{Bmatrix}\varepsilon_x\\ \varepsilon_y\\ \varepsilon_{xy}\end{Bmatrix} = \frac{1}{4ab}\begin{bmatrix} -(b-y) & 0 & -(b+y) & 0 & (b+y) & 0 & (b-y) & 0\\ 0 & -(a-x) & 0 & (a-x) & 0 & (a+x) & 0 & -(a+x)\\ -(a-x) & -(b-y) & (a-x) & -(b+y) & (a+x) & (b+y) & -(a+x) & (b-y)\end{bmatrix}\begin{Bmatrix}u_1\\ v_1\\ u_2\\ v_2\\ u_3\\ v_3\\ u_4\\ v_4\end{Bmatrix} \tag{2-96}$$

Using Eqs. (2-11) and (2-96), the strain interpolation matrix can be written as:

$$[Z] = \frac{1}{4ab}\begin{bmatrix} -(b-y) & 0 & -(b+y) & 0 & (b+y) & 0 & (b-y) & 0\\ 0 & -(a-x) & 0 & (a-x) & 0 & (a+x) & 0 & -(a+x)\\ -(a-x) & -(b-y) & (a-x) & -(b+y) & (a+x) & (b+y) & -(a+x) & (b-y)\end{bmatrix} \tag{2-97}$$

Since the number of displacement degree of freedom of the element are eight, and number of rigid body modes are three, therefore minimum five independent forces are required to interpolate the stress field and to obtain the correct rank of the equilibrium matrix. The higher order stress interpolation can be used with more than five independent forces to obtain better approximation of stress at the expense of computational cost. The stresses $\sigma_x$ and $\sigma_y$ are interpolated linearly and constant interpolation is used for shear stress $\tau_{xy}$. Thus, the stress field interpolation can be written as:

$$\sigma_x = F_1 + F_4 y \tag{2-98}$$

$$\sigma_y = F_2 + F_5 x \tag{2-99}$$

$$\tau_{xy} = F_3 \tag{2-100}$$

Based on Eqs. (2-11) and (2-98-100) the stress-interpolation matrix can be written as:

$$[Y] = \begin{bmatrix} 1 & 0 & 0 & y & 0 \\ 0 & 1 & 0 & 0 & x \\ 0 & 0 & 1 & 0 & 0 \end{bmatrix} \tag{2-101}$$

and also from Eq. (2-20), the equilibrium matrix can be written as:

$$[B_e]_M = \int_{-a}^{a}\int_{-b}^{b} [Z]^T [Y] t \, dydx \tag{2-102}$$

where $t$ is the thickness of the element. Substituting Eqs. (2-97) and (2-101) into Eq. (2-102) yields the equilibrium matrix as:

$$[B_e]_M = \begin{bmatrix} -b & 0 & -a & \frac{b^2}{3} & 0 \\ 0 & -a & -b & 0 & \frac{a^2}{3} \\ -b & 0 & a & -\frac{b^2}{3} & 0 \\ 0 & a & -b & 0 & -\frac{a^2}{3} \\ b & 0 & a & \frac{b^2}{3} & 0 \\ 0 & a & b & 0 & \frac{a^2}{3} \\ b & 0 & -a & -\frac{b^2}{3} & 0 \\ 0 & -a & b & 0 & -\frac{a^2}{3} \end{bmatrix} \tag{2-103}$$

Similarly, substituting Eq. (2-101) into Eq. (2-26) yields the flexibility matrix as:

$$[G_e]_M = \left(\frac{4ab}{tE}\right) \times \begin{bmatrix} 1 & -\nu & 0 & 0 & 0 \\ -\nu & 1 & 0 & 0 & 0 \\ 0 & 0 & \frac{E}{S} & 0 & 0 \\ 0 & 0 & 0 & \frac{b^2}{3} & 0 \\ 0 & 0 & 0 & 0 & \frac{a^2}{3} \end{bmatrix} \tag{2-104}$$

### 2.8.5 4-Node Quadrilateral Kirchhoff's Bending Element

The 4-node quadrilateral Kirchhoff's bending element is formulated to perform the bending analysis of plate's type structures. The shape and node numbering of the element are shown in the Figure 2-5. Element has three degrees of freedoms at each node, transverse deflection, rotation about $x$ direction and rotation about $y$ direction. The Kirchhoff's thin plate assumption is imposed such that plane normal to the element remains straight and normal after the rotation and shear stress in neglected.

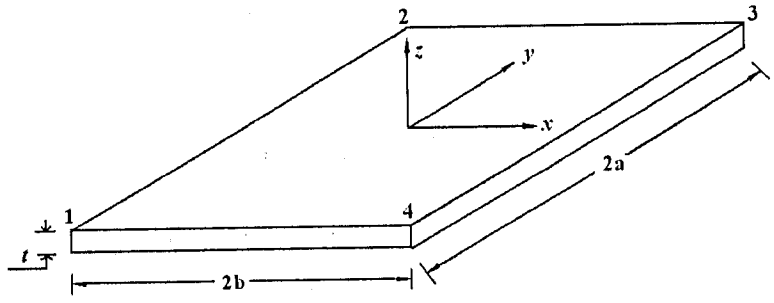


**Figure 2-5** 4-Node quadrilateral bending element

The displacement field is interpolated in terms of nodal displacements using hermite polynomial. The transverse deflection within the element is interpolated as:

$$
\begin{aligned}
w = {} & H_{01}(x)H_{01}(y)w_1 + H_{01}(x)H_{11}(y)\theta_{x1} + H_{11}(x)H_{01}(y)\theta_{y1} \\
& H_{01}(x)H_{02}(y)w_2 + H_{01}(x)H_{12}(y)\theta_{x2} + H_{11}(x)H_{02}(y)\theta_{y2} \\
& H_{02}(x)H_{02}(y)w_3 + H_{02}(x)H_{12}(y)\theta_{x3} + H_{12}(x)H_{02}(y)\theta_{y3} \\
& H_{02}(x)H_{01}(y)w_4 + H_{02}(x)H_{11}(y)\theta_{x4} + H_{12}(x)H_{01}(y)\theta_{y4}
\end{aligned}
\tag{2-105}
$$

where shape functions are:

$$
\begin{aligned}
H_{01}(x) &= \frac{x^3 - 3a^2x + 2a^3}{4a^3} \quad , \quad H_{02}(x) = -\frac{x^3 - 3a^2x - 2a^3}{4a^3} \\
H_{11}(x) &= \frac{x^3 - ax^2 - a^2x + a^3}{4a^2} \quad , \quad H_{12}(x) = \frac{x^3 + ax^2 - a^2x - a^3}{4a^2}
\end{aligned}
\tag{2-106}
$$

Strain field within the element can be obtained from the strain-displacement relation, which can be written as [16]:

$$
\begin{Bmatrix} \varepsilon_x \\ \varepsilon_y \\ \lambda_{xy} \end{Bmatrix} = -z \begin{Bmatrix} \dfrac{\partial^2 w}{\partial^2 x} \\ \dfrac{\partial^2 w}{\partial^2 y} \\ \dfrac{2\partial^2 w}{\partial x \partial y} \end{Bmatrix}
\tag{2-107}
$$

where $z$ is the distance from the centroidal axis. The strain interpolation matrix $[Z]$ can be obtained by closed or numerical differentiation of Eq. (2-107).

Similar to beam element, moment field within the element is interpolated in terms of independent forces, and then stresses are interpolated by using moment-stress relation. The element have twelve displacement degrees of freedom and three rigid body modes, therefore moment field is interpolated in term of nine independent forces:

$$
\begin{aligned}
M_x &= F_1 + F_2 x + F_3 y + F_4 xy \\
M_y &= F_5 + F_6 x + F_7 y + F_8 xy \\
M_{xy} &= F_9
\end{aligned}
\tag{2-108}
$$

The variation of normal moments in the field is linear, but the twisting moment is constant. Stress interpolation is obtained from stress-moment relation, which can be stated as:

$$\begin{Bmatrix} \sigma_x \\ \sigma_y \\ \tau_{xy} \end{Bmatrix} = \frac{12z}{t^3} \begin{Bmatrix} M_x \\ M_y \\ M_{xy} \end{Bmatrix} \tag{2-109}$$

where $t$ is the thickness of the element. Now using Eqs. (2-11), (2-108) and (2-109), the stress-interpolation matrix can be described as:

$$[Y] = \frac{12z}{t^3} \begin{bmatrix} 1 & x & y & xy & 0 & 0 & 0 & 0 & 0 \\ 0 & 0 & 0 & 0 & 1 & x & y & xy & 0 \\ 0 & 0 & 0 & 0 & 0 & 0 & 0 & 0 & 1 \end{bmatrix} \tag{2-110}$$

Substituting Eq. (2-110) into Eq. (2-26) yields the flexibility matrix as:

$$[G_e]_P = \frac{48ab}{t^3} \begin{bmatrix} 1 & 0 & 0 & 0 & -v & 0 & 0 & 0 & 0 \\ 0 & \frac{a^2}{3} & 0 & 0 & 0 & -v\frac{a^2}{3} & 0 & 0 & 0 \\ 0 & 0 & \frac{b^2}{3} & 0 & 0 & 0 & -v\frac{b^2}{3} & 0 & 0 \\ 0 & 0 & 0 & \frac{a^2b^2}{9} & 0 & 0 & 0 & -v\frac{a^2b^2}{9} & 0 \\ v & 0 & 0 & 0 & 1 & 0 & 0 & 0 & 0 \\ 0 & -v\frac{a^2}{3} & 0 & 0 & 0 & \frac{a^2}{3} & 0 & 0 & 0 \\ 0 & 0 & -v\frac{b^2}{3} & 0 & 0 & 0 & \frac{b^2}{3} & 0 & 0 \\ 0 & 0 & 0 & -v\frac{a^2b^2}{9} & 0 & 0 & 0 & \frac{a^2b^2}{9} & 0 \\ 0 & 0 & 0 & 0 & 0 & 0 & 0 & 0 & 2(1+v) \end{bmatrix} \tag{2-111}$$

The equilibrium matrix obtained from Eq. (2-20) is:

$$[B_e]_P=\begin{bmatrix}
0 & b & 0 & -\frac{2b^2}{5} & 0 & 0 & a & -\frac{2a^2}{5} & -2 \\
0 & \frac{b^2}{3} & 0 & -\frac{b^3}{15} & -a & \frac{2a^2}{5} & ab & -\frac{2a^2b}{5} & 0 \\
-b & ab & \frac{2b^2}{5} & -\frac{2ab^2}{5} & 0 & 0 & \frac{a^2}{3} & -\frac{a^3}{15} & 0 \\
0 & b & 0 & \frac{2b^2}{5} & 0 & 0 & -a & \frac{2a^2}{5} & 2 \\
0 & -\frac{b^2}{3} & 0 & -\frac{b^3}{15} & a & -\frac{2a^2}{5} & ab & -\frac{2a^2b}{5} & 0 \\
-b & ab & -\frac{2b^2}{5} & \frac{2ab^2}{5} & 0 & 0 & -\frac{a^2}{3} & \frac{a^3}{15} & 0 \\
0 & -b & 0 & -\frac{2b^2}{5} & 0 & 0 & -a & -\frac{2a^2}{5} & -2 \\
0 & \frac{b^2}{3} & 0 & \frac{b^3}{15} & a & \frac{2a^2}{5} & ab & \frac{2a^2b}{5} & 0 \\
b & ab & \frac{2b^2}{5} & \frac{2ab^2}{5} & 0 & 0 & \frac{a^2}{3} & \frac{a^3}{15} & 0 \\
0 & -b & 0 & \frac{2b^2}{5} & 0 & 0 & a & \frac{2a^2}{5} & 2 \\
0 & -\frac{b^2}{3} & 0 & \frac{b^3}{15} & -a & -\frac{2a^2}{5} & ab & \frac{2a^2b}{5} & 0 \\
b & ab & -\frac{2b^2}{5} & -\frac{2ab^2}{5} & 0 & 0 & -\frac{a^2}{3} & -\frac{a^3}{15} & 0
\end{bmatrix} \tag{2-112}$$

## 2.9 Illustrative Examples

In this section, two numerical examples are presented to validate the FE formulation based on the IFM. The results are compared with those obtained from the DM and analytical solutions. First example is the analysis of beam subjected to end loading using 4-node quadrilateral membrane elements, and the second is analysis of plate subjected to point load at the center using 4-node quadrilateral bending elements.

### 2.9.1 Beam Analysis

A beam of length 12m and uniform rectangular cross section, subjected to concentrated force P at the free end as shown in Figure 2-6 is analyzed.

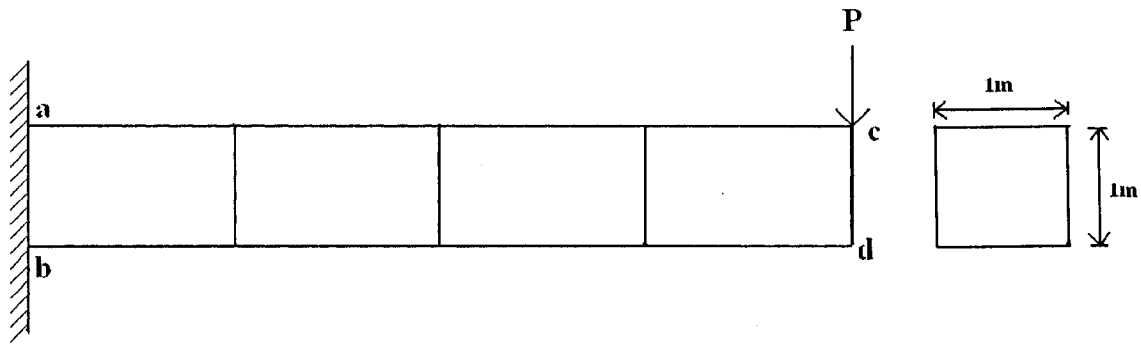


**Figure 2-6** Beam meshed with quadrilateral membrane element

The analysis is performed using two dimensional finite element discretizations, assuming the state of plane stress case, and using the 4-node quadrilateral membrane element. The response of the beam is also obtained using the DM 4-node quadrilateral membrane element having displacement interpolation similar to the IFM element. The support conditions for the clamped end are modeled such that point b is completely fixed and horizontal displacement at point a, is fixed. The concentrated force at the end is generally modeled as parabolic shear force along the edge. Here, since we have two nodes at the edge, P is distributed equally on nodes c and d with 0.5P on each node. The value of the P taken for the analysis is 12 KN.

The compatibility conditions are generated by using both direct and indirect approach. It has been observed using indirect approach that only interface compatibility condition exists for this problem. A MATLAB computer program has been written to generate the

interface compatibility at each interface, and then finally to assemble into the global compatibility condition. The responses from the analysis program are the maximum stress at the constrained end and the tip displacement at the free end of the beam. The exact value of the stress at the constraint end in the outer most fiber ($\text{at}\, y = \frac{h}{2}$) is 864 KPa and the tip displacement is 0.395mm. The results for stress and tip displacement, for both the IFM and the DM are provided in Table 2-1.

**Table 2-1** Stress at the constrained end and tip displacement

| | Stress at Constrained End (KPa) | | Tip Displacement (mm) | |
|---|---|---|---|---|
| El. No. | DM | IFM | DM | IFM |
| 5 | 260 | 778 | 0.1198 | 0.3926 |
| 10 | 549 | 821 | 0.2402 | 0.3956 |
| 15 | 686 | 835 | 0.2952 | 0.3962 |
| 20 | 752 | 842 | 0.3208 | 0.3964 |
| 25 | 788 | 847 | 0.3343 | 0.3965 |
| 30 | 809 | 850 | 0.3421 | 0.3966 |
| 35 | 822 | 852 | 0.3470 | 0.3966 |

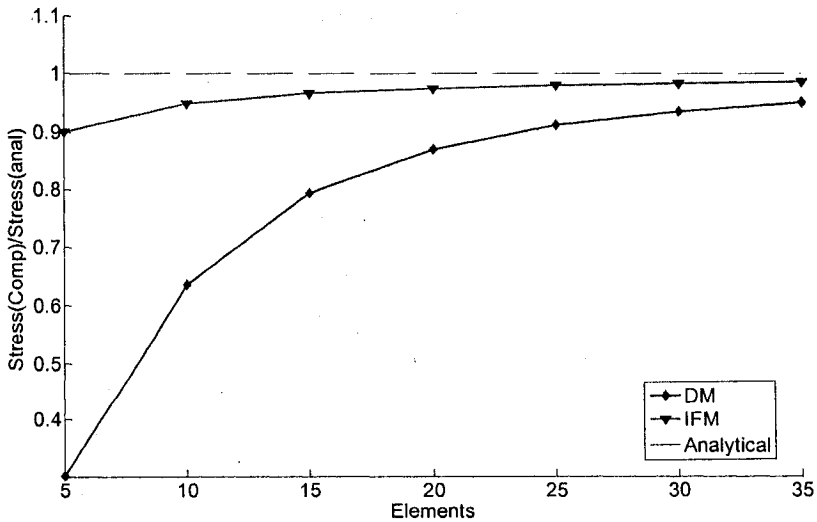


**Figure 2-7** Convergence of stress with number of elements

It can be realized that the IFM not only show high accuracy in calculation of stresses, but also give very accurate results for the tip displacement. The IFM achieves 90% of accuracy in stress calculation only with five elements; on the other hand the DM achieves this accuracy with more than 20 elements. Figure 2-7 shows the convergence study for the normalized stress at the constrained end versus the number of elements. As it can be seen that the IFM converge very rapidly; on the other hand the DM shows slow convergence.

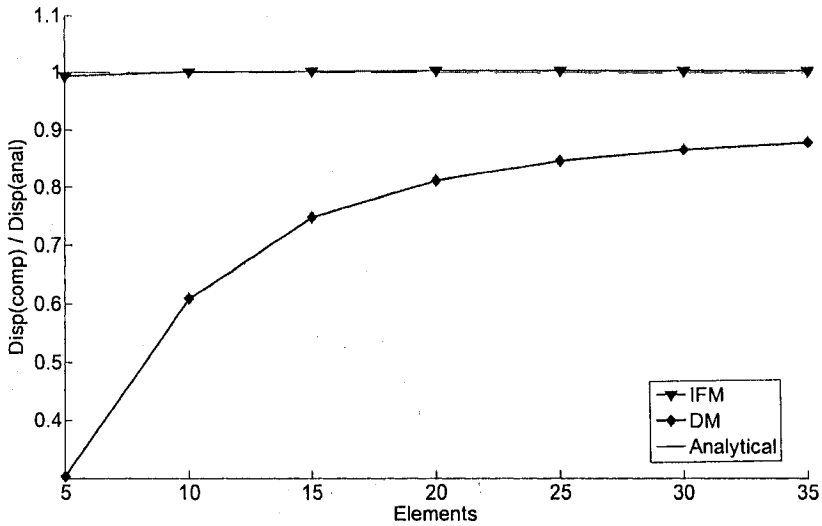


**Figure 2-8** Convergence of tip displacement with number of elements

Surprisingly, the tip displacement results obtained from the IFM are far more accurate than those obtained from the DM. The results for the convergence study of the normalized tip displacement are presented graphically in Figure 2-8. The IFM method achieves sufficient accuracy with error less than only 1% using 5 elements, where as the DM gives an error of 70 % using the same number of elements. It has been noted that the SVD and indirect approach to generate the compatibility generate similar results, and computational time for both the cases is almost the same.

## 2.9.2 Plate Analysis

The plate dimensions, loading and material properties are shown in the Figure 2-8. The problem is analyzed using, 4-node quadrilateral Kirchhoff's IFM bending element and 4-node quadrilateral Kirchhoff's DM bending element having displacement interpolation similar to the IFM element. The FE equations of 4-node IFM element are formulated previously and those of 4-node DM element are well documented in the literature [16]. The global equilibrium and flexibility matrices are assembled from element matrices, and the compatibility matrix is generated by SVD approach.

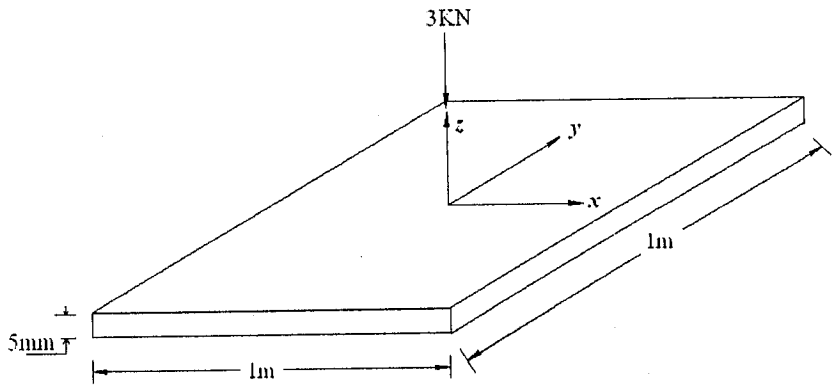


Modulus of Elasticity=210e9 , Poisson ratio=0.3

**Figure 2-9** Clamped plate subjected to loading at the center

The transverse deflection at the center of the plate and the moment per unit length about y axis $M_y$ at $\left(x=0, y=-\frac{b}{2}\right)$ are responses from the analysis. The central deflection and moment at the specified point, given by Timoshenko [40], are 0.699 cm and 377.1N/m, respectively. The results obtained from the IFM and the DM are presented in the Table 2.2.

**Table 2-2** Center deflection and moment $M_y$ for different element numbers

| El. No. | Deflection at the center of plate(cm) | | $M_y$ at $x$=0, $y$= -b/2 (N/m) | |
|---|---|---|---|---|
| | DM | IFM | DM | IFM |
| 16 | 0.6548 | 0.6975 | 324.7864 | 372.3855 |
| 36 | 0.6671 | 0.6975 | 341.9589 | 373.1158 |
| 64 | 0.6735 | 0.697 | 352.686 | 373.2155 |
| 100 | 0.6768 | 0.696 | 359.0042 | 373.441 |
| 144 | 0.6788 | 0.696 | 362.9558 | 373.9 |

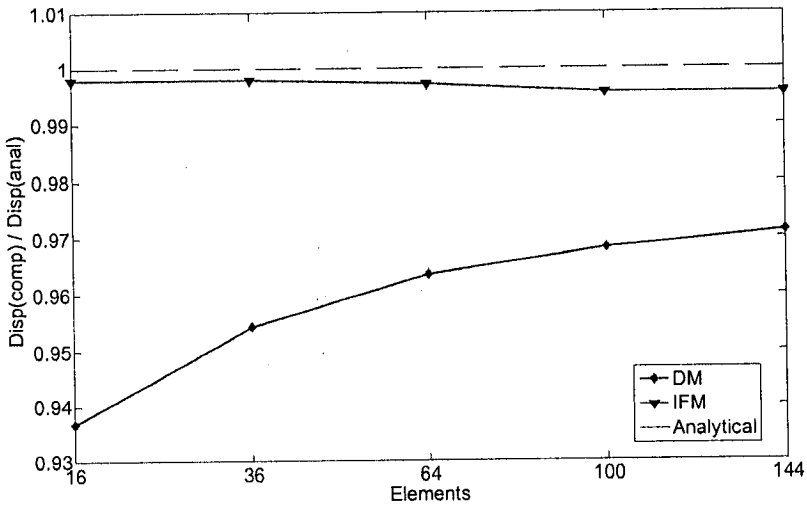


**Figure 2-10** Convergence of central deflection with number of elements

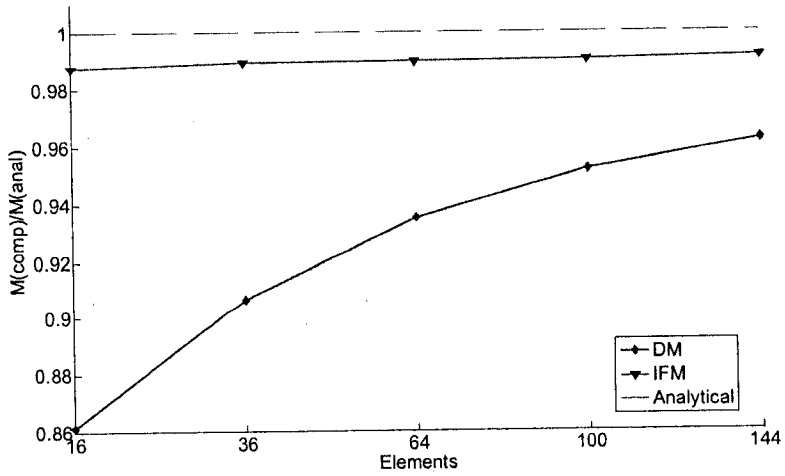


**Figure 2-11** Convergence of the moment with number of elements.

The rate of convergence of the normalized central deflection versus number of elements for both the analysis methods is shown graphically in Figure 2-10. It can be seen that the IFM element provides accurate results using just16 elements, where as the DM struggle to do so. The DM requires very fine mesh to converge to accurate results, and it shows error of 2.9% even for FE model consisting of 144 elements.

The calculation of moments in the IFM is far more accurate than the DM. The graphical presentation of normalized moment per unit length with increasing numbers of element is shown in Figure 2-11. The IFM shows 1.25% error with respect to analytical solution with only 16 elements model, where as DM shows 13.87% error with same numbers of elements. Using 144 elements, the error reduces to 3.75% using the DM which is still higher than the 1.25% of the IFM with 16 elements. The IFM is also more efficient for stress calculation because it calculate stress directly from the independent forces which are unknown in the formulation, where as in the DM stresses are calculated from the back substituting of the nodal displacement.

It can be realized from these investigations that the IFM yields accurate results for both stresses and displacements even for very coarse meshes. The equations of the IFM are amenable to computer automation and can be easily automated. Therefore accuracy and efficiency of the IFM structural analysis has motivated to use it for structural optimization.

# Chapter 3

# STRUCTURAL OPTIMIZATION AND SENSITIVITY ANALYSIS

## 3.1 Introduction

Structural optimization deals with engineering design problem with aim of finding an optimal structure that satisfies a number of given constraints. Structural optimization problems are characterized by various objective and constraint functions, which are generally non-linear function of design variables. These functions are usually implicit, discontinuous and non-convex. The mathematical formulation of the structural optimization problem with respect to the design variables, the objective and constraint functions depend on the type of application. However, all structural optimization problems can be expressed in standard mathematical form as a non-linear programming problem which in general can be stated as follows [50]:

Minimize $f(X)$ (3-1)

Subject to, $n_e$ equality constraints:

$$h_i(X) = 0 \qquad i = 1.....n_e \tag{3-2}$$

$n_{ie}$ inequality constraints:

$$g_j(X) \leq 0 \qquad j = 1.....n_{ie} \tag{3-3}$$

and $n_d$ side constraints:

$$\{X_l\}_k \leq \{X\}_k \leq \{X_u\}_k \qquad k = 1.....n_d \tag{3-4}$$

where, $\{X\}$ is the vector of design variables, $f(X)$ is the objective function to be minimized, $h_i(X)$ are the equality behavior constraints, $g_j(X)$ are inequality behavior constraints, $\{X_l\}_k$ and $\{X_u\}_k$ are the upper and lower bounds on design variables $\{X\}_k$.

The FE method is most widely used analyzer for the structural optimization to find the performance measures of the structure. The accuracy and efficiency of the FE formulation affect the success of the optimization algorithm. Nowadays, the DM is dominant as analyzer and most of the optimization algorithms are based on the DM. Very few investigations have been done on structural optimization using force method and its comparison with the DM. This chapter is focused on developing size optimization algorithms for the discrete structures using the IFM. In a general purpose computer aided environment for design optimization, sensitivity analysis is an important enabling tool. The numerical and analytical techniques are generally used to find the design sensitivity. The analytical techniques are more preferred because of high computational efficiency and accuracy. It should be noted that most of the reference work on the analytical sensitivity analysis is based on the DM and few work have been reported related to sensitivity analysis based on the force method [33-34]. In this study, the sensitivity analysis of behavior constraints such as stress, displacement, frequency with respect to design variables is formulated using the IFM.

## 3.2 Size Optimization

A structural design problem can be represented as a mathematical model whose constituent elements are design parameters, constraints and objective function. The design parameters

specify the geometry and shape of the structures and physical properties of its members. From the design parameters, a set of derived parameters are obtained which are defined as behavior constraints e.g., stress, displacement, natural frequency and buckling loads etc. The lower and upper limits on the design parameters are known as side constraints.

In size structural optimization problem, the design variables are typically the cross sectional area of structural components and objective function is to minimize the weight of the structure. The objective function of the problem can be stated as:

$$f(A) = M = \rho \{A\}^T \{L\} \tag{3-5}$$

where $\{A\}$ is vector of design variables, and its elements are the cross sectional area of the structural components.

Practical structural optimization problems are usually subjected to different types of constraint such as stress, displacement, frequency and system stability, and these constraints can be cast into the following forms:

*Stress Constraint*

$$g_i = \left|\frac{\sigma_i}{\overline{\sigma}_i}\right| - 1 \le 0 \qquad i = 1,.....,n_{sc} \tag{3-6}$$

where $n_{sc}$ are the number of stress constraints, and $\sigma_i$ and $\overline{\sigma}_i$ are von Mises stress and its relative allowable for the *i*th element, respectively.

*Displacement Constraint*

$$g_j = \left|\frac{U_j}{\overline{U}_j}\right| - 1 \le 0 \qquad j = 1,.....,n_{dc} \tag{3-7}$$

where $n_{dc}$ are the number of displacement constraints, and $U_j$ and $\overline{U}_j$ are the $j$th displacement and its relative allowable, respectively.

*Frequency Constraints*

$$g_k = -\frac{|\omega_k|}{|\overline{\omega}_k|} + 1 \le 0 \qquad k = 1,\ldots\ldots,n_{fc} \tag{3-8}$$

where $n_{fc}$ are the number of frequency constraints, and $\omega_k$ and $\overline{\omega}_k$ are the $k$th frequency and its relative allowable, respectively.

*Stability Constraint*

$$g_c = -\frac{N_c}{\overline{N}_c} + 1 \le 0 \tag{3-9}$$

where $N_c$ and $\overline{N}_c$ are critical buckling load and its relative allowable, respectively.

## 3.3 Optimality Conditions

In unconstrained optimization, a local minimum has to satisfy the necessary condition $\nabla f(X) = 0$, and non-negative curvature in any direction at the optimum. This implies that there is no descent direction at the optimum for the unconstrained problem. The condition for the constrained case can be written similar to the unconstrained case if problem can be transformed into a single function. This leads to the use of Lagrange multipliers $\lambda$ to combine the objective and constraint function into Lagrangian function. The Lagrangian function for the constraint optimization problem can be written as [50, 51]:

$$L(X,\lambda) = f(X) - \sum_{i=1}^{n_e} \lambda_i h_i(X) + \sum_{j=1}^{n_{ie}} \lambda_j g_j(X) \tag{3-10}$$

Consider a design point that is optimum for the constrained problems and the functions are continuously differentiable. The set of optimality conditions are:

$$\nabla L(X^*,\lambda^*) = 0 \tag{3-11}$$

$$h_i(X^*) = 0, \qquad i = 1,\ldots..,n_e \tag{3-12}$$

$$g_j(X^*) \le 0, \qquad j = 1,\ldots..,n_{ie} \tag{3-13}$$

$$\lambda_j^* \ge 0, \qquad j = 1,\ldots..,n_{ie} \tag{3-14}$$

$$\lambda_i^* h_i(X^*) = 0, \qquad i = 1,\ldots..,n_e \tag{3-15}$$

$$\lambda_i^* g_i(X^*) = 0, \qquad j = 1,\ldots..,n_{ie} \tag{3-16}$$

Eqs. (3-11) to (3-16) are collectively known as the Karush-Kuhn-Tucker (KKT) conditions. KKT conditions are necessary and sufficient for optimality based on the first-order conditions. The set of optimum design variables and Lagrange multipliers $(X^*,\lambda^*)$ that satisfies the KKT conditions are referred to as the KKT points. The condition of Eq. (3-16) is referred to as the complimentarily condition and implies that $\lambda^*$ and $g_j$ cannot be both non-zero. For cases that the condition is not hold, the constraint is considered inactive with a feasible descent direction defined with respect to the constraint.

## 3.4 Sequential Quadratic Programming

Sequential Quadratic Programming (SQP) method is mathematical programming technique for solving Non-Linear Programming (NLP) optimization problems. They are also considered to be the most robust and powerful mathematical programming optimization algorithm available today. In this method a Quadratic Programming (QP)

sub problem is constructed from the initial NLP problem. A local minimizer is then found by solving a sequence of these QP sub problems using a quadratic approximation of the objective function. Each sub problem has the following form:

Minimize:

$$\nabla f^T \{s^{(p)}\} + \frac{1}{2} \{s^{(p)}\}^T [H^{(p)}] \{s^{(p)}\} \tag{3-17}$$

Subject to:

$$\nabla h^T \{s^{(p)}\} + h(X^{(p)}) = 0 \tag{3-18}$$

$$\nabla g^T \{s^{(p)}\} + g(X^{(p)}) \leq 0, \tag{3-19}$$

where $p$ in the parentheses is the current iteration number, $[H^{(p)}]$ is the Hessian of the Lagrangian function at the current design point $\{X^{(p)}\}$, with the current estimate of the Lagrange multipliers $\lambda^{(k)}$, and $\{s\}$ is the vector of design variables in this sub-problem representing the search direction to be defined in the original optimization problem. The solution of the QP sub-problem produces an estimate of the Lagrange multiplier $\lambda$, and a search direction vector $\{s\}$ at iteration $p$, which are used to form a new iteration as:

$$\{X^{(p+1)}\} = \{X^{(p)}\} + \alpha_p \{s^{(p)}\} \tag{3-20}$$

The step length parameter $\alpha_p$ is determined through a one-dimensional minimization in order to produce a sufficient decrease in the merit function. At the end of the one dimensional minimization, Hessian of Lagrangian, required for the solution of the next QP problem is updated using Broyden-Fletcher-Goldfarb-Shanno (BFGS) [52-53] update formula:

$$[H^{(p+1)}] = [H^{(p)}] + \frac{\{y^{(p)}\}\{y^{(p)}\}^T}{\{y^{(p)}\}^T \{\delta^{(p)}\}} - \frac{[H^{(p)}]^T \{\delta^{(p)}\} \{\delta^{(p)}\}^T [H^{(p)}]}{\{s^{(p)}\}^T [H^{(p)}] \{s^{(p)}\}} \tag{3-21}$$

where

$$\{\delta^p\} = \{X^{p+1}\} - \{X^{(p)}\} \tag{3-22}$$

$$\{y^{(p)}\} = \nabla L(\mathrm{X}^{p+1}, \lambda^{p+1}) - \nabla L(\mathrm{X}^{p}, \lambda^{p}) \tag{3-23}$$

BFGS formula may lead to indefinite Hessian. In order to keep Hessian positive definite, Powel [52] recommends replacing $\{y^{(p)}\}$ by:

$$\chi\{y^{(p)}\} + (1-\chi)[H^p]\{\delta^p\} \tag{3-24}$$

where $\{y^{(p)}\}$ is given by Eq.(3-22) and $\chi$ is determined by:

$$\chi = \begin{cases} 1 & \text{if } \{\delta^{(p)}\}^T\{y^{(p)}\} \geq 0.2\{\delta^{(p)}\}^T[H]\{\delta^{(p)}\} \\ \dfrac{0.8\{\delta^{(p)}\}^T[H]\{\delta^{(p)}\}}{0.8\{\delta^{(p)}\}^T[H]\{\delta^{(p)}\} - \{\delta^{(v)}\}^T\{y^{(p)}\}} & \text{if } \{\delta^{(p)}\}^T\{y^{(p)}\} < 0.2\{\delta^{(p)}\}^T[H]\{\delta^{(p)}\} \end{cases} \tag{3-25}$$

From Eqs. (3-21) and (3-23), it can be observed that gradient of Lagrangian is required at the start of each iteration in SQP problem. Lagrangian gradient consists of the gradient of both the objective function and the constraint. Therefore the correct evaluation of the gradient of the objective and constraint function is necessary for the success of the optimization algorithm.

## 3.5 Sensitivity Analysis

The structural optimization problems are mostly solved using the gradient based SQP algorithm, which requires accurate sensitivity analysis to find the search direction and step size. Sensitivity analysis is also used to ascertain how the structural performance measures depend on the design variables. The performance measures of the structure can be stress, displacement, natural frequency and system stability. Design sensitivity of

functions explicitly defined in terms of design variables can be easily evaluated by direct differentiation. However in structural analysis, performance measures are mostly implicit function of the design variables, therefore the direct differentiation is not possible.

The sensitivity analysis of the performance measures in the structural optimization problems can be performed by numerical and analytical techniques. The finite difference approach has been largely used for the numerical sensitivity analysis. This approach to sensitivity analysis is not computationally efficient, but can be used as reliable reference method. Therefore the analytical methods are commonly used for the efficient and accurate evaluation of the design sensitivity. The finite difference and analytical approaches to evaluate the design sensitivity are discussed in the next section.

### 3.5.1 Finite Difference Technique

Finite differencing is the simplest way of estimating sensitivities transformed from the definition of the function derivative. For any continuous function, Taylor expansion can be written as:

$$f(X+\Delta X) = f(X) + f'(X)\Delta X + f''(X)\frac{\Delta X^2}{2!} + f'''(X)\frac{\Delta X^3}{3!} + \ldots\ldots\ldots \tag{3-26}$$

where $\Delta X$ is the step size, and it is generally defined relative to the magnitude of the design variable in order to ensure the robustness of the calculation regardless of the dimensions and range of the design variable. By truncating the series at second derivative term, we can rearrange formula and obtain the forward-step finite difference as:

$$f'(X) = \frac{f(X+\Delta X) - f(X)}{\Delta X} \tag{3-27}$$

Whenever a finite difference scheme is used to approximate derivatives, there are two sources of error: truncation and condition errors. The truncation error is the results of the neglected terms in the Taylor series expansion in the perturbed function in Eq. (3-26). This source of error can be reduced by using a small perturbation. The reduction in step size results in improved accuracy of the formulation, however reduction of step size leads to condition error, which can drastically reduce the number of significant digits in the sensitivity value. As the step size is reduced, the function value of the perturbed point and the reference value become increasingly similar and when subtracted, the matching digits will cancel each other, thus reducing the accuracy of the resulting sensitivity. These opposite demands to the magnitude of the perturbation may give rise to the so-called "step size dilemma" referred by Haftka and Adelman[57]. As noted by Haftka and Adelman, the "step-size dilemma" may be reduced if a higher order finite difference approximation is used, e.g. a second order central difference approximation, but this implies additional computational cost. The finite difference method is also not very efficient because of large numbers of structure analysis required to find a single gradient. The number of structural analysis increases with increase in number of design variables leading to large computational expense. For example, if problem has $n_d$ design variables, the total number of structural analysis required to find the sensitivity of one performance measure are $(n_d + 1)$.

### 3.5.2 Analytical Sensitivity Analysis of Behavior Constraints

As the finite difference method is computationally inefficient for the design sensitivity analysis, the analytical approaches are generally used. The analytical sensitivity analysis

can be divided into discrete and continuum methods. In the discrete method, the sensitivity analysis is obtained by taking the design derivatives of the discrete governing equations obtained by the FE method. For this purpose, it is necessary to take the derivatives of the FE matrices with respect to design variables. If these derivatives are obtained analytically using the explicit expression of the derivatives of the matrices with respect to design variables, it is known as analytical methods. However, if derivatives are obtained using a finite difference method, then method is called semi analytical method. In the continuum approach, the design derivatives of the variational equations are taken before it discretized.

The issue of which approach of sensitivity analysis is better is a much debated subject and several authors, e.g., Keulen, Haftka and Kim [58], Choi and Twu [59], have presented comparisons between the continuum and the discrete approaches. The conclusive argument for selection of method for the design sensitivity analysis has been that continuum approach takes a lot of analytical work in order to develop the expression for design sensitivity. The discrete approach seems much easier to implement and to be just as applicable to solve problem as continuum approach.

In this study, the discrete approach to design sensitivity analysis has been chosen due to its ease of implementation. The expression for the discrete sensitivity analysis of the stress, displacement, natural frequency and system stability constraints are formulated using the IFM for the discrete structures. The efficiency of the discrete sensitivity analysis will be discussed in Chapter 4.

## 3.6 Sensitivity Analysis of Truss Structures

The IFM FE formulation for truss structure is presented in the section 2.8.1. The truss element has two displacement degrees of freedom and one force degree of freedom. Generally for the truss structure, the numbers of force degrees of freedom $n$ are the same as the numbers of member in the structure $n_d$. The design variables are the cross sectional area of the members. These types of structure may be subjected to stress, displacement, frequency and buckling constraints. The discrete sensitivity analysis for each of these constraints is formulated in this section.

In the force based finite element method, the sensitivity analysis of various performance criteria is based on the design sensitivity of the force field. Thus, when the force design sensitivities are known, other sensitivities, e.g. stress, displacement and frequency etc., can be easily computed. Therefore, the sensitivity analysis of force field is evaluated first.

The discrete approach to obtain design sensitivity of the force field is based on implicitly differentiation of the system equilibrium equation of the IFM. The system equilibrium equations of the IFM from Eq. (2-4) can be stated as:

$$[S]\{F\} = \{P\}$$

Suppose that truss structure has $n_d$ number of members, and the design variables are the vector $\{A\}$ consisting of the cross sectional area of the members. It should be noted that Eq. (2-4) is implicit function of the member cross sectional area. Thus taking the derivative of the Eq. (2-4) with respect to the cross sectional area of the $j$th member $A_j$ yields:

$$[S]\frac{\partial\{F\}}{\partial A_j}+\frac{\partial[S]}{\partial A_j}\{F\}=\frac{\partial\{P\}}{\partial A_j} \tag{3-28}$$

The applied external load $\{P\}$ is usually independent of the design variables, therefore $\frac{\partial\{P\}}{\partial \mathrm{A}_j}=0$. Substituting in Eq. (3-28) yields:

$$\frac{\partial\{F\}}{\partial A_j}=-[S]^{-1}\frac{\partial[S]}{\partial A_j}\{F\} \tag{3-29}$$

As given in Eq. (2-5), the matrix $[S]$ can be written in term of equilibrium and compatibility equations as:

$$[S]=\begin{bmatrix}[B]\\ \hline [C][G]\end{bmatrix}$$

The compatibility equation in Eq. (2-5) can be expanded as:

$$[C][G]=\begin{bmatrix}C_1 & C_2 & \cdots & C_{n_d}\end{bmatrix}\begin{bmatrix}G_{e1} & 0 & \cdots & 0\\ 0 & G_{e2} & \cdots & 0\\ \vdots & \vdots & \ddots & \vdots\\ 0 & 0 & 0 & G_{en_d}\end{bmatrix}=\begin{bmatrix}C_1G_{e1} & C_2G_{e2} & \cdots & C_nG_{en_d}\end{bmatrix} \tag{3-30}$$

where $C_i$ is the $i$th column of $[C]$ and $[G_{ei}]$ is the flexibility matrix of $i$th member of the structure. $[G_{ei}]$ can be obtained from Eq.(2-81) as:

$$G_{ei}=\frac{\mathrm{L_i}}{A_i E} \tag{3-31}$$

It is important to note that in $[S]$matrix, only flexibility matrix depends on the design variables, and the equilibrium and the compatibility matrices are independent of design variables. Furthermore, in the system flexibility matrix, the flexibility matrix of only $j$th element depends on the $A_j$, therefore the derivative of flexibility matrices of

other elements with respect to $A_j$ is zero. Substituting Eq. (3-30) in Eq. (3-29) and taking derivative of the final equation with respect to $A_j$ yields:

$$\frac{\partial[S]}{\partial A_j} = -\begin{bmatrix} [0] \\ \hline [0 \quad 0 \quad \dots \quad C_j \overline{G}_{ej} \quad \dots \quad 0] \end{bmatrix} \tag{3-32}$$

where

$$\overline{G}_{ej} = \frac{G_{ej}}{A_j} \tag{3-33}$$

Eq. (3-32) can also be written as:

$$\frac{\partial[S]}{\partial A_j} = -[0 \quad 0 \quad \dots \quad \overline{S}_j \quad \dots \quad 0] \quad \text{where} \quad [\overline{S}_j] = \begin{bmatrix} 0 \\ \hline C_j \overline{G}_{ej} \end{bmatrix} \tag{3-34}$$

Substituting Eq. (3-34) into Eq. (3-29) yields:

$$\frac{\partial\{F\}}{\partial A_j} = [S]^{-1} [\overline{S}_j]\{F_j\} \tag{3-35}$$

Expanding the terms of Eq. (3-35), for $j = 1.....n_d$, the final equation for the sensitivity analysis of the force field can be written as:

$$\begin{bmatrix} \frac{\partial F}{\partial A_1} \\ \frac{\partial F}{\partial A_2} \\ \vdots \\ \frac{\partial F}{\partial A_{n_d}} \end{bmatrix}^T = [S]^{-1}[\overline{S}][\overline{F}_T] = [Y_T] \tag{3-36}$$

where

$$[\overline{F}_T] = \begin{bmatrix} F_1 & 0 & \dots & 0 \\ 0 & F_2 & \dots & 0 \\ \vdots & \vdots & \ddots & \vdots \\ 0 & 0 & 0 & F_{n_d} \end{bmatrix} \quad \text{and} \quad [\overline{S}] = [\overline{S}_1 \quad \overline{S}_2 \quad \cdots \quad \overline{S}_{n_d}] \tag{3-37}$$

### 3.6.1 Sensitivity Analysis of Stress Constraint

Truss structures are subjected to only axial stresses. The normalized stress constraint can be written from Eq. (3-6) as:

$$g_i(F,A) = \frac{\sigma_i}{\overline{\sigma}_i} - 1 \qquad i = 1.....n_d \tag{3-38}$$

It is supposed that each member is subjected to stress constraint; therefore the numbers of stress constraints are same as number of design variables $n_d$. For the truss structure, the stress in terms of axial member force $F_i$ can be written as:

$$\sigma_i = \frac{F_i}{A_i} \tag{3-39}$$

Substituting Eq. (3-39) into Eq. (3-38) yields the stress constraint as:

$$g_i(F,A) = \frac{F_i}{A_i\overline{\sigma}_i} - 1 \qquad i = 1.....n_d \tag{3-40}$$

The gradients are the rate of change of the performance measures with respect to design variables, and can be stated as:

$$\nabla g_i = \left[ \frac{dg_i}{dA_1} \quad \frac{dg_i}{dA_2} \quad \cdots \quad \frac{dg_i}{dA_{n_d}} \right]^T \qquad i = 1.....n_d \tag{3-41}$$

As discussed previously, $g_i$ is not explicit function of design variables, it depends indirectly on the design variables, so we can not find its derivative directly. The total derivative of $g_i$ with respect to $A_j$ can be evaluated by using the chain rule of differentiation as:

$$\frac{dg_i}{dA_j} = \frac{\partial g_i}{\partial A_j} + \frac{\partial g_i}{\partial \{F\}}^T \frac{\partial \{F\}}{\partial A_j} \tag{3-42}$$

The $\frac{\partial\{F\}}{\partial A}$ can be obtained from the Eq. (3-36), therefore to calculate the design sensitivity of stress constraint only the partial derivatives $\frac{\partial g_i}{\partial A_j}$ and $\frac{\partial g_i}{\partial\{F\}}$ are required to be evaluated. The $\frac{\partial g_i}{\partial A_j}$ can be obtained by taking the partial derivative of Eq. (3-40) with respect to $A_j$:

$$\frac{\partial g_i}{\partial A_j} = \begin{Bmatrix} -\frac{F_i}{\bar{\sigma}_i A_i^2} & if\ i = j \\ 0 & if\ i \neq j \end{Bmatrix} \tag{3-43}$$

Extending the terms of Eq. (3-43), for $i = 1.....n_d$ and $j = 1.....n_d$ yields:

$$\begin{bmatrix} \frac{\partial g_1}{\partial A_1} & \frac{\partial g_1}{\partial A_2} & \cdots & \frac{\partial g_1}{\partial A_{n_d}} \\ \frac{\partial g_2}{\partial A_1} & \frac{\partial g_2}{\partial A_2} & \cdots & \frac{\partial g_2}{\partial A_{n_d}} \\ \vdots & \vdots & \ddots & \vdots \\ \frac{\partial g_{n_d}}{\partial A_1} & \frac{\partial g_{n_d}}{\partial A_2} & \cdots & \frac{\partial g_{n_d}}{\partial A_{n_d}} \end{bmatrix} = \begin{bmatrix} -\frac{F_1}{\bar{\sigma}_1 A_1^2} & 0 & \cdots & 0 \\ 0 & -\frac{F_2}{\bar{\sigma}_2 A_2^2} & \cdots & 0 \\ \vdots & \vdots & \ddots & \vdots \\ 0 & 0 & 0 & -\frac{F_{n_d}}{\bar{\sigma}_i A_{n_d}^2} \end{bmatrix} = [Q_T] \tag{3-44}$$

The $\frac{\partial g_i}{\partial\{F\}}$ can be obtained by taking the partial derivative of Eq. (3-40) with respect to force field $\{F\}$:

$$\frac{\partial g_i}{\partial\{F\}} = \begin{bmatrix} \frac{\partial g_i}{\partial F_1} \\ \frac{\partial g_i}{\partial F_2} \\ \vdots \\ \frac{\partial g_i}{\partial F_i} \\ \vdots \\ \frac{\partial g_i}{\partial F_{n_d}} \end{bmatrix} = \begin{Bmatrix} 0 \\ 0 \\ \vdots \\ Z_i \\ \vdots \\ 0 \end{Bmatrix} \tag{3-45}$$

where

$$Z_i = \frac{1}{\overline{\sigma}_i A_i} \tag{3-46}$$

Expanding the terms of Eq. (3-45), for $i = 1.....n_d$ and $j = 1.....n_d$ yields:

$$\begin{bmatrix} \frac{\partial g_1}{\partial F_1} & \frac{\partial g_2}{\partial F_1} & \cdots & \frac{\partial g_{n_d}}{\partial F_1} \\ \frac{\partial g_1}{\partial F_2} & \frac{\partial g_2}{\partial F_2} & \cdots & \frac{\partial g_{n_d}}{\partial F_2} \\ \vdots & \vdots & \ddots & \vdots \\ \frac{\partial g_1}{\partial F_{n_d}} & \frac{\partial g_2}{\partial F_{n_d}} & \cdots & \frac{\partial g_{n_d}}{\partial F_{n_d}} \end{bmatrix} = \begin{bmatrix} Z_1 & 0 & \cdots & 0 \\ 0 & Z_2 & \cdots & 0 \\ \vdots & \vdots & \ddots & \vdots \\ 0 & 0 & 0 & Z_{n_d} \end{bmatrix} = [R_T] \tag{3-47}$$

Substituting Eqs. (3-36), (3-44), (3-47) into Eq. (3-42) and then substituting the final equation in Eq. (3-41) yields the stress gradient as:

$$\begin{bmatrix} \nabla g_1 \\ \nabla g_2 \\ \vdots \\ \nabla g_{n_d} \end{bmatrix} = \begin{bmatrix} \frac{dg_1}{dA_j} \\ \frac{dg_2}{dA_j} \\ \vdots \\ \frac{dg_{n_d}}{dA_j} \end{bmatrix}^T = [Q_T]^T + [Y_T]^T [R_T] \tag{3-48}$$

## 3.6.2 Sensitivity Analysis of Displacement Constraints

Generally, the nodal displacements are constrained in the structure, and a general expression for the displacement constraints of the truss structure can be stated from Eq. (3-7) as:

$$g_i = \frac{U_i}{\overline{U}_i} - 1 \qquad i = 1.....m \tag{3-49}$$

Similarly to the stress gradient, the displacement gradient can be stated as in Eq. (3-41). The displacement constraints are not explicit function of design variables, so their derivatives can be evaluated as given in Eq. (3-42). As mentioned before, $\frac{\partial\{F\}}{\partial A_j}$ can be obtained from the Eq. (3-36), according to Eq. (3-42) $\frac{\partial g_i}{\partial A_j}$ and $\frac{\partial g_i}{\partial\{F\}}$ are required to be evaluated to find the design sensitivity of the displacement constraints.

To calculate $\frac{\partial g_i}{\partial\{F\}}$, take the partial derivative of Eq. (3-49) with respect to $\{F\}$:

$$\frac{\partial g_i}{\partial\{F\}} = \frac{1}{\overline{U}_i}\frac{\partial U_i}{\partial\{F\}} \tag{3-50}$$

The term $\frac{\partial U_i}{\partial\{F\}}$ in Eq. (3-50) can be obtained by taking the partial derivative of Eq. (2-6) with respect to $\{F\}$:

$$\frac{\partial\{U_e\}}{\partial\{F\}} = [J][G] \tag{3-51}$$

Expanding the terms of Eq. (3-50) for $i = 1.....m$ and then substituting Eq. (3-51) into it yields:

$$\begin{bmatrix} \frac{\partial g_1}{\partial F} \\ \frac{\partial g_2}{\partial F} \\ \vdots \\ \frac{\partial g_{n_d}}{\partial F} \end{bmatrix} = [\overline{U}_T][J][G], \quad \text{where} [\overline{U}_T] = \begin{bmatrix} \frac{1}{\overline{U}_1} & 0 & 0 & 0 \\ 0 & \frac{1}{\overline{U}_2} & 0 & 0 \\ 0 & 0 & 0 & 0 \\ 0 & 0 & 0 & \frac{1}{\overline{U}_m} \end{bmatrix} \tag{3-52}$$

The term $\frac{\partial g_i}{\partial A_j}$ can be obtained by taking partial derivative of Eq. (3-49) with respect to $A_j$:

$$\frac{\partial g_i}{\partial A_j} = \frac{1}{\overline{U}_i} \frac{\partial U_i}{\partial A_j} \tag{3-53}$$

To calculate $\frac{\partial U_i}{\partial A_j}$, take the partial derivative of Eq. (2-6) with respect to $A_j$:

$$\frac{\partial U_i}{\partial A_j} = [J] \frac{\partial [G]}{\partial A_j} \{F\} \tag{3-54}$$

Eq. (3-54) can be expanded as:

$$\frac{\partial U_i}{\partial A_j} = [J] \begin{bmatrix} 0 & 0 & 0 & \dots & 0 & \dots & 0 \\ 0 & 0 & 0 & \dots & 0 & \dots & 0 \\ 0 & 0 & 0 & \dots & 0 & \dots & 0 \\ \vdots & \vdots & \vdots & \ddots & \vdots & \ddots & \vdots \\ 0 & 0 & 0 & \dots & -\frac{G_{ej}}{A_j} & \dots & 0 \\ \vdots & \vdots & \vdots & \ddots & \vdots & \ddots & \vdots \\ 0 & 0 & 0 & 0 & 0 & 0 & 0 \end{bmatrix}_{(n_d \times n_d)} \begin{Bmatrix} F_1 \\ F_2 \\ F_3 \\ \vdots \\ F_j \\ \vdots \\ F_{n_d} \end{Bmatrix} \tag{3-55}$$

Substituting Eq. (3-55) into Eq. (3-53) and extending the terms for $i = 1 \dots\dots\dots m$ and $j = 1 \dots\dots\dots n_d$ yields:

$$\begin{bmatrix} \frac{\partial g_1}{\partial A_1} & \frac{\partial g_1}{\partial A_2} & \dots & \frac{\partial g_1}{\partial A_{n_d}} \\ \frac{\partial g_2}{\partial A_1} & \frac{\partial g_2}{\partial A_2} & \dots & \frac{\partial g_2}{\partial A_{n_d}} \\ \vdots & \vdots & \ddots & \vdots \\ \frac{\partial g_m}{\partial A_1} & \frac{\partial g_m}{\partial A_2} & \dots & \frac{\partial g_m}{\partial A_{n_d}} \end{bmatrix} = [\overline{U}_T][J][W_T] \tag{3-56}$$

where

$$[W_T]=\begin{bmatrix} -F_1\frac{G_1}{A_2} & 0 & \cdots & 0 \\ 0 & -F_2\frac{G_2}{A_2} & \cdots & 0 \\ \vdots & \vdots & \ddots & \vdots \\ 0 & 0 & \cdots & -F_{n_d}\frac{G_{n_d}}{A_{n_d}} \end{bmatrix} \tag{3-57}$$

Substituting Eqs. (3-36), (3-51) and (3-56) into Eq. (3-42) and then substituting the final equation in Eq. (3-41) yields the gradients of the displacement constraints as:

$$\begin{bmatrix} \nabla g_1 \\ \nabla g_2 \\ \vdots \\ \nabla g_m \end{bmatrix} = \begin{bmatrix} \frac{dg_1}{dA_j} \\ \frac{dg_2}{dA_j} \\ \vdots \\ \frac{dg_m}{dA_j} \end{bmatrix}^T = [[\overline{U}_T][J][W_T]+[\overline{U}_T][J][G][Y_T]]^T \qquad j=1.....n_d \tag{3-58}$$

### 3.6.3 Sensitivity Analysis of Eigen Values

The eigen value problem appears in both the vibration and buckling analysis of the structure, therefore the sensitivity analysis of eigen value problem is necessary for the optimization of the structures subjected to frequency and buckling constraints. A general eigen value problem in the IFM can be stated as:

$$([S]-\mu[M_f])\{V_R\}=\{0\} \tag{3-59}$$

where $\mu$ is the eigen value, $\{V_R\}$ is the corresponding right eigen vector and

$$[M_f]=\begin{bmatrix} [M][J][G] \\ \hline [0] \end{bmatrix} \tag{3-60}$$

where $[M]$ is the mass matrix of the structure. Eq. (3-59) can also be written as:

$$\{V_L\}^T([S]-\mu[M_f])=\{0\} \tag{3-61}$$

where $\{V_L\}$ is the left eigen vector corresponding to eigen value $\mu$. Pre multiplying Eq. (3-59) by $\{V_L\}^T$ yields:

$$\{V_L\}^T([S]-\mu[M_f])\{V_R\}=\{0\} \tag{3-62}$$

Differentiating Eq (3-61) with respect to $A_j$ yields:

$$\begin{aligned}&\{V_L\}^T\left(\frac{d[S]}{dA_j}-\mu\frac{d[M_f]}{dA_j}-[M_f]\frac{d\mu}{dA_j}\right)\{V_R\}+\frac{d\{V_L\}^T}{dA_j}([S]-\mu[M_f])\{V_R\}\\&+\{V_L\}^T([S]-\mu[M_f])\frac{d\{V_R\}}{dA_j}=0\end{aligned} \tag{3-63}$$

Substituting Eqs. (3-59) and (3-61) into Eq. (3-63) yields:

$$\frac{d\mu}{dA_j}=\frac{\{V_L\}^T\left(\frac{d[S]}{dA_j}-\mu\frac{d[M_f]}{dA_j}\right)\{V_R\}}{\{V_L\}^T[M_f]\{V_R\}} \tag{3-64}$$

Eq. (3-64) is the general equation for the sensitivity analysis of the eigen value problem. Therefore in addition to the eigen value analysis results, the matrices $\frac{d[S]}{dA_j}$ and $\frac{d[M_f]}{dA_j}$ are required to be evaluated, to perform the design sensitivity analysis of eigen value. The $\frac{\partial[S]}{\partial A_j}$ can be obtained from the Eq. (3-34), and to evaluate $\frac{d[M_f]}{dA_j}$, we differentiate Eq. (3-60) with respect to $A_j$:

$$\frac{d[M_f]}{dA_j}=\begin{bmatrix}\frac{d[M]}{dA_j}[J][G]+[M]\frac{d[J]}{dA_j}[G]+[M][J]\left[\frac{d[G]}{dA_j}\right]\\ [0]_{(r\times n_d)}\end{bmatrix} \tag{3-65}$$

All the matrices, except $\frac{d[J]}{dA_j}$ are evaluated in the previous section. $[J]$ represents the top $m$ rows of the transpose of $[S]^{-1}$, and its derivative can be calculated from the following relation:

$$\frac{d[S]^{-1}}{dA_j} = -[S]^{-1}\frac{d[S]}{dA_j}[S]^{-1} \tag{3-66}$$

## 3.7 Sensitivity Analysis of Frame Structures

Frame structures are subjected to both the axial and the bending loadings. The FE formulation for the frame structures is discussed in section 2.8.3. Frame element have three force degrees of freedom, one related to axial displacement and other two related to bending moments. Element have three displacement degrees of freedom at each node. It is supposed that structure have $n$ force degrees of freedoms, $m$ displacement degrees of freedoms, and $n_d$ are the number of members in the structure. The design variables are the cross sectional area of the members, and other parameters such as moment of area and section modulus can be related to the cross sectional area by standard relations [61].

As discussed previously, the design sensitivity of the force field is required to evaluate the design sensitivities of various other performance measures. Therefore the design sensitivity of the force field of the frame structure is evaluated first. The general expression for the design sensitivity of the force field is given in Eq. (3-29). It should be noted that the global flexibility matrix of the frame structure is $(3n_d \times 3n_d)$ which is

assembled from $(3\times3)$ elemental flexibility matrices of each member; therefore $[S]$ can be discretized as:

$$[S]=\left[\begin{array}{c}[B]\\ \hline [C_1][G_e]_1 \quad [C_2][G_e]_2 \quad \cdots \quad [C_{n_d}][G_e]_{n_d}\end{array}\right] \tag{3-67}$$

where $[G_e]_j$ is the $(3\times3)$ flexibility matrix of the $j$th frame member, and given in Eq.(2-93), and $[C_i]$ are the corresponding columns of the compatibility matrix. Taking the partial derivative of Eq. (3-67) with respect to $A_j$ yields:

$$\frac{\partial[S]}{\partial A_j}=-\left[\begin{array}{c}[0]\\ \hline [0 \quad 0 \quad \cdots \quad [C_j][\overline{G}_e]_j \quad \cdots \quad 0]\end{array}\right] \tag{3-68}$$

where $[\overline{G}_e]_j$ is derivative of the flexibility matrix of the $j$th element, and its value can be obtained by differentiating Eq.(2-93) :

$$[\overline{G}_e]_j=\frac{1}{E}\begin{bmatrix} -\frac{L_j}{A_j^2} & 0 & 0 \\ 0 & \frac{-L_j}{I_j^2}\frac{dI_j}{dA_j} & \frac{-L_j^2}{2I_j^2}\frac{dI_j}{dA_j} \\ 0 & \frac{-L_j^2}{2I_j^2}\frac{dI_j}{dA_j} & \frac{-L_j^3}{3I_j^2}\frac{dI_j}{dA_j} \end{bmatrix} \tag{3-69}$$

Eq. (3-68) can also be written as:

$$\frac{\partial[S]}{\partial A_j}=-[0 \quad 0 \quad \cdots \quad [\overline{S}_j] \quad \cdots \quad 0] \quad \text{where} \quad [\overline{S}_j]=\left[\begin{array}{c}0\\ \hline [C_j][G_e]_j\end{array}\right] \tag{3-70}$$

Substituting Eq. (3-70) into Eq. (3-29) yields:

$$\frac{\partial\{F\}}{\partial A_j} = [S]^{-1}\begin{bmatrix}0 & 0 & \cdots & [\bar{S}_j] & \cdots & 0\end{bmatrix}\begin{Bmatrix}F_1\\F_2\\\vdots\\F_{3j-2}\\F_{3j-1}\\F_{3j}\\\vdots\\F_{3n_d}\end{Bmatrix} = [S]^{-1}[\bar{S}_j]\begin{bmatrix}F_{3j-2}\\F_{3j-1}\\F_{3j}\end{bmatrix} \tag{3-71}$$

Extending the terms of Eq. (3-71), for $j = 1.....n_d$ yields the sensitivity of force field as:

$$\begin{bmatrix}\frac{\partial F}{\partial A_1}\\\frac{\partial F}{\partial A_2}\\\vdots\\\frac{\partial F}{\partial A_{n_d}}\end{bmatrix}^T = [Y_F] \tag{3-72}$$

where

$$[Y_F] = [S]^{-1}[\bar{S}][\bar{F}_F], \text{ and } [\bar{F}_F] = \begin{bmatrix}F_1 & 0 & \cdots & 0\\F_2 & 0 & \cdots & 0\\F_3 & 0 & \cdots & 0\\0 & F_4 & \cdots & 0\\0 & F_5 & \cdots & 0\\0 & F_6 & \cdots & 0\\\vdots & \vdots & \ddots & \vdots\\0 & 0 & 0 & F_{3n_d-2}\\0 & 0 & 0 & F_{3n_d-1}\\0 & 0 & 0 & F_{3n_d}\end{bmatrix} \tag{3-73}$$

### 3.7.1 Stress Gradients

The frame structures are subjected to the axial and the bending stresses. The maximum stress in the frame member is the sum of the axial stress and the maximum bending stress. The maximum stress in the *i*th member can be written as:

$$\sigma_i = \frac{F_{3i-2}}{A_i} + \frac{M_i}{SH_i} \tag{3-74}$$

where $F_{3i-2}$ is the internal axial force, $SH_i$ is the shear modulus which is function of the cross sectional area of the member and $M_i$ is the maximum bending moment in the member. Maximum bending moment in frame element will at one of its two ends, and from Eq. (2-85) can be written as:

$$M_i = \begin{cases} F_{3i-1} & \text{if } F_{3i-1} \geq F_{3i-1} + F_{3i}\mathrm{L} \quad \text{Case1} \\ F_{3i-1} + F_{3i}\mathrm{L} & \text{if } F_{3i-1} \leq F_{3i-1} + F_{3i}\mathrm{L} \quad \text{Case2} \end{cases} \tag{3-75}$$

The numbers of stress constraints for the frame element are generally same as the number of members in the structure. A general expression for the stress constraint for the frame element can be stated similar to Eq. (3-38). Substituting Eq. (3-74) into Eq. (3-38) yields the stress constraint as:

$$g_i = \frac{F_{3i-2}}{\bar{\sigma}_i A_i} + \frac{M_i}{\bar{\sigma}_i SH_i} \qquad i = 1.....n_d \tag{3-76}$$

Similarly to the truss structure, the stress gradient can be stated as in Eqs. (3-41) and (3-42). The term $\frac{\partial\{F\}}{\partial A_j}$ in Eq. (3-42) can be obtained from the Eq. (3-72), therefore only $\frac{\partial g_i}{\partial A_j}$ and $\frac{\partial g_i}{\partial\{F\}}$ are required to be evaluated in order to find the gradients.

To calculate the term $\frac{\partial g_i}{\partial A_j}$, Let us take the partial derivative of Eq. (3-76) with respect to $A_j$:

$$\frac{\partial g_i}{\partial A_j} = \left\{ \begin{array}{cc} -\frac{F_i}{\overline{\sigma}_i A_i^2} - \frac{M_i}{\overline{\sigma}_i SH_i^2}\frac{\partial SH_i}{\partial A_i} & \text{if } i = j \\ 0 & \text{if } i \neq j \end{array} \right\} \tag{3-77}$$

For $i = 1.....n_d$ and $j = 1.....n_d$, Eq. (3-77) can be extended as:

$$\begin{bmatrix} \frac{\partial g_1}{\partial A_1} & \frac{\partial g_1}{\partial A_2} & \cdots & \frac{\partial g_1}{\partial A_{n_d}} \\ \frac{\partial g_2}{\partial A_1} & \frac{\partial g_2}{\partial A_2} & \cdots & \frac{\partial g_2}{\partial A_{n_d}} \\ \vdots & \vdots & \ddots & \vdots \\ \frac{\partial g_{n_d}}{\partial A_1} & \frac{\partial g_{n_d}}{\partial A_2} & \cdots & \frac{\partial g_{n_d}}{\partial A_{n_d}} \end{bmatrix} = [Q_F] \tag{3-78}$$

where

$$[Q_F] = \begin{bmatrix} -\frac{F_1}{\overline{\sigma}_1 A_1^2} - \frac{M_1}{\overline{\sigma}_1 SH_1^2}\frac{\partial SH_1}{\partial A_1} & 0 & \cdots & 0 \\ 0 & -\frac{F_4}{\overline{\sigma}_2 A_2^2} - \frac{M_2}{\overline{\sigma}_2 SH_2^2}\frac{\partial SH_2}{\partial A_2} & \cdots & 0 \\ \vdots & \vdots & \ddots & \vdots \\ 0 & 0 & 0 & -\frac{F_{3n_d-2}}{\overline{\sigma}_{n_d} A_{n_d}^2} - \frac{M_{n_d}}{\overline{\sigma}_{n_d} SH_{n_d}^2}\frac{\partial SH_{n_d}}{\partial A_{n_d}} \end{bmatrix} \tag{3-79}$$

The $\frac{\partial g_i}{\partial \{F\}}$ can be obtained by taking the partial derivative of Eq. (3-76) with respect to $\{F\}$:

$$\frac{\partial g_i}{\partial \{F\}} = \begin{bmatrix} \frac{\partial g_i}{\partial F_1} \\ \frac{\partial g_i}{\partial F_1} \\ \vdots \\ \frac{\partial g_i}{\partial F_{3i-2}} \\ \frac{\partial g_i}{\partial F_{3i-1}} \\ \frac{\partial g_i}{\partial F_{3i}} \\ \vdots \\ \frac{\partial g_{n_d}}{\partial F_{3n_d}} \end{bmatrix} = \begin{Bmatrix} 0 \\ 0 \\ \vdots \\ \Omega_i \\ \Sigma_i \\ I_i \\ 0 \\ 0 \end{Bmatrix} \tag{3-80}$$

where

$$\Omega_i = \frac{1}{\bar{\sigma}_i A_i} \tag{3-81}$$

The values of $\Sigma_i$ and $I_i$ depend on the location of the maximum moment in the frame element, and for two different locations can be written as:

Case1: When $M_i = F_{3i-1}$

$$\Sigma_i = \frac{1}{\bar{\sigma}_i SH_i} \quad \text{and} \quad I_i = 0 \tag{3-82}$$

Case 2: When $M_i = F_{3i-1} + F_{3i}\mathrm{L}$

$$\Sigma_i = \frac{\mathrm{L}_i}{\bar{\sigma}_i SH_i} \quad \text{and} \quad I_i = \frac{1}{\bar{\sigma}_i SH_i} \tag{3-83}$$

For $i = 1.....n_d$ and $j = 1.....n_d$ , Eq.(3-80) can be extended as:

$$\begin{bmatrix} \frac{\partial g_1}{\partial F_1} & \frac{\partial g_2}{\partial F_1} & \cdots & \frac{\partial g_{n_d}}{\partial F_1} \\ \frac{\partial g_1}{\partial F_2} & \frac{\partial g_2}{\partial F_2} & \cdots & \frac{\partial g_{n_d}}{\partial F_2} \\ \frac{\partial g_1}{\partial F_3} & \frac{\partial g_2}{\partial F_3} & \cdots & \frac{\partial g_{n_d}}{\partial F_3} \\ \vdots & \vdots & \ddots & \vdots \\ \frac{\partial g_1}{\partial F_{3n_d-2}} & \frac{\partial g_2}{\partial F_{3n_d-2}} & \cdots & \frac{\partial g_{n_d}}{\partial F_{3n_d-2}} \\ \frac{\partial g_1}{\partial F_{3n_d-1}} & \frac{\partial g_2}{\partial F_{3n_d-1}} & \cdots & \frac{\partial g_{n_d}}{\partial F_{3n_d-1}} \\ \frac{\partial g_1}{\partial F_{3n_d}} & \frac{\partial g_2}{\partial F_{3n_d}} & \cdots & \frac{\partial g_{n_d}}{\partial F_{3n_d}} \end{bmatrix} = [R_F] \quad \text{where} \quad [R_F] = \begin{bmatrix} \Omega_1 & 0 & \cdots & 0 \\ \Sigma_1 & 0 & \cdots & 0 \\ I_1 & 0 & \cdots & 0 \\ \vdots & \vdots & \ddots & \vdots \\ 0 & 0 & \cdots & \Omega_{n_d} \\ 0 & 0 & \cdots & \Sigma_{n_d} \\ 0 & 0 & \cdots & I_{n_d} \end{bmatrix} \tag{3-84}$$

Substituting Eqs. (3-72), (3-78) and (3-84) into Eq. (3-42) yields the stress gradient as:

$$\begin{bmatrix} \nabla g_1 \\ \nabla g_2 \\ \vdots \\ \nabla g_{n_d} \end{bmatrix} = \begin{bmatrix} \frac{\partial g_1}{\partial A_j} \\ \frac{\partial g_2}{\partial A_j} \\ \vdots \\ \frac{\partial g_{n_d}}{\partial A_j} \end{bmatrix}^T = [Q_F]^T + [Y_F]^T [R_F] \tag{3-85}$$

### 3.7.2 Displacement Gradient

A general expression for the normalized displacement constraint for the frame element can also be stated similar to Eq. (3-49) and the expression for the sensitivity analysis is given in Eqs.(3-41) and (3-42). The term $\frac{\partial \{F\}}{\partial A_j}$ can be obtained from Eq. (3-72), therefore to calculate gradient of displacement constraints, only the partial derivatives $\frac{\partial g_i}{\partial A_j}$ and $\frac{\partial g_i}{\partial \{F\}}$ are required to be evaluated.

The term $\frac{\partial g_i}{\partial \{F\}}$ can be calculated similar to as calculated in section 3.6.2 for the truss element and can be written similar to Eq. (3-51) as:

$$\begin{bmatrix} \frac{\partial g_1}{\partial F} \\ \frac{\partial g_2}{\partial F} \\ \vdots \\ \frac{\partial g_m}{\partial F} \end{bmatrix}^T = [\overline{U}_F][J][G] \tag{3-86}$$

The term $\frac{\partial g_i}{\partial A_j}$ can be obtained from the Eq. (3-53) and the term $\frac{\partial U_i}{\partial A_j}$ in Eq. (3-54) can be written similar to Eq. (3-55) as:

$$\frac{\partial \{U_e\}}{\partial A_j} = [J] \begin{bmatrix} 0 & 0 & 0 & \dots & 0 & \dots & 0 \\ 0 & 0 & 0 & \dots & 0 & \dots & 0 \\ 0 & 0 & 0 & \dots & 0 & \dots & 0 \\ \vdots & \vdots & \vdots & \ddots & \vdots & \ddots & \vdots \\ 0 & 0 & 0 & \dots & [\overline{G}_e]_j & \dots & 0 \\ \vdots & \vdots & \vdots & \ddots & \vdots & \ddots & \vdots \\ 0 & 0 & 0 & 0 & 0 & 0 & 0 \end{bmatrix}_{(3n_d \times 3n_d)} \begin{Bmatrix} F_1 \\ F_2 \\ F_3 \\ \vdots \\ F_{3j-2} \\ F_{3j-1} \\ F_{3j} \\ \vdots \\ F_{3n_d-2} \\ F_{3n_d-1} \\ F_{3n_d} \end{Bmatrix} \tag{3-87}$$

$$\frac{\partial \{U_e\}}{\partial A_j} = [J_j] \begin{Bmatrix} F_{3j-2} \\ F_{3j-1} \\ F_{3j} \end{Bmatrix} [\overline{G}_e]_j \tag{3-88}$$

where $J_j$ is the $j$th column of $[J]$. Extending the terms of Eq. (3-88) for $j = 1.....n_d$ and substituting into Eq. (3-54) yields:

$$\begin{bmatrix} \frac{\partial g_1}{\partial A_1} & \frac{\partial g_1}{\partial A_2} & \cdots & \frac{\partial g_1}{\partial A_{n_d}} \\ \frac{\partial g_2}{\partial A_1} & \frac{\partial g_2}{\partial A_2} & \cdots & \frac{\partial g_2}{\partial A_{n_d}} \\ \vdots & \vdots & \ddots & \vdots \\ \frac{\partial g_{n_d}}{\partial A_1} & \frac{\partial g_{n_d}}{\partial A_2} & \cdots & \frac{\partial g_{n_d}}{\partial A_{n_d}} \end{bmatrix} = [\overline{U}_F][J][\overline{G}_F][\overline{F}_F] \tag{3-89}$$

where

$$[\overline{G}_F] = \begin{bmatrix} [G_e]_1 & 0 & \cdots & 0 \\ 0 & [G_e]_2 & \cdots & 0 \\ \vdots & \vdots & \ddots & \vdots \\ 0 & 0 & 0 & [G_e]_{n_d} \end{bmatrix} \tag{3-90}$$

Substituting Eqs. (3-85), (3-86) and (3-89) into Eq. (3-42) yields the displacement constraint as:

$$\begin{bmatrix} \nabla g_1 \\ \nabla g_2 \\ \vdots \\ \nabla g_{n_d} \end{bmatrix} = \begin{bmatrix} \frac{\partial g_1}{\partial A_j} \\ \frac{\partial g_2}{\partial A_j} \\ \vdots \\ \frac{\partial g_{n_d}}{\partial A_j} \end{bmatrix}^T = [[\overline{U}_F][J][\overline{G}_F][\overline{F}_F] + [\overline{U}_F][J][G][Y_F]]^T \qquad j = 1.....n_d \tag{3-91}$$

### 3.7.3 Sensitivity Analysis of Eigen Values

The sensitivity analysis of eigen value using the IFM for truss structures is discussed in the section 3.6.3. The basic equation for the design sensitivity analysis for the frame structure is same, and can be stated from Eq. (3-64) as:

$$\frac{d\mu}{dA_j} = \frac{\{V_L\}^T \left( \frac{d[S]}{dA_j} - \mu \frac{d[M_f]}{dA_j} \right) \{V_R\}}{\{V_L\}^T [M_f] \{V_R\}}$$

Similar to Eq. (3-65), $\frac{d[M_f]}{dA_j}$ can be obtained as:

$$\frac{d[M_f]}{dA_j} = \begin{bmatrix} \frac{d[M]}{dA_j}[J][G] + [M]\frac{d[J]}{dA_j}[G] + [M][J]\left[\frac{d[G]}{dA_j}\right] \\ \hline [0]_{(r \times 3n_d)} \end{bmatrix}$$

Except matrix $\frac{d[J]}{dA_j}$, all the required matrices for the sensitivity analysis are evaluated in previous section. $[J]$ represents the top m rows of the transpose of the matrix $[S]^{-1}$ and its derivative can be calculated from Eq. (3-66):

# Chapter-4

# CASE STUDY-STRUCTURAL OPTIMIZATION

## 4.1 Introduction

In this chapter, several examples of sizing design optimization for the discrete structures are presented. The objective of this study is to implement and investigate, the design optimization and sensitivity analysis method using the IFM for small and large scale size optimization problems. A size optimization algorithm has been developed in which the IFM as analyzer is combined with SQP technique as optimizer. SQP algorithm is implemented using MATLAB optimization toolbox [60]. An efficient analytical design sensitivity analysis technique, developed in previous chapter, has been implemented for evaluating the gradient of the behavior constraints. The analytical sensitivity analysis is implemented using MATLAB programming, and then integrated with optimization algorithm. It should be noted that for all the optimization problems considered in this chapter stopping tolerance of 0.001 is considered for objective function, constraints and search direction.

The structures ranging from small to large scale are designed for the stress, displacement and frequency constraints. The problems are also investigated using the DM and the IFM(NG). Various performance criteria's like optimum design, numbers of iterations, computational time, convergence and number of active constraints are compared for all the cases. The numerical tests presented demonstrate the computational advantages of the IFM for stress and displacement constraints, which become more pronounced in the

large-scale optimization problems. It has been shown that path of the optimization algorithm depends on the analysis procedure, and the small difference in the response from the analysis procedure can change the path of the optimization algorithm. The optimization problems subjected to frequency constraints have numbers of local optimums and it has been observed that the IFM and the DM leads to different optimum design while starting with same initial design. The efficiency and accuracy of analytical sensitivity analysis is also compared with numerical sensitivity analysis.

## 4.2 Size optimization-Stress and Displacement constraints

### 4.2.1 10-Member Truss Structure

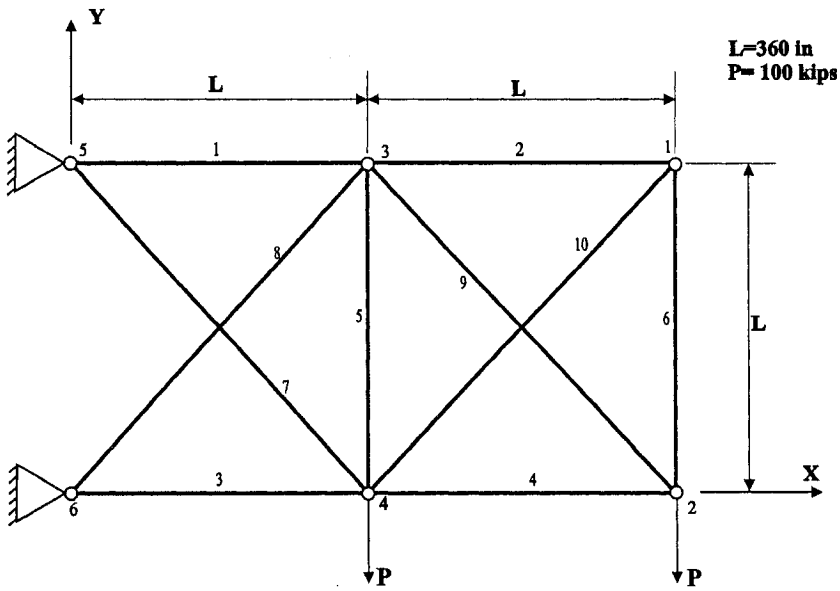


**Figure 4.1** The 10-bar planar truss structure

The 10-bar planar truss structure is shown in Figure 4.1. This structural design optimization problem is a classical benchmark problem for testing optimization algorithms. The objective is to minimize the mass of the structure under stress and displacement constraints, and design variables are the cross sectional area of the

elements. The material is aluminum with Young's modulus $E = 10^7$ psi ($6.895 \times 10^{11}$ Pa) and density $\rho = 0.1$ lbm/in$^3$ (2767.99 Kg/m$^3$). Structure is statically indeterminate having 10 force degrees of freedom and 8 displacement degrees of freedom. Thus, the degree of indeterminacy is 2. The maximum allowable stress of ±25000 psi is imposed on all the members. Vertical displacement constraints of ±2 in are imposed on nodes 1-4. The minimum area for all elements was set at 0.1 in$^2$. The cross sectional area of 1in$^2$ is considered as initial design for all the members.

**Table 4.1** Optimum design of the 10-bar planar truss structure

| | Area of Cross Section (m$^2$) | | |
|---|---|---|---|
| Member No. | IFM(NG) | IFM(AG) | DM |
| 1 | 30.5219 | 30.5219 | 30.5219 |
| 2 | 0.1 | 0.1 | 0.1 |
| 3 | 23.1999 | 23.1999 | 23.1999 |
| 4 | 15.2229 | 15.2229 | 15.2229 |
| 5 | 0.1 | 0.1 | 0.1 |
| 6 | 0.5514 | 0.5514 | 0.5514 |
| 7 | 7.4572 | 7.4572 | 7.4572 |
| 8 | 21.0364 | 21.0364 | 21.0364 |
| 9 | 21.5284 | 21.5284 | 21.5284 |
| 10 | 0.1 | 0.1 | 0.1 |
| Mass (Kg) | 5060.9 | 5060.9 | 5060.9 |
| CPU time(sec) | 2.956 | 2.14 | 3.187 |
| No. of Iterations | 26 | 22 | 44 |
| A.S.C | 5 | 5 | - |
| A.D.C. | V1 | V1 | V1 |
| A.L.B.C. | 2,5,10 | 2,5,10 | 2,5,10 |

*A.S.C.-Active Stress Constraint, A.D.C-Active Displacement Constraint*
*A.L.B.C-Active Lower Bound Constraint, V1-Vertical Displacement at Node 1*
*V1- Vertical Displacement at node 1*

The optimization results for the 10-bar structures are shown in Table 4.1. It can be seen that all the optimization algorithms converge to similar optimum mass of 5060.9 Kg, but

differ in number of iterations. The results of the optimization analysis match exactly with those in literature by Haftka and Gurdal [51], and Fleury and Schmit [62], which are based on the DM. The IFM (AG) required 22 iterations, where as the IFM (NG) and the DM required 26 and 44 iterations, respectively. The DM takes maximum number of iterations.

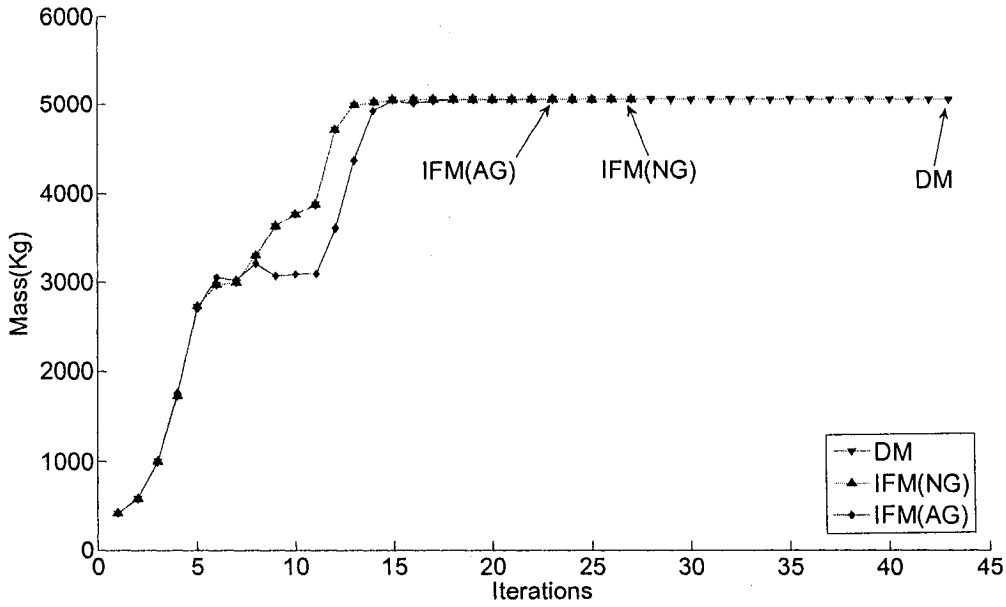


**Figure 4.2** Convergence curves of the 10-bar truss structure.

The axial stress in the 5th member and vertical displacement at node 1 (V1) reached to their maximum values at the optimum design. The cross sectional area of the elements 2, 5 and 10 reach to their minimum value. The convergence of the all the optimization algorithms has been presented graphically in Figure 4.2. It can be seen that the IFM(AG) and the IFM(NG) take different optimization path. Therefore small error in numerical gradient can change the path of optimization algorithm and results in large number of iterations. The optimization has also been performed with different initial point and same

optimum results have been obtained for most of the initial designs. The results show that the IFM is robust analyzer for the optimization.

### 4.2.2 10- Members Frame Structure

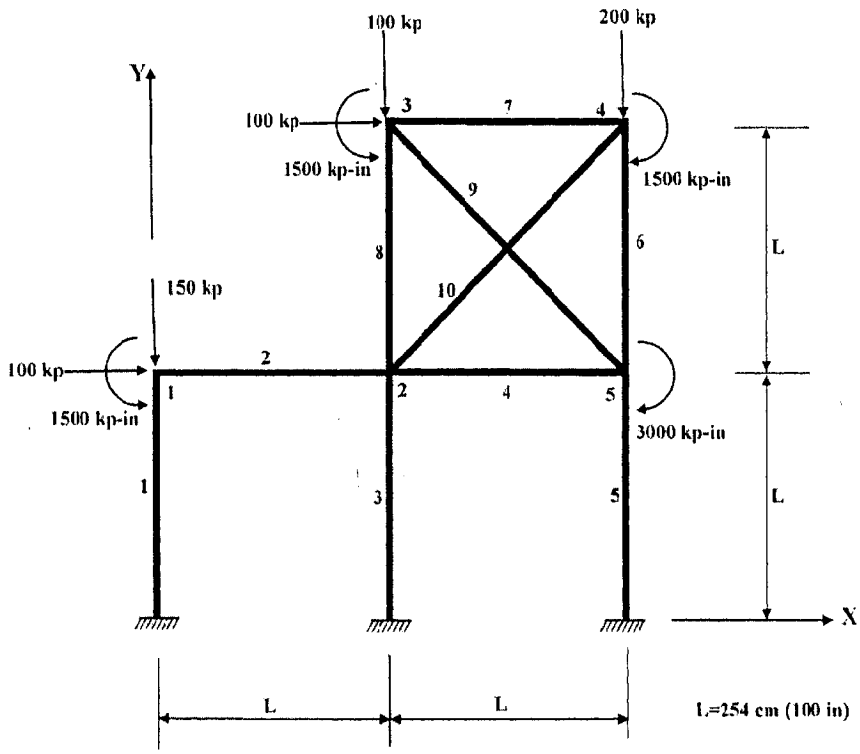


**Figure 4.3** The 10-member frame structure

The 10-member frame structure and applied loading are shown in Figure 4.3. It is made of steel with $E = 207\,KN/m^3$ and $\rho = 7830\,Kg/m^3$. The structure is statically indeterminate having 30 force degrees of freedoms and 15 displacement degrees of freedoms. The degree of indeterminacy is 15. The objective is to minimize the mass of the structure and the design variables are the cross sectional area of the members. The second moment of area and section modulus, are related to cross sectional area by the following relations:

$$\begin{cases} SH = 1.6634A^{1.511} \\ I = 4.592A^2 \end{cases} \qquad 0 \le A \le 15 \qquad (4\text{-}1)$$

$$\begin{cases} SH = (281.077A^2 + 84100)^{0.5} - 290 \\ I = 4.638A^2 \end{cases} \qquad 15 \le A \le 44 \qquad (4\text{-}2)$$

$$\begin{cases} SH = 13.76A - 103.906 \\ I = 256.229A - 2300 \end{cases} \qquad 15 \le A \le 44 \qquad (4\text{-}3)$$

where *SH, I* and *A* are the section modulus, moment of area and cross sectional area of the member, respectively. The above relations are stated for steel section in accordance with AISC codes [61]. The stress limit for all members is 165.474 Kg/m$^3$ and the horizontal displacement of all joints is limited to 0.00127m. A minimum and maximum area limit of 0.003226 m$^2$ and 0.064516 m$^2$ are enforced on each member.

**Table 4.2** Optimum design of the10-members frame structure

| | Cross Sectional Area (m$^2$) | | |
|---|---|---|---|
| Member No. | IFM(NG) | IFM(AG) | DM |
| 1 | 0.028387 | 0.028386 | 0.028387 |
| 2 | 0.023753 | 0.023654 | 0.023681 |
| 3 | 0.003226 | 0.003226 | 0.003226 |
| 4 | 0.003226 | 0.003226 | 0.003226 |
| 5 | 0.046245 | 0.046202 | 0.046256 |
| 6 | 0.01025 | 0.010243 | 0.010241 |
| 7 | 0.007201 | 0.007228 | 0.0072355 |
| 8 | 0.016323 | 0.016459 | 0.016429 |
| 9 | 0.016296 | 0.016281 | 0.016245 |
| 10 | 0.003226 | 0.003226 | 0.003226 |
| Mass | 3305.8 | 3305.63 | 3305.8 |
| CPU time(sec) | 3.203 | 2.281 | 4.814 |
| No. of Iterations | 36 | 33 | 46 |
| A.S.C. | 6 | 6 | 6 |
| A.D.C. | H4 | H4 | H4 |
| A.L.B. C. | 3,4,10 | 3,4,10 | 3,4,10 |

The problem was solved using number of different initial points and the best optimum result is obtained by considering an initial design of 0.012903 $m^2$ for the cross sectional area for all the members. The results of the optimization analysis are presented in Table 4.2. The IFM (NG) and the DM converge to same value of minimum mass of 3305.8 Kg, and almost same value of mass of 3305.63 Kg is obtained by using the IFM(AG). At the optimum point, stress in member 6 and horizontal displacement of node 4 (H4) reached to their maximum value. The cross sectional area of the members 3, 4 and 10 reached to their minimum value. The problem was also investigated by Khan [63] using the DM and the optimal criteria method, and a mass of 3390.39 Kg was obtained.

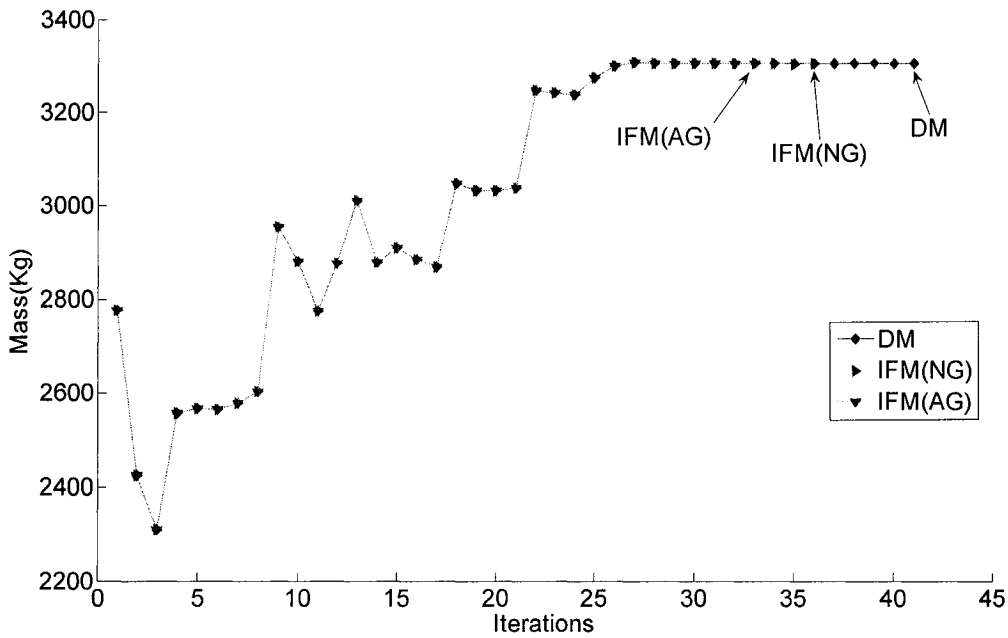


**Figure 4.4** Convergence curves for the10-member frame structure

The iteration history for the optimization algorithms is shown in Figure 4.4. All the algorithms follow almost the same path, but differ in numbers of iterations required for the convergence. The numbers of iteration taken by the IFM(AG) are 33 which are less than 36 and 46 taken by the IFM(NG) and the DM, respectively. The computational time

taken by the IFM is less than the DM, and it is further reduced by calculating the gradient analytically.

### 4.2.3 25- Member Frame Structure

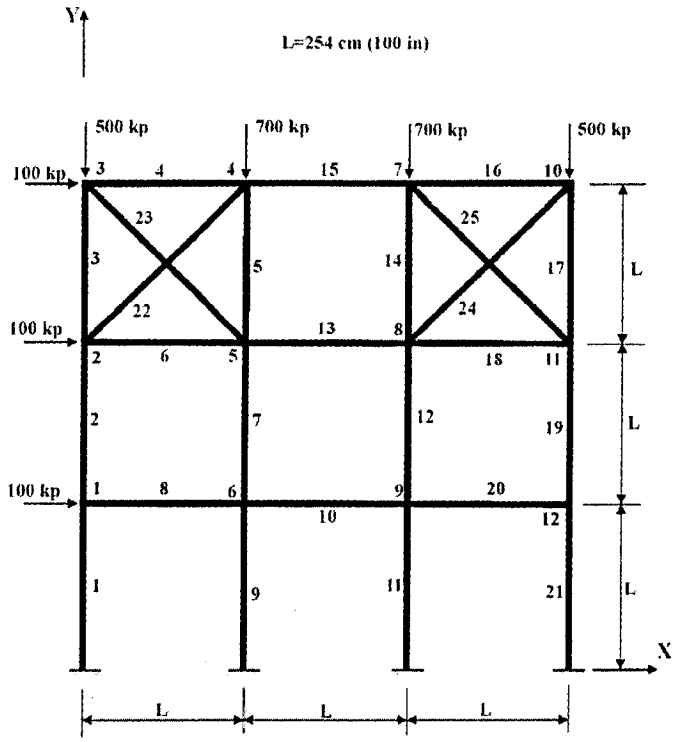


**Figure 4.5** The 25-member frame structure

The 25-member frame structure and the applied loading are shown in Figure 4.5. The structure has the same material properties and the stress limit as those of the 10-member frame structure and the objective is to minimize the mass of the structure. The numbers of design variables are 25 and those are the cross sectional area of the members. The section modulus and moment of area are related to the cross sectional area according to Eqs. (4-1), (4-2) and (4-3). The horizontal displacement of nodes 1, 2, 3, 10, 11 and 12 are limited to 0.00127m and the limits for minimum and maximum cross sectional area are 0.003226 $m^2$ and 0.064516 $m^2$, respectively. The numbers of stress and displacement constraints are 25 and 12, respectively. The numbers of force and displacement degrees

of freedom are 75 and 36, respectively, and the degree of redundancy of the structure is 39.

The optimization results are given in Table 4.3. The problem is solved with number of different initial points and the best design is obtained with initial cross sectional area of 0.06 $m^2$. Almost same minimum mass of 9504 Kg is obtained by using all formulations. It should be noted that a minimum mass of 10049 Kg was obtained by Khan [63] using the DM and the optimal criteria method. At the optimum point, the stress in the members 1, 2, 3, 5, 9, 12, 14 and 17, and the cross sectional area of member 11 reached to their maximum values, for both the IFM and the DM. The horizontal displacements of nodes 2 and 10 (H2 and H10) are active for the IFM, and the horizontal displacements of nodes 3, 10 and 12 (H3, H10 and H12) are active for the DM. The total numbers of active constraint for the DM are 19, where as those for the IFM(AG) and the IFM(NG) are 17. The computational efficiency of the IFM in this problem is more prominent as compared to the 10 member frame structure due to large size of the problem. It can be seen from Table 4.3 that the IFM takes significant less computational time than the DM. Further, it is interesting to note that the gradient calculation by analytical method reduces this computational time to almost half of the original computational time. The gradient calculation by analytical method decreases the computational efficiency significantly. The iteration history of the optimization algorithms is shown in Figure 4.6. It is seen that the IFM(AG) and the IFM(NG) almost follow the same path, but the DM follows a different path. The IFM converge to optimal solution quite rapidly as compared to the DM. So it can be concluded that path of the optimization algorithm depends on the

analysis method, and the small difference in the calculation of performance measures can change the convergence path.

**Table 4.3** Optimum design of the 25-members frame structure

| Member No. | Cross Sectional Area ($m^2$) | | |
|---|---|---|---|
| | DM | IFM(NG) | IFM(AG) |
| 1 | 0.010004 | 0.010011 | 0.010008 |
| 2 | 0.0071444 | 0.0071558 | 0.0071489 |
| 3 | 0.0042334 | 0.0042296 | 0.0042338 |
| 4 | 0.016201 | 0.016231 | 0.016193 |
| 5 | 0.020244 | 0.020239 | 0.020239 |
| 6 | 0.003226 | 0.003226 | 0.003226 |
| 7 | 0.051763 | 0.051774 | 0.05172 |
| 8 | 0.014865 | 0.014786 | 0.014866 |
| 9 | 0.031431 | 0.031422 | 0.031425 |
| 10 | 0.053884 | 0.053883 | 0.053879 |
| 11 | 0.064516 | 0.064516 | 0.064516 |
| 12 | 0.020579 | 0.020582 | 0.020583 |
| 13 | 0.003226 | 0.003226 | 0.003226 |
| 14 | 0.019579 | 0.019578 | 0.01958 |
| 15 | 0.003226 | 0.003226 | 0.003226 |
| 16 | 0.0048218 | 0.0048456 | 0.0048354 |
| 17 | 0.013149 | 0.013153 | 0.013153 |
| 18 | 0.003226 | 0.003226 | 0.003226 |
| 19 | 0.016149 | 0.016177 | 0.016145 |
| 20 | 0.003226 | 0.003226 | 0.003226 |
| 21 | 0.01874 | 0.018719 | 0.018781 |
| 22 | 0.013523 | 0.013536 | 0.013543 |
| 23 | 0.046809 | 0.046808 | 0.046788 |
| 24 | 0.003226 | 0.003226 | 0.003226 |
| 25 | 0.003226 | 0.003226 | 0.003226 |
| Mass(kg) | 9504.2 | 9504.4 | 9504.2 |
| CPU time(sec) | 20.2 | 12.78 | 6.25 sec |
| No. of Iterations | 62 | 48 | 47 |
| A.S.C. | 1,2,3,5,9,12,14,17 | 1,2,3,5,9,12,14,17 | 1,2,3,5,9,12,14,17 |
| A.D.C. | H3,H10,H12 | H2,H10 | H2,H10 |
| A.L.B.C. | 6,13,15,18,20,24,25 | 6,13,18,20,24,25 | 6,13,18,20,24,25 |
| A. U.B.C. | 11 | 11 | 11 |

*A.U.B.C.-Active Upper Bound Constraints*

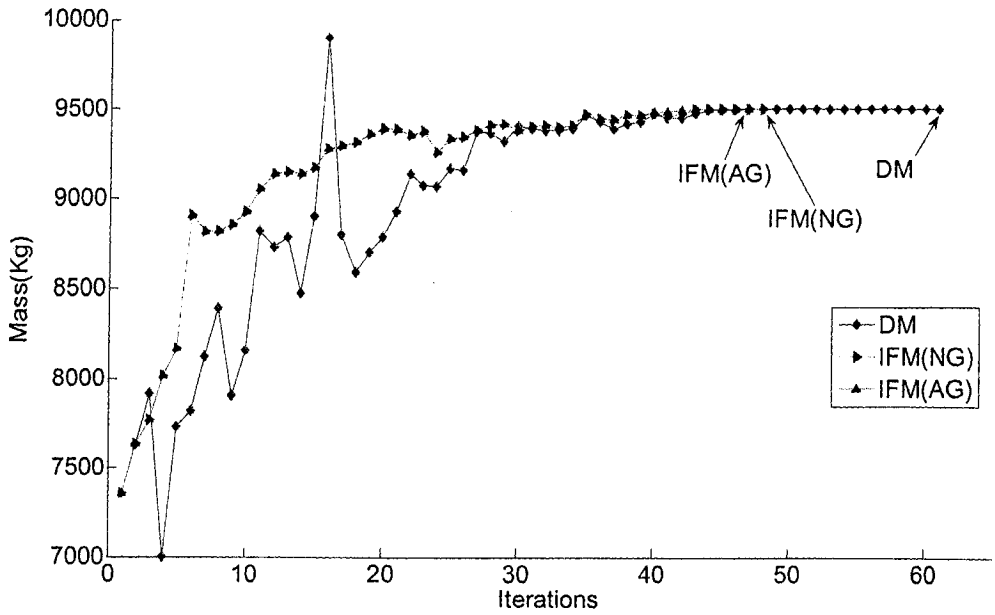


**Figure 4.6** Convergence curve for the 25-members frame structure

### 4.2.4 70 Member Frame Structure

The 70 member frame structure and loading on the structure are shown in Figure 4.7. The material properties of the structure, side constraints on the cross sectional area and stress limits are assigned the same values, as those used for the 10 members frame structure. The design variables are the cross sectional area of the members, and other parameters such as section modulus and moment of area are related to cross sectional area according to Eqs. (4-1), (4-2) and (4-3). The horizontal displacements of all joints are limited to 0.03810m. The numbers of force and displacement degrees of freedom are 210 and 120, respectively, and the degree redundancy is 90.

The mass of the structure is minimized for the following two cases:

Case 1- Subjected to both the stress and displacement constraints.

Case 2- Subjected to only stress constraints.

The two cases are considered to study the efficiency of the IFM under stress-displacement constraints and under only stress constraints.

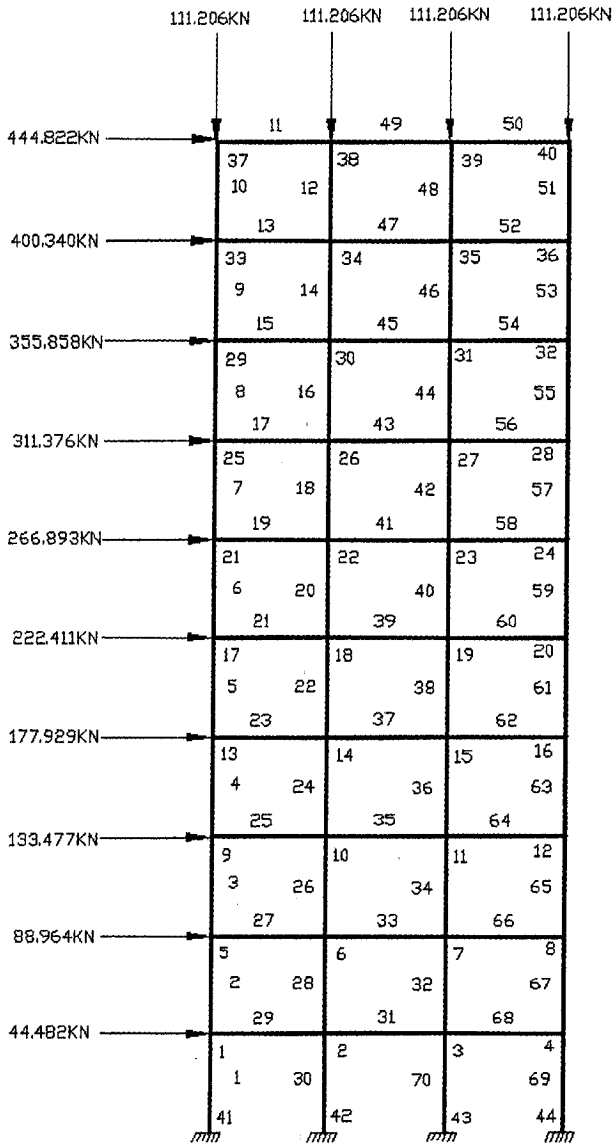


**Figure 4.7** The 70-members frame structure.

### 4.2.4.1 Case1: Stress and Displacement Constraints

The structure is designed for both stress and displacement constraints. In the literature, the problem was investigated by Khan [63] using the DM and the optimal criteria

method, and optimum mass of 43691.4 Kg was obtained. An initial design of 0.06 $m^2$ is taken for the cross sectional area of all members. The optimum mass and finial design for the cross sectional areas are given in Tables 4.4 and 4.5, respectively. The performance parameters such as CPU time, number of iteration, active constraints are also given in Table 4.4.

**Table 4.4** Final design of the 70-members frame structure with both displacement and stress constraints.

| | IFM (NG) | IFM (AG) | DM |
|---|---|---|---|
| MASS(Kg) | 43520 | 43520 | 43521 |
| CPU time(sec) | 925.836 | 323.312 | 1179.5 |
| No. of Iterations | 191 | 186 | 194 |
| Active D.C. | H37 | H37 | H37 |
| Active L.B.C. | 48,49,50,51,52,53 | 48,49,50,51,52,53 | 48,49,50,51,52,53 |
| Active U.B.C. | 1,2,3,63,65,67,69 | 1,2,3,63,65,67,69 | 1,2,3,63,65,67,69 |

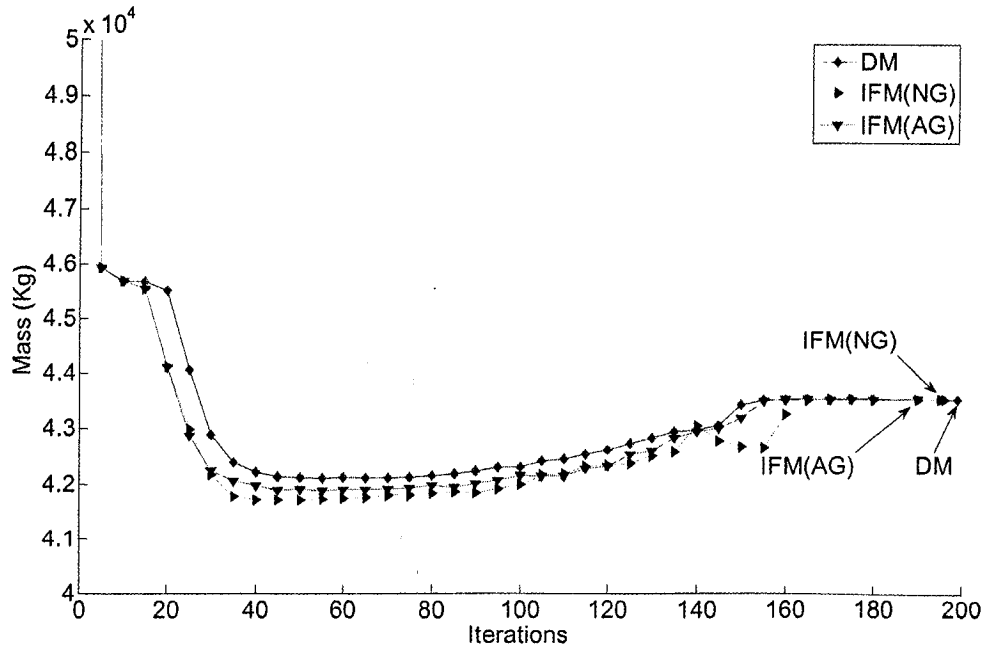


**Figure 4.8** Convergence for the 70-member frame structure for both stress and displacement constraints.

**Table 4.5** Optimum design for the cross sectional area ($m^2$) of the 70-members frame structure with both displacement and stress constraints

| Member No. | IFM(NG) | IFM(AG) | DM | Member No. | IFM(NG) | IFM(AG) | DM |
|---|---|---|---|---|---|---|---|
| 1 | 0.064516 | 0.064516 | 0.06452 | 36 | 0.030281 | 0.030672 | 0.031075 |
| 2 | 0.064516 | 0.064516 | 0.06452 | 37 | 0.02922 | 0.029454 | 0.029671 |
| 3 | 0.064516 | 0.064516 | 0.06452 | 38 | 0.029814 | 0.029505 | 0.029509 |
| 4 | 0.064405 | 0.064345 | 0.0645 | 39 | 0.028391 | 0.028415 | 0.028399 |
| 5 | 0.051467 | 0.051489 | 0.05171 | 40 | 0.028567 | 0.028565 | 0.02859 |
| 6 | 0.039302 | 0.039416 | 0.03961 | 41 | 0.028367 | 0.02844 | 0.028387 |
| 7 | 0.028481 | 0.028363 | 0.02839 | 42 | 0.028734 | 0.028857 | 0.028896 |
| 8 | 0.019963 | 0.020181 | 0.0202 | 43 | 0.028368 | 0.028412 | 0.028346 |
| 9 | 0.013922 | 0.014028 | 0.01406 | 44 | 0.029272 | 0.029543 | 0.029344 |
| 10 | 0.02252 | 0.022644 | 0.0226 | 45 | 0.028466 | 0.028441 | 0.028457 |
| 11 | 0.026668 | 0.026604 | 0.0266 | 46 | 0.034474 | 0.034561 | 0.034889 |
| 12 | 0.028396 | 0.028386 | 0.0284 | 47 | 0.034448 | 0.033963 | 0.033957 |
| 13 | 0.025203 | 0.02522 | 0.02531 | 48 | 0.003226 | 0.003226 | 0.003226 |
| 14 | 0.026567 | 0.026675 | 0.02653 | 49 | 0.003226 | 0.003226 | 0.003226 |
| 15 | 0.013918 | 0.014202 | 0.01386 | 50 | 0.003226 | 0.003226 | 0.003226 |
| 16 | 0.022553 | 0.022257 | 0.02246 | 51 | 0.003226 | 0.003226 | 0.003226 |
| 17 | 0.022725 | 0.022781 | 0.02277 | 52 | 0.003226 | 0.003226 | 0.003226 |
| 18 | 0.028392 | 0.028374 | 0.02837 | 53 | 0.003226 | 0.003226 | 0.003226 |
| 19 | 0.028379 | 0.02836 | 0.02839 | 54 | 0.029087 | 0.028941 | 0.02927 |
| 20 | 0.028435 | 0.028376 | 0.02846 | 55 | 0.02839 | 0.028331 | 0.028386 |
| 21 | 0.028492 | 0.02844 | 0.02839 | 56 | 0.030181 | 0.030254 | 0.029641 |
| 22 | 0.028522 | 0.028534 | 0.02847 | 57 | 0.031367 | 0.031256 | 0.031248 |
| 23 | 0.029221 | 0.029013 | 0.02932 | 58 | 0.028737 | 0.028705 | 0.028575 |
| 24 | 0.029726 | 0.029836 | 0.02917 | 59 | 0.04264 | 0.042636 | 0.042682 |
| 25 | 0.028971 | 0.029588 | 0.02918 | 60 | 0.028648 | 0.029012 | 0.028696 |
| 26 | 0.031741 | 0.031618 | 0.0308 | 61 | 0.054881 | 0.055038 | 0.054774 |
| 27 | 0.030977 | 0.030634 | 0.0302 | 62 | 0.029234 | 0.029587 | 0.029664 |
| 28 | 0.03027 | 0.030112 | 0.03124 | 63 | 0.064516 | 0.064516 | 0.064516 |
| 29 | 0.028418 | 0.02841 | 0.02841 | 64 | 0.029705 | 0.02913 | 0.029821 |
| 30 | 0.028393 | 0.028325 | 0.02838 | 65 | 0.064516 | 0.064516 | 0.064516 |
| 31 | 0.028354 | 0.028361 | 0.02836 | 66 | 0.030207 | 0.030562 | 0.030374 |
| 32 | 0.031454 | 0.031048 | 0.03098 | 67 | 0.064516 | 0.064516 | 0.064516 |
| 33 | 0.029742 | 0.029686 | 0.03047 | 68 | 0.028393 | 0.028369 | 0.028415 |
| 34 | 0.032002 | 0.031728 | 0.03193 | 69 | 0.064516 | 0.064516 | 0.064516 |
| 35 | 0.031437 | 0.031233 | 0.03035 | 70 | 0.028391 | 0.028443 | 0.028438 |

An optimized mass of 43520 Kg is obtained using the IFM(AG) and the IFM(NG), and almost similar mass of 43521 Kg is obtained using the DM. The horizontal displacement at node 37 (H37) is active at the optimized result and there is no active stress constraint. Therefore displacement constraints are more dominating for this problem and decide the final optimum design of the structure. The cross sectional area of elements 48, 49, 50, 51, 52 and 53 reached to their minimum value, while that of elements 1, 2, 3, 63, 65, 67 and 69 reached to their maximum value. It is evident from Table 4.4 that the IFM is computationally more efficient as compared to the DM. It should also be noted that again there is significant increase in computational efficiency using IFM combined with analytically evaluated gradients technique. The calculation of gradient by analytical method reduces the computational time to one third of that with numerical gradient. The convergence of the optimization algorithms is presented in Figure 4.8. It can be seen that all the optimization algorithms take the different path. The number of iteration required to converge to the optimized result are also different. The IFM(AG), the IFM(NG) and the DM take 186, 191 and 196 iterations, respectively.

### 4.2.4.2 Case 2-Stress Constraints

In order to investigate the efficiency of the IFM for problems under only stress constraints, the 70-member frame structure is again designed for only stress constraints. It has been demonstrated that the IFM is very efficient for stress dominating optimization problems. The optimum mass and finial design for the 70-member frame structure subjected to only stress constraints are provided in Tables 4.6 and 4.7, respectively. The CPU time, numbers of iterations, active constraints are also shown in Table 4.6. A

minimum value of mass of 28033 Kg is obtained using both the IFM(NG) and the DM, and the IFM(AG) converges to slightly lighter mass of 28027 Kg. It can be seen from Table 4.6 that IFM(NG) takes almost one fourth of the computational time than that taken by the DM. This illustrates the high computational efficiency of the IFM for stress dominating problems. Therefore, it can be concluded that the efficiency of the IFM increases with increase in number of active stress constraints in the optimization problem. Furthermore, the computational time for the IFM is reduced by one third with calculation of gradient by the analytical method. It can be observed that the IFM(AG) take insignificant computational time of 18.54 sec as compared to 227.83 sec taken by the DM. The numbers of iterations taken by the IFM are also significantly less than the DM. The numbers of active stress constraints, active lower bound constraints and active upper bound constraints, for the IFM(AG), the IFM(NG) and the DM, are the same and shown in Table 4.6.

**Table 4.6** Final design of the 70-memebrs frame structure with stress constraints

| | IFM(AG) | IFM(NG) | DM |
|---|---|---|---|
| MASS(Kg) | 28027 | 28033 | 28033 |
| CPU time(sec) | 18.54 | 54.172 | 227.828 |
| No. of Iterations | 29 | 30 | 47 |
| A. S. C. | 1-7,10-17,19,20,22, 24-28,31,34,36-40,44-47,56-59,61-67,69,70 | 1-7,10-7,19,20,22,24-28,31,34,36-40,44-47, 56-59,61-67,69,70 | 1-7,10-7,19,20,22,24-28,31,34,36-40,44-47, 56-59,61-67,69,70 |
| A.L.B.C. | 8,9,18,21,29,33,35,41, 43,48-55,60,68 | 8,9,18,21,29,33,35, 41,43,48-55,60,68 | 8,9,18,21,29,33,35,41, 43,48-55,60,68 |
| A.U.B.C. | 69 | 69 | 69 |

**Table 4.7** Optimum design for the cross sectional area ($m^2$) of the 70-members frame structure under only stress constraints

| Member No. | IFM(AG) | IFM(NG) | DM | Member No. | IFM(AG) | IFM(NG) | DM |
|---|---|---|---|---|---|---|---|
| 1 | 0.064237 | 0.064207 | 0.064231 | 36 | 0.031562 | 0.031566 | 0.031537 |
| 2 | 0.040219 | 0.040197 | 0.040221 | 37 | 0.031748 | 0.031751 | 0.031725 |
| 3 | 0.039618 | 0.03963 | 0.039627 | 38 | 0.034329 | 0.034316 | 0.03439 |
| 4 | 0.024374 | 0.024368 | 0.024357 | 39 | 0.043387 | 0.043379 | 0.043411 |
| 5 | 0.015836 | 0.015848 | 0.015811 | 40 | 0.027629 | 0.027633 | 0.027592 |
| 6 | 0.011141 | 0.011143 | 0.011142 | 41 | 0.003226 | 0.003226 | 0.003226 |
| 7 | 0.023185 | 0.023182 | 0.023197 | 42 | 0.005065 | 0.005065 | 0.00508 |
| 8 | 0.003226 | 0.003226 | 0.003226 | 43 | 0.003226 | 0.003226 | 0.003226 |
| 9 | 0.003226 | 0.003226 | 0.003226 | 44 | 0.032609 | 0.032617 | 0.032609 |
| 10 | 0.010023 | 0.009943 | 0.009939 | 45 | 0.028012 | 0.028007 | 0.028002 |
| 11 | 0.009621 | 0.010054 | 0.010056 | 46 | 0.015084 | 0.015105 | 0.015114 |
| 12 | 0.011228 | 0.011206 | 0.011209 | 47 | 0.015622 | 0.01566 | 0.015666 |
| 13 | 0.013169 | 0.013069 | 0.013062 | 48 | 0.003226 | 0.003226 | 0.003226 |
| 14 | 0.018158 | 0.018129 | 0.018118 | 49 | 0.003226 | 0.003226 | 0.003226 |
| 15 | 0.003981 | 0.003983 | 0.003984 | 50 | 0.003226 | 0.003226 | 0.003226 |
| 16 | 0.01859 | 0.018594 | 0.018605 | 51 | 0.003226 | 0.003226 | 0.003226 |
| 17 | 0.019374 | 0.019375 | 0.019386 | 52 | 0.003226 | 0.003226 | 0.003226 |
| 18 | 0.003226 | 0.003226 | 0.003226 | 53 | 0.003226 | 0.003226 | 0.003226 |
| 19 | 0.024718 | 0.024714 | 0.024736 | 54 | 0.003226 | 0.003226 | 0.003226 |
| 20 | 0.027962 | 0.027957 | 0.027989 | 55 | 0.003226 | 0.003226 | 0.003226 |
| 21 | 0.003226 | 0.003226 | 0.003226 | 56 | 0.030772 | 0.030779 | 0.030772 |
| 22 | 0.033784 | 0.033798 | 0.033716 | 57 | 0.031345 | 0.031349 | 0.031331 |
| 23 | 0.017424 | 0.017455 | 0.017329 | 58 | 0.027906 | 0.027904 | 0.027892 |
| 24 | 0.032429 | 0.032426 | 0.032494 | 59 | 0.015133 | 0.015133 | 0.015143 |
| 25 | 0.032009 | 0.032014 | 0.032049 | 60 | 0.003226 | 0.003226 | 0.003226 |
| 26 | 0.01956 | 0.01952 | 0.019539 | 61 | 0.017391 | 0.017387 | 0.017407 |
| 27 | 0.036274 | 0.036269 | 0.036296 | 62 | 0.018022 | 0.018014 | 0.018065 |
| 28 | 0.025003 | 0.025007 | 0.025016 | 63 | 0.027486 | 0.027482 | 0.027503 |
| 29 | 0.003226 | 0.003226 | 0.003226 | 64 | 0.030952 | 0.030958 | 0.030934 |
| 30 | 0.028377 | 0.028435 | 0.028387 | 65 | 0.039544 | 0.03955 | 0.039533 |
| 31 | 0.031616 | 0.031624 | 0.031628 | 66 | 0.032676 | 0.032685 | 0.032661 |
| 32 | 0.02091 | 0.020911 | 0.020869 | 67 | 0.041584 | 0.041586 | 0.041589 |
| 33 | 0.003226 | 0.003226 | 0.003226 | 68 | 0.003226 | 0.003226 | 0.003226 |
| 34 | 0.020255 | 0.020258 | 0.020261 | 69 | 0.064516 | 0.064516 | 0.064516 |
| 35 | 0.003226 | 0.003226 | 0.003226 | 70 | 0.032503 | 0.032492 | 0.032506 |

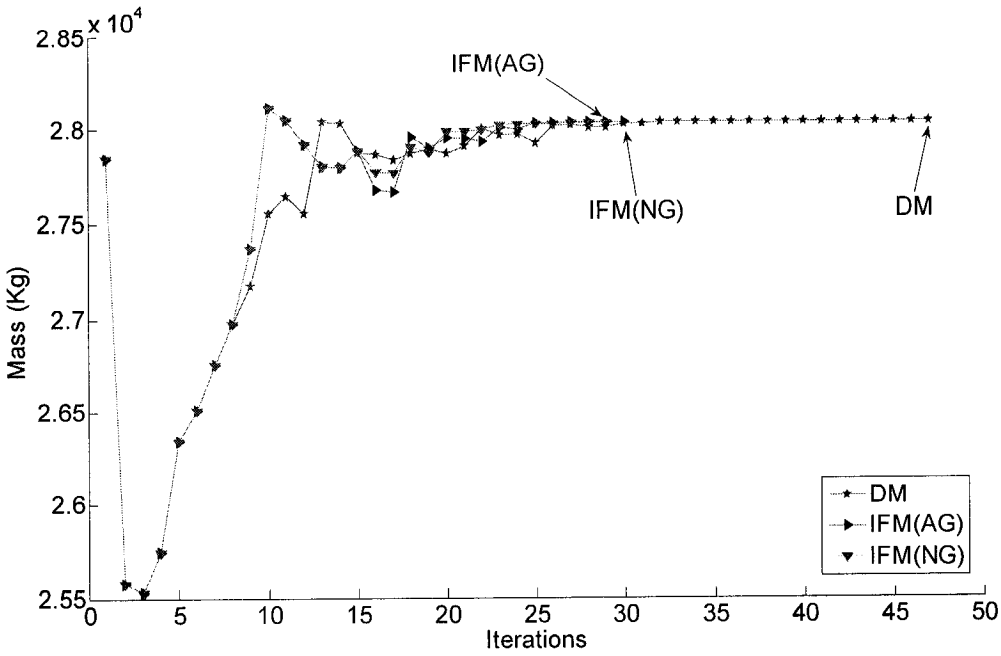


**Figure 4.9** Convergence curve for the 70-members frame structure under stress constraints

The convergence curves of all optimization algorithms are shown in Figure 4.9. It can be seen that the IFM(NG) and the IFM(AG) almost follow the same path, but the DM follows the different path. The IFM converges to optimized result quite rapidly as compared to DM.

It can be concluded that the IFM is very efficient for the stress dominating optimization problem, and is also equally efficient for displacement dominated problems. Moreover evaluating the gradient of constraints analytically significantly improves the efficiency of the optimization algorithm.

## 4.3 Size Optimization -Frequency Constraints

Here, the efficiency and accuracy of the IFM for the frequency constraints are investigated, and compared with those of the DM, and also those reported in the literature. The 70 member frame structure as shown in Figure 4.7 is considered, but now it is subjected to different loading. All the horizontal members of the structure carry the uniformly distributed nonstructural weight of 450 Kg/m. Frames are made from steel having weight density of 7757 Kg/m$^3$ and an elastic modulus of $2\times10^{11}$ Pa. The minimum area limit for all the members is specified at 0.0019355 m$^2$, while the maximum area limit is set at 0.056955m$^2$. The mass of the frame structure is minimized for three different cases of frequency constraints:

Case 1: The second natural frequency is 7 Hz. ($\omega_2 = 7$ HZ).

Case 2: The first and second natural frequencies are greater than 2 Hz and 7Hz, respectively. ($\omega_1 \geq 2, \omega_2 \geq 7$).

Case 3: The first, second and third natural frequencies are greater than 2Hz, 7 Hz and 15 Hz, respectively. ($\omega_1 \geq 2, \omega_2 \geq 7, \omega_3 \geq 15$).

The problem is investigated using the IFM(NG), the IFM(AG) and the DM. The results of the optimization analysis are also compared with those obtained by McGee and Phan [64] who investigated the problem using optimal criteria method and the DM. The design variables are the cross sectional area of the members, and the other parameters such as shear modulus and moment of area are related to cross sectional area by relation given by McGee and Phan [64]. Similar to other problems multiple of random initial point has been generated to find the optimal solution. Here, it has been observed that the problem has number of local optimums and different initial points converge to different local

optimum point. It has been found that the two best optimal results obtained are associated with initial points of 0.0129032 $m^2$ and 0.0258064 $m^2$, for the cross sectional area of all members. The optimal results corresponding to these two initial points are presented for all the following cases.

### 4.3.1 Case1: 70 Member Frame Structure-Single Frequency Constraint

The mass of 70 member frame structure as shown in Figure 4.7 is minimized under equality constraint that the second natural frequency to be 7 Hz. The problem was investigated with different initial designs, and the minimum optimum mass is obtained at starting design of 0.0258064 $m^2$ for all the algorithms. The results of the optimization algorithm for the first five natural frequencies with two best starting design are given in Table 4.8. The finial optimum results for the cross sectional areas corresponding to initial point of 0.0258064 $m^2$ are tabulated in Tables 4.8. A minimum mass of 34839 Kg is obtained using the DM, and minimum mass of 34694 Kg and 34520 Kg are obtained using the IFM(NG) and the IFM(AG), respectively. A minimum mass of 36292.82Kg was obtained by McGee and Phan [64] using optimal criteria and the DM. It can be seen that the IFM converges to lighter design than the DM. The optimization problem subjected to frequency constraints is numerically expensive using the IFM due to presence of null rows in the mass matrix. The problem of large computation time is alleviated by calculating the gradients by analytical method. It has been observed that in some cases calculation of gradient by analytical method led to the lighter optimum design. This is because that numerical sensitivity analysis is not very accurate, and small

error in the gradient calculation can change the path of the optimization algorithm and it can converge to other local minima.

**Table 4.8** Final five frequencies of the 70-members frame structure at the optimum point, designed for Case 1.

| Analysis Method | Initial Design -0.0019355 $m^2$ | | | Initial Design-0.0258064 $m^2$ | | |
|---|---|---|---|---|---|---|
| | DM | IFM(NG) | IFM(AG) | DM | IFM(NG) | IFM(AG) |
| First | 1.1798 | 1.1841 | 1.2311 | 1.2076 | 1.2144 | 1.2451 |
| Second | 7 | 7 | 6.9999 | 7 | 7 | 7 |
| Third | 7.3265 | 7.0934 | 7.0001 | 7.2225 | 7 | 8.0522 |
| Fourth | 8.7866 | 9.4406 | 8.7001 | 9.1372 | 9.1918 | 8.935 |
| Fifth | 12.103 | 11.742 | 11.631 | 12.42 | 11.636 | 12.267 |
| Mass(Kg) | 35580 | 35288 | 35666 | 34839 | 34694 | 34520 |

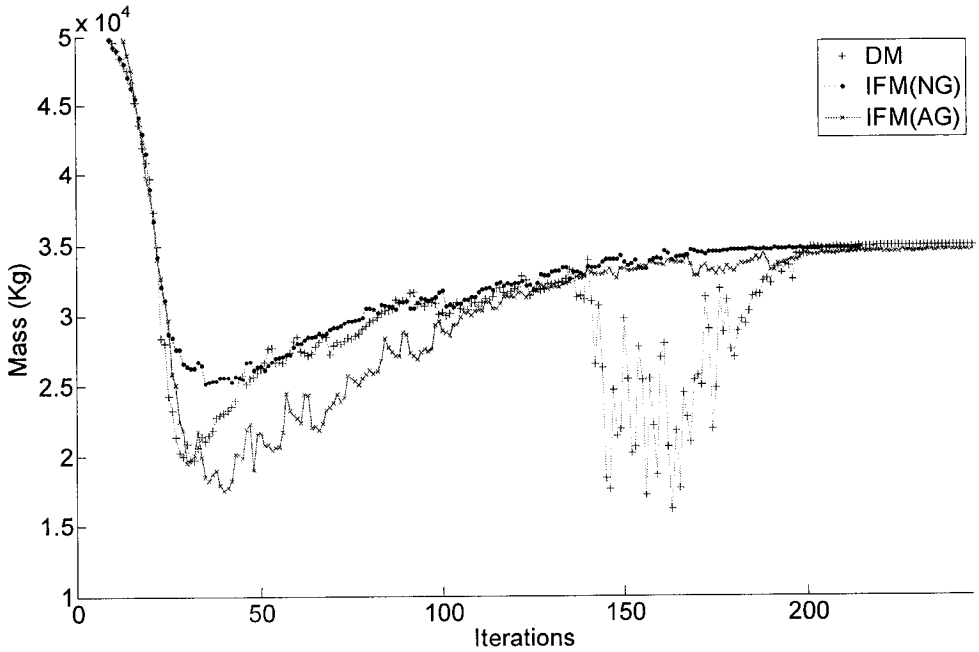


**Figure 4.10** Convergence curve for the 70-member frame structure optimized for Case1

**Table 4.9** Optimum design for the cross sectional area ($m^2$) of the 70 member frame structure designed for Case1

| Member No. | IFM(AG) | IFM(NG) | DM | Member No. | IFM(AG) | IFM(NG) | DM |
|---|---|---|---|---|---|---|---|
| 1 | 0.039 | 0.0337 | 0.0329 | 36 | 0.0025 | 0.0019 | 0.0019 |
| 2 | 0.0284 | 0.0166 | 0.0164 | 37 | 0.0019 | 0.0019 | 0.0019 |
| 3 | 0.0191 | 0.0219 | 0.0213 | 38 | 0.0024 | 0.0019 | 0.0019 |
| 4 | 0.0248 | 0.0284 | 0.0268 | 39 | 0.002 | 0.0025 | 0.0024 |
| 5 | 0.0243 | 0.0207 | 0.0178 | 40 | 0.0025 | 0.0019 | 0.0019 |
| 6 | 0.0166 | 0.0284 | 0.0284 | 41 | 0.0019 | 0.0019 | 0.0019 |
| 7 | 0.0381 | 0.0019 | 0.0019 | 42 | 0.0025 | 0.0019 | 0.0019 |
| 8 | 0.0019 | 0.0019 | 0.0019 | 43 | 0.0019 | 0.0459 | 0.0526 |
| 9 | 0.0019 | 0.0019 | 0.0019 | 44 | 0.0022 | 0.0421 | 0.0474 |
| 10 | 0.0019 | 0.0019 | 0.0019 | 45 | 0.0369 | 0.023 | 0.0019 |
| 11 | 0.0019 | 0.0019 | 0.0019 | 46 | 0.0321 | 0.0058 | 0.0152 |
| 12 | 0.0019 | 0.0022 | 0.0138 | 47 | 0.0019 | 0.0019 | 0.0161 |
| 13 | 0.0019 | 0.0019 | 0.0019 | 48 | 0.003 | 0.0287 | 0.0265 |
| 14 | 0.0019 | 0.0198 | 0.0021 | 49 | 0.0019 | 0.0023 | 0.0019 |
| 15 | 0.0019 | 0.0019 | 0.0019 | 50 | 0.004 | 0.0019 | 0.0019 |
| 16 | 0.0429 | 0.0062 | 0.0032 | 51 | 0.0284 | 0.0019 | 0.0019 |
| 17 | 0.0477 | 0.0019 | 0.0019 | 52 | 0.0313 | 0.0319 | 0.0284 |
| 18 | 0.0084 | 0.0422 | 0.0443 | 53 | 0.0067 | 0.0284 | 0.0284 |
| 19 | 0.0351 | 0.0393 | 0.0373 | 54 | 0.0019 | 0.0302 | 0.0378 |
| 20 | 0.0284 | 0.0198 | 0.0178 | 55 | 0.0071 | 0.0124 | 0.0125 |
| 21 | 0.0019 | 0.0247 | 0.0264 | 56 | 0.0019 | 0.0019 | 0.0019 |
| 22 | 0.0284 | 0.0039 | 0.0095 | 57 | 0.0071 | 0.0111 | 0.0111 |
| 23 | 0.0019 | 0.0027 | 0.0019 | 58 | 0.0019 | 0.0019 | 0.0019 |
| 24 | 0.0284 | 0.0029 | 0.0062 | 59 | 0.0065 | 0.0101 | 0.0102 |
| 25 | 0.0019 | 0.0029 | 0.0032 | 60 | 0.0019 | 0.0019 | 0.0019 |
| 26 | 0.0225 | 0.0041 | 0.0033 | 61 | 0.0064 | 0.0104 | 0.0102 |
| 27 | 0.0338 | 0.0284 | 0.0284 | 62 | 0.0019 | 0.0019 | 0.0019 |
| 28 | 0.0252 | 0.0281 | 0.0278 | 63 | 0.0065 | 0.0118 | 0.0116 |
| 29 | 0.0471 | 0.0338 | 0.0331 | 64 | 0.0019 | 0.0019 | 0.0019 |
| 30 | 0.045 | 0.031 | 0.0316 | 65 | 0.0066 | 0.0108 | 0.0108 |
| 31 | 0.0019 | 0.0019 | 0.0019 | 66 | 0.0019 | 0.0019 | 0.0019 |
| 32 | 0.0035 | 0.002 | 0.0019 | 67 | 0.0076 | 0.0125 | 0.012 |
| 33 | 0.0019 | 0.0019 | 0.0019 | 68 | 0.0019 | 0.0019 | 0.0019 |
| 34 | 0.0031 | 0.0019 | 0.0019 | 69 | 0.0116 | 0.0282 | 0.0254 |
| 35 | 0.0022 | 0.0019 | 0.0019 | 70 | 0.0043 | 0.002 | 0.0019 |

It is seen from the convergence study shown in Figure 4-10 that the IFM converge to the optimized solution more rapidly as compared to the DM and also led to lighter design. The deviation of the DM from the optimized solution is more as compared to any other analysis procedure. It can be concluded from this study that path of the optimization algorithm depends on the analysis procedure, and the IFM is better in comparison of convergence and accuracy of the results. Further, the IFM(AG) and the IFM(NG) follow the different optimization path. The numerically calculated gradient deviate the path of the IFM and led to premature convergence which result in the heavier optimum design corresponding to other local optima.

### 4.3.2 Case 2:70-Member Frame Structure-Two Frequency Constraint

In this case, the mass of the structure is minimized such that the first and second natural frequencies are greater than 2 Hz and 7 Hz, respectively. The optimization results for the first five natural frequencies with two best starting designs are shown in Table 4.11, and the finial optimum design of the structure is tabulated in Table 4.10.

It can be observed that the initial point that give the minimum optimal solution for the IFM can be different from the initial point that give the minimum optimal solution for the DM. It is interesting to note that for this problem the IFM produce minimum mass using initial design of 0.0019355 $m^2$, where as the DM produce minimum mass using initial design of 0.0258064 $m^2$. A minimum mass of 38356 Kg and 38354 Kg is obtained using the IFM(NG) and IFM(AG), respectively with initial design of 0.0019355$m^2$. A minimum mass of 38802Kg is obtained using the DM with initial design of 0.0258064$m^2$.

**Table 4.10** Optimum design for the cross sectional area ($m^2$) of the 70-members frame structure designed for Case2.

| Member No | IFM(AG) | IFM(NG) | DM | Member No | IFM(AG) | IFM(NG) | DM |
|---|---|---|---|---|---|---|---|
| 1 | 0.0441 | 0.0019 | 0.0514 | 36 | 0.0118 | 0.0115 | 0.0251 |
| 2 | 0.0284 | 0.0019 | 0.0284 | 37 | 0.0019 | 0.0019 | 0.0019 |
| 3 | 0.0248 | 0.0019 | 0.0135 | 38 | 0.0136 | 0.0088 | 0.0228 |
| 4 | 0.0243 | 0.0019 | 0.0119 | 39 | 0.0019 | 0.0019 | 0.0019 |
| 5 | 0.0225 | 0.0019 | 0.0126 | 40 | 0.0144 | 0.025 | 0.0284 |
| 6 | 0.0172 | 0.0019 | 0.0115 | 41 | 0.0286 | 0.0289 | 0.0296 |
| 7 | 0.0123 | 0.0019 | 0.0117 | 42 | 0.0314 | 0.0142 | 0.0283 |
| 8 | 0.0153 | 0.0019 | 0.0124 | 43 | 0.0394 | 0.0394 | 0.0399 |
| 9 | 0.0314 | 0.0019 | 0.0312 | 44 | 0.0019 | 0.0389 | 0.0191 |
| 10 | 0.0019 | 0.0019 | 0.0019 | 45 | 0.0019 | 0.0019 | 0.0019 |
| 11 | 0.0019 | 0.0019 | 0.0019 | 46 | 0.0019 | 0.0059 | 0.0019 |
| 12 | 0.0285 | 0.0019 | 0.0286 | 47 | 0.0019 | 0.0019 | 0.0019 |
| 13 | 0.0314 | 0.0019 | 0.0328 | 48 | 0.0019 | 0.0284 | 0.0019 |
| 14 | 0.0059 | 0.0019 | 0.008 | 49 | 0.002 | 0.002 | 0.0022 |
| 15 | 0.0393 | 0.0019 | 0.0345 | 50 | 0.0019 | 0.0019 | 0.0019 |
| 16 | 0.0388 | 0.0019 | 0.0347 | 51 | 0.0019 | 0.0019 | 0.0019 |
| 17 | 0.0019 | 0.0019 | 0.0019 | 52 | 0.0019 | 0.0311 | 0.0019 |
| 18 | 0.0142 | 0.0314 | 0.0285 | 53 | 0.0019 | 0.0314 | 0.0019 |
| 19 | 0.0019 | 0.0019 | 0.0019 | 54 | 0.0019 | 0.0395 | 0.0019 |
| 20 | 0.0251 | 0.0144 | 0.0022 | 55 | 0.0019 | 0.0153 | 0.0019 |
| 21 | 0.0233 | 0.0019 | 0.0019 | 56 | 0.0019 | 0.0019 | 0.0019 |
| 22 | 0.0087 | 0.0136 | 0.0019 | 57 | 0.0019 | 0.0123 | 0.0019 |
| 23 | 0.0125 | 0.0019 | 0.0019 | 58 | 0.0019 | 0.0019 | 0.0019 |
| 24 | 0.0114 | 0.0119 | 0.002 | 59 | 0.0019 | 0.0171 | 0.0019 |
| 25 | 0.0284 | 0.0019 | 0.0019 | 60 | 0.0019 | 0.0232 | 0.0235 |
| 26 | 0.0248 | 0.0118 | 0.0278 | 61 | 0.0019 | 0.0223 | 0.0173 |
| 27 | 0.0361 | 0.0019 | 0.0284 | 62 | 0.0019 | 0.0125 | 0.0142 |
| 28 | 0.0284 | 0.0132 | 0.0284 | 63 | 0.0019 | 0.0243 | 0.0044 |
| 29 | 0.049 | 0.0019 | 0.0532 | 64 | 0.0019 | 0.0284 | 0.0019 |
| 30 | 0.047 | 0.0284 | 0.0387 | 65 | 0.0019 | 0.0247 | 0.0042 |
| 31 | 0.0019 | 0.0019 | 0.0019 | 66 | 0.0019 | 0.036 | 0.0019 |
| 32 | 0.0131 | 0.0283 | 0.0076 | 67 | 0.0019 | 0.0285 | 0.0044 |
| 33 | 0.0019 | 0.0019 | 0.0211 | 68 | 0.0019 | 0.0491 | 0.0019 |
| 34 | 0.0117 | 0.0249 | 0.0187 | 69 | 0.0019 | 0.0442 | 0.006 |
| 35 | 0.0027 | 0.0027 | 0.0284 | 70 | 0.0284 | 0.0468 | 0.0094 |

**Table 4.11** Final five frequencies of the 70-members frame structure at the optimum point, designed for Case 2.

| Analysis Method | Initial Design -0.0019355 $m^2$ | | | Initial Design-0.0258064 $m^2$ | | |
|---|---|---|---|---|---|---|
| | DM | IFM(NG) | IFM(AG) | DM | IFM(NG) | IFM(AG) |
| First | 2 | 2 | 2 | 2 | 2 | 1.9999 |
| Second | 7 | 7 | 6.9997 | 7 | 7 | 6.9997 |
| Third | 7.6296 | 8.7088 | 8.7087 | 7.6357 | 8.709 | 9.1821 |
| Fourth | 10.815 | 9.5094 | 9.5204 | 10.62 | 9.3599 | 10.443 |
| Fifth | 13.715 | 12.231 | 12.228 | 12.412 | 12.452 | 11.035 |
| Mass(Kg) | 41155 | 38356 | 38354 | 38802 | 38476 | 40378 |

The optimized cross sectional areas corresponding to these optimum designs are given in Table 4.10. It is noted that again the IFM converges to lighter design in comparison to the DM. Further, analytical gradient increases the performance of the IFM, and produced even lighter design than that with numerical gradient. It should be noted that a minimum mass 46494.67 Kg was obtained by McGee and Phan [64] using optimal criteria method and the DM.

### 4.3.3 Case3:70-Member Frame Structure-Three Frequency Constraint

Finally, the mass of the structure is minimized so that the first, second and third natural frequencies be greater than 2 Hz, 7 Hz and 15 Hz, respectively. The first five natural frequencies and optimized mass using all the analysis methods are shown in Table 4-12. For both the IFM and the DM, the minimum optimum mass is obtained using starting design of 0.0258064$m^2$. A mass of 55418 Kg is obtained using the DM, and a mass of 54557 Kg and 54252 Kg are obtained using the IFM(NG) and the IFM(AG), respectively. It should be noted that a minimum mass of 61369.05 Kg was obtained by McGee and Phan [64] using optimal criteria method and the DM. The cross sectional area of all the

members corresponding to optimum solution using the IFM(AG), the IFM(NG) and the DM are provided in Table 4.13.

**Table 4.12** Final five frequencies of the 70-members frame structure at the optimum point, designed for Case 3.

| Analysis Method | Initial Design -0.0019355 $m^2$ | | | Initial Design-0.0258064 $m^2$ | | |
|---|---|---|---|---|---|---|
| | DM | IFM(NG) | IFM(AG) | DM | IFM(NG) | FM(AG) |
| First | 2 | 2 | 2 | 2 | 2.0478 | 2 |
| Second | 7 | 7 | 7 | 7 | 7 | 7 |
| Third | 15 | 15 | 15 | 15 | 15 | 15 |
| Fourth | 17.616 | 16.382 | 16.382 | 15.09 | 15.325 | 15.306 |
| Fifth | 18.441 | 17.465 | 17.004 | 18.3 | 17.111 | 18.072 |
| Mass(Kg) | 56389 | 54891 | 54797 | 55418 | 54557 | 54252 |

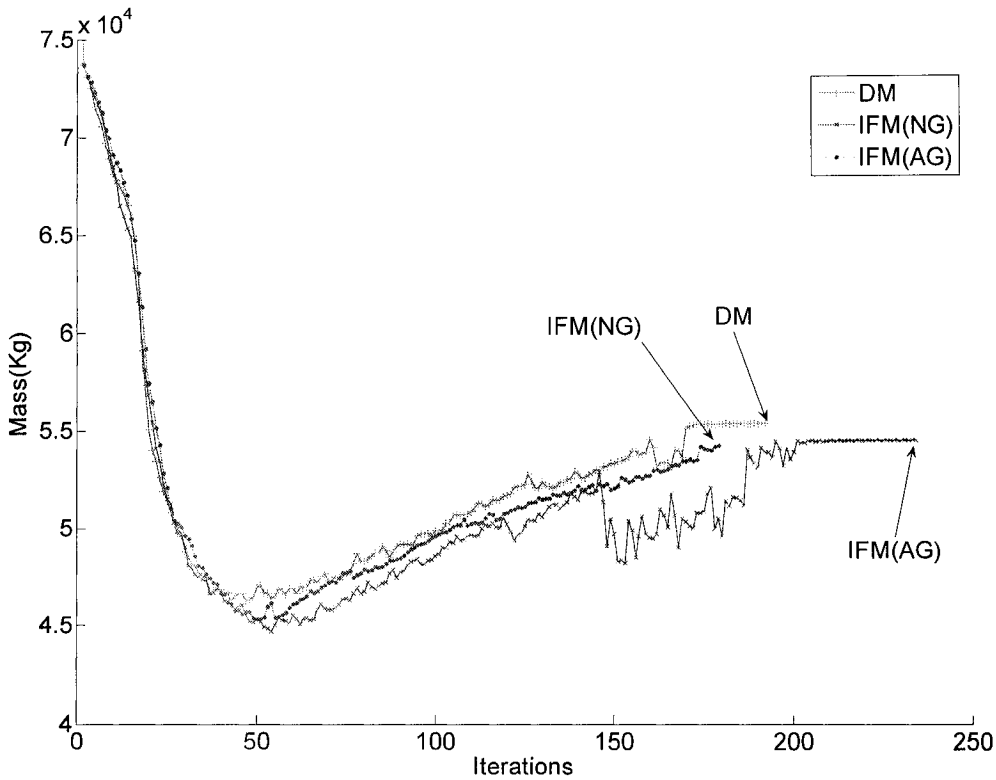


**Figure 4-11** Convergence curve for the 70-members frame structure optimized for case3

**Table 4.13** Optimum design for the cross sectional area ($m^2$) of the 70-members frame structure designed for Case3

| Member No. | IFM(AG) | IFM(NG) | DM | Member No. | IFM(AG) | IFM(NG) | DM |
|---|---|---|---|---|---|---|---|
| 1 | 0.034 | 0.0434 | 0.0355 | 36 | 0.0242 | 0.0285 | 0.0212 |
| 2 | 0.0217 | 0.0207 | 0.0268 | 37 | 0.0019 | 0.0019 | 0.0019 |
| 3 | 0.0228 | 0.0249 | 0.028 | 38 | 0.0324 | 0.0298 | 0.0356 |
| 4 | 0.0222 | 0.0244 | 0.0265 | 39 | 0.0371 | 0.0336 | 0.0472 |
| 5 | 0.0133 | 0.0309 | 0.0214 | 40 | 0.0291 | 0.0286 | 0.0284 |
| 6 | 0.01 | 0.0272 | 0.0161 | 41 | 0.0289 | 0.0284 | 0.032 |
| 7 | 0.01 | 0.0266 | 0.0196 | 42 | 0.0213 | 0.0283 | 0.024 |
| 8 | 0.0258 | 0.0283 | 0.0284 | 43 | 0.0019 | 0.0284 | 0.0019 |
| 9 | 0.0019 | 0.0325 | 0.0019 | 44 | 0.0199 | 0.0284 | 0.0281 |
| 10 | 0.0019 | 0.0019 | 0.0019 | 45 | 0.0029 | 0.0284 | 0.0203 |
| 11 | 0.0019 | 0.0019 | 0.0019 | 46 | 0.0275 | 0.0172 | 0.0285 |
| 12 | 0.0224 | 0.04 | 0.0287 | 47 | 0.0347 | 0.0412 | 0.0495 |
| 13 | 0.0019 | 0.0354 | 0.0019 | 48 | 0.0293 | 0.0294 | 0.0409 |
| 14 | 0.0293 | 0.033 | 0.0288 | 49 | 0.0206 | 0.0019 | 0.0019 |
| 15 | 0.0289 | 0.0418 | 0.0299 | 50 | 0.0019 | 0.0019 | 0.0019 |
| 16 | 0.0173 | 0.0292 | 0.028 | 51 | 0.0019 | 0.0019 | 0.0019 |
| 17 | 0.0208 | 0.0019 | 0.0304 | 52 | 0.0286 | 0.0019 | 0.0284 |
| 18 | 0.0225 | 0.0262 | 0.0284 | 53 | 0.0283 | 0.0021 | 0.0284 |
| 19 | 0.0019 | 0.0019 | 0.0019 | 54 | 0.0314 | 0.0019 | 0.0286 |
| 20 | 0.0281 | 0.0286 | 0.0284 | 55 | 0.0241 | 0.003 | 0.0159 |
| 21 | 0.0019 | 0.0295 | 0.0019 | 56 | 0.0233 | 0.0019 | 0.0019 |
| 22 | 0.0277 | 0.0342 | 0.0284 | 57 | 0.0216 | 0.0037 | 0.0131 |
| 23 | 0.0274 | 0.0465 | 0.0284 | 58 | 0.0019 | 0.0019 | 0.0019 |
| 24 | 0.0122 | 0.0316 | 0.0129 | 59 | 0.0196 | 0.0043 | 0.013 |
| 25 | 0.0019 | 0.0019 | 0.0019 | 60 | 0.0289 | 0.0019 | 0.0019 |
| 26 | 0.0115 | 0.0284 | 0.011 | 61 | 0.0273 | 0.0054 | 0.0238 |
| 27 | 0.0019 | 0.0019 | 0.0019 | 62 | 0.0386 | 0.0019 | 0.036 |
| 28 | 0.0138 | 0.0217 | 0.0129 | 63 | 0.0278 | 0.0049 | 0.0276 |
| 29 | 0.0287 | 0.033 | 0.0285 | 64 | 0.0278 | 0.0019 | 0.0225 |
| 30 | 0.034 | 0.0374 | 0.0358 | 65 | 0.0241 | 0.0056 | 0.0228 |
| 31 | 0.0019 | 0.0019 | 0.0019 | 66 | 0.0019 | 0.0019 | 0.0019 |
| 32 | 0.0205 | 0.0274 | 0.025 | 67 | 0.0226 | 0.008 | 0.0219 |
| 33 | 0.0019 | 0.0019 | 0.0019 | 68 | 0.0288 | 0.0285 | 0.0319 |
| 34 | 0.0207 | 0.0281 | 0.0216 | 69 | 0.0389 | 0.0389 | 0.0377 |
| 35 | 0.0019 | 0.0282 | 0.0019 | 70 | 0.0317 | 0.0378 | 0.0396 |

The iteration history for the DM, the IFM (AG) and the IFM(NG) is presented in the Figure 4-11. It can be seen that all optimization algorithms take the different optimization path and converge to the different optimum results. The small difference in the gradient calculation and performance measures can change the path of the optimization algorithms. Although the numbers of iterations for the IFM(AG) are more than IFM(NG), but it converge to the lighter result. The inaccuracy in the numerical gradient leads to the premature convergence using the IFM(NG).

It can be concluded that the IFM and the DM can converge to the different optimum results for structures subjected to single or multiple frequency constraints. The gradient calculation with analytical method can change the path of the optimization algorithm and can lead to the better design. As discussed in last chapter, the numerically gradient calculation highly depends on the step size and choosing appropriate step size for the finite difference gradient is challenging task. Therefore analytical calculated gradient can provide the best direction to the optimization algorithm.

# Chapter 5

# DESIGN OPTIMIZATION OF STIFFENED PANELS USING IFM

## 5.1 Introduction

Stiffened panels are structural components, consisting of plates reinforced by a system of stiffeners to enhance their load carrying capacity. The advantage of stiffening a plate lies in achieving an economical and light weight design. While stiffening elements add negligible weight to the structure, their influence on strength and stability is enormous. These structures are widely used in aircraft, ship, bridge, building and some other engineering activities. In many circumstances, these structures are found to be exposed to in-plane loading. The buckling characteristics of these structures subjected to uniform in-plane loading is of considerable importance, while designing for the aerospace [64], naval [65] and civil engineering applications.

In this chapter, the FE formulation based on the IFM is developed for the elastic buckling analysis of eccentrically stiffened panels. The panel and the stiffener are modeled using two different IFM finite elements, and the compatibility between them is maintained. The force finite element buckling analysis is performed for different sizes of stiffened panels and convergence with increasing mesh size is studied. Further, the force FE buckling analysis is combined with SQP technique to develop a design optimization methodology to optimize the size of the stiffened panel while guarding against the elastic buckling. The

analytical expressions of the design sensitivity of the buckling load with respect to the plate and the stiffener dimensions are also formulated using the IFM. The sensitivity analysis is then integrated with the optimization algorithm to provide the gradient information to SQP gradient based optimization technique. Finally, the developed design optimization methodology is used to optimize the unflange and the flange stiffened panels subjected to uniform compression loading.

## 5.2 Finite Element Formulation

The FE model for the elastic stability analysis of the eccentrically stiffened panels based on the IFM is developed. The stiffened panel and references axis are shown in Figure 5-1. The mid plane of the panel is considered as reference plane for both the panel and the stiffener. The centroidal axis of the stiffener is eccentric from the reference axis by the distance *e* which is called eccentricity of the stiffener.

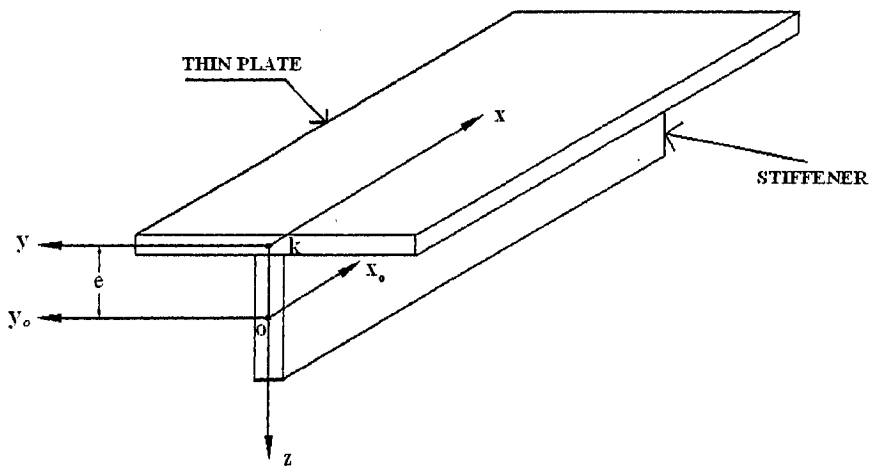


**Figure 5-1** Stiffened panel

The stiffener and the panel are assumed to buckle simultaneously and the formulation is based on the behavior of the panel-stiffener system, and not on the behavior of separate components. The stiffener is assumed to be of solid cross section, i.e. warping effects are neglected. The bending strain developed due to the action of in plane loading is considered for the buckling analysis. The panel and the stiffener are descretized by using 4-node shell element and 2-node space frame element, respectively. The expressions for the equilibrium, the geometric stiffness and the flexibility matrices for both the panel and the stiffener elements are formulated in the next section.

### 5.2.1 Shell Element

The shell element and the corresponding displacement degrees of freedom are shown in Figure 5-2. The shell element is combination of the plate and the membrane element. The bending and the membrane deformations are considered independent of each other and the FE matrices are formulated separately for these cases. The final matrices are obtained by superposition of plate and membrane matrices.

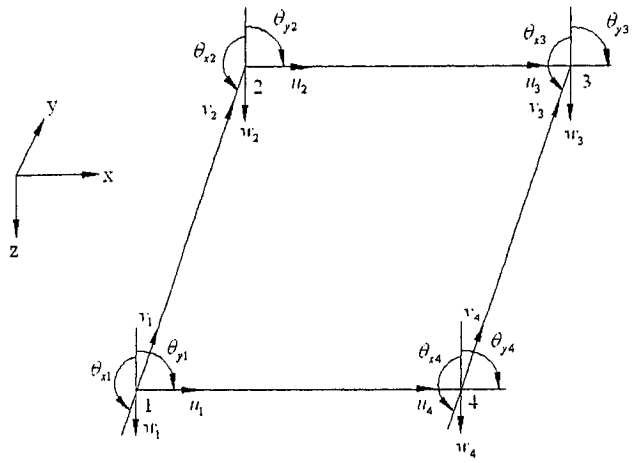


**Figure 5-2** The displacement degrees of freedom of 4-node shell element

The element has four nodes and five displacement degrees of freedom at each node as shown in Figure 5-2. Three displacement degrees of freedom are corresponding to the plate element and two are corresponding to membrane element.

*Plate Element*

The bending state displacement $w$ within the element is interpolated in terms of deflection $w_i$, rotation about $x$ direction $\theta_{xi}$ and rotation about y direction $\theta_{yi}$. The Kirchhoff's assumption that line normal to the surface of the plate remain normal after the bending, is assumed, thus transverse shear deformation is neglected. Due to this assumption, the rotational displacements are related to transverse displacements as:

$$\theta_{xi} = -\frac{\partial w_i}{\partial y}, \quad \theta_{yi} = \frac{\partial w_i}{\partial x} \tag{5-1}$$

The negative sign in $\theta_{xi}$ is due to the fact that to have positive moment along $x$ direction, negative displacement $w$ is required. The displacement field within the element is interpolated with hermitian interpolation, and is given by:

$$\begin{aligned} w = {} & N_{1p} w_1 + N_{2p} \theta_{x1} + N_{3p} \theta_{y1} + N_{4p} w_2 \\ & + N_{5p} \theta_{x2} + N_{6p} \theta_{y2} + N_{7p} w_3 + N_{8p} \theta_{x3} \\ & + N_{9p} \theta_{y3} + N_{10p} w_4 + N_{11p} \theta_{x4} + N_{12p} \theta_{y4} \end{aligned} \tag{5-2}$$

where

$$\begin{aligned} & N_{1p} = H_{01}(x)H_{01}(y), \quad N_{2p} = -H_{01}(x)H_{11}(y), \quad N_{3p} = H_{11}(x)H_{01}(y) \\ & N_{4p} = H_{01}(x)H_{02}(y), \quad N_{5p} = -H_{01}(x)H_{12}(y), \quad N_{6p} = H_{11}(x)H_{02}(y), \\ & N_{7p} = H_{02}(x)H_{02}(y), \quad N_{8p} = -H_{02}(x)H_{12}(y), \quad N_{9p} = H_{12}(x)H_{02}(y) \\ & N_{10p} = H_{02}(x)H_{01}(y), \quad N_{11p} = -H_{02}(x)H_{11}(y), \quad N_{12p} = H_{12}(x)H_{01}(y) \end{aligned} \tag{5-3}$$

where $H_{01}(x), H_{02}(x), H_{11}(x)$ and $H_{12}(x)$ can be obtained from Eq.(2-106), and $H_{01}(y)$

$H_{02}(y), H_{11}(y)$ and $H_{12}(y)$ can be obtained from Eq.(2-106) by changing $x$ to $y$ and $a$ to $b$.

The moment field is interpolated similar to Eq. (2-108) and the stress interpolation matrix is obtained from Eq. (2-110). The equilibrium matrix for 4-node plate element corresponding to the bending deformations is obtained by substituting the displacement and stress interpolation from Eqs. (5-2) and (2-110), respectively into Eq. (2-20), and is given by:

$$[B_e]_B = \begin{bmatrix}
0 & b & 0 & -\frac{2b^2}{5} & 0 & 0 & a & -\frac{2a^2}{5} & -2 \\
0 & -\frac{b^2}{3} & 0 & \frac{b^3}{15} & a & -\frac{2a^2}{5} & -ab & \frac{2a^2b}{5} & 0 \\
-b & ab & \frac{2b^2}{5} & -\frac{2ab^2}{5} & 0 & 0 & \frac{a^2}{3} & -\frac{a^3}{15} & 0 \\
0 & b & 0 & \frac{2b^2}{5} & 0 & 0 & -a & \frac{2a^2}{5} & 2 \\
0 & \frac{b^2}{3} & 0 & \frac{b^3}{15} & -a & \frac{2a^2}{5} & -ab & \frac{2a^2b}{5} & 0 \\
-b & ab & -\frac{2b^2}{5} & \frac{2ab^2}{5} & 0 & 0 & -\frac{a^2}{3} & \frac{a^3}{15} & 0 \\
0 & -b & 0 & -\frac{2b^2}{5} & 0 & 0 & -a & -\frac{2a^2}{5} & -2 \\
0 & -\frac{b^2}{3} & 0 & -\frac{b^3}{15} & -a & -\frac{2a^2}{5} & -ab & -\frac{2a^2b}{5} & 0 \\
b & ab & \frac{2b^2}{5} & \frac{2ab^2}{5} & 0 & 0 & \frac{a^2}{3} & \frac{a^3}{15} & 0 \\
0 & -b & 0 & \frac{2b^2}{5} & 0 & 0 & a & \frac{2a^2}{5} & 2 \\
0 & \frac{b^2}{3} & 0 & -\frac{b^3}{15} & a & \frac{2a^2}{5} & -ab & -\frac{2a^2b}{5} & 0 \\
b & ab & -\frac{2b^2}{5} & -\frac{2ab^2}{5} & 0 & 0 & -\frac{a^2}{3} & -\frac{a^3}{15} & 0
\end{bmatrix} \qquad (5\text{-}4)$$

The flexibility matrix corresponding to stress filed of Eq. (2-110) can be obtained from Eq. (2-115).

*Membrane Element*

The equilibrium and flexibility matrices for the membrane degrees of freedom are formulated in the section 2.8.4, and can be obtained from the Eqs. (2-103) and (2-104), respectively.

The geometric stiffness matrix corresponding to the membrane degrees of freedom is null matrix. Therefore, the geometric stiffness matrix of shell element contains terms only corresponding to the bending degrees of freedom, and those can be evaluated from the following equation [16]:

$$[K_g]_p = \int_{-b}^{b}\int_{-a}^{a}[A]^T\begin{bmatrix} n_x & n_{xy} \\ n_{xy} & n_y \end{bmatrix}dx\,dy \tag{5-5}$$

where

$$[A]=\begin{bmatrix} \frac{\partial N_{1p}}{\partial x} & \frac{\partial N_{2p}}{\partial x} & \cdots & \frac{\partial N_{ip}}{\partial x} & \cdots & \frac{\partial N_{12p}}{\partial x} \\ \frac{\partial N_{1p}}{\partial y} & \frac{\partial N_{2p}}{\partial y} & \cdots & \frac{\partial N_{ip}}{\partial y} & \cdots & \frac{\partial N_{12p}}{\partial y} \end{bmatrix} \tag{5-6}$$

and $n_x$ and $n_y$ are load vector along $x$ and $y$ direction, respectively, and $n_{xy}$ is shear load vector. The panel is subjected to in plane compression loading only and shear load factor $n_{xy}$ is considered as zeros. The closed form integration of the Eq. (5-5) is performed, and the analytical expression for the geometric stiffness matrix is obtained for compressive loading along $x$ direction as:

$$[K_g]_P = \left(\frac{n_x b}{1050}\right) \times \begin{bmatrix}
\frac{468}{a} & \frac{-132b}{a} & 78 & \frac{162}{a} & \frac{78b}{a} & 27 & \frac{-162}{a} & \frac{-78b}{a} & 27 & \frac{-468}{a} & \frac{132b}{a} & 78 \\
\frac{-132b}{a} & \frac{48b^2}{a} & -22b & \frac{-78b}{a} & \frac{-36b^2}{a} & -13b & \frac{78b}{a} & \frac{36b^2}{a} & -13b & \frac{132b}{a} & \frac{-48b^2}{a} & -22b \\
78 & -22b & 208a & 27 & 13b & 72a & -27 & -13b & -18a & -78 & 22b & -52a \\
\frac{162}{a} & \frac{-78b}{a} & 27 & \frac{468}{a} & \frac{132b}{a} & 78 & \frac{-468}{a} & \frac{-132b}{a} & 78 & \frac{-162}{a} & \frac{78b}{a} & 27 \\
\frac{78b}{a} & \frac{-36b^2}{a} & 13b & \frac{132b}{a} & \frac{48b^2}{a} & 22b & \frac{-132b}{a} & \frac{48b^2}{a} & 22b & \frac{-78b}{a} & \frac{36b^2}{a} & 13b \\
27 & -13b & 72a & 78 & 22b & 208a & -78 & -22b & -52a & -27b & 13b & -18a \\
\frac{-162}{a} & \frac{78b}{a} & -27 & \frac{-468}{a} & \frac{-132b}{a} & -78 & \frac{468}{a} & \frac{132b}{a} & -78 & \frac{162}{a} & \frac{-78b}{a} & -27 \\
\frac{-78b}{a} & \frac{36b^2}{a} & -13b & \frac{-132b}{a} & \frac{48b^2}{a} & -22b & \frac{132b}{a} & \frac{48b^2}{a} & -22b & \frac{78b}{a} & \frac{36b^2}{a} & -13b \\
27 & -13b & -18a & 78 & 22b & -52a & -78 & -22b & 208a & -27 & 13b & 72a \\
\frac{-468}{a} & \frac{132b}{a} & -78 & \frac{-162}{a} & \frac{-78b}{a} & -27b & \frac{162}{a} & \frac{78b}{a} & -27 & \frac{468}{a} & \frac{-132b}{a} & -78 \\
\frac{132b}{a} & \frac{-48b^2}{a} & 22b & \frac{78b}{a} & \frac{36b^2}{a} & 13b & \frac{-78b}{a} & \frac{36b^2}{a} & 13b & \frac{-132b}{a} & \frac{48b^2}{a} & 22b \\
78 & -22b & -52a & 27 & 13b & -18a & -27 & -13b & 72a & -78 & 22b & 208a
\end{bmatrix} \quad (5\text{-}7)$$

The expression for the geometric stiffness matrix corresponding to the compression loading along $y$ direction can be obtained by changing $a$ to $b$ and $n_x$ to $n_y$ in Eq. (5-7). If the stiffened panel is compressed along both directions, then the resulting geometric stiffness matrix is sum of previous two matrices.

### 5.2.2 Space Frame Element

A space frame element as shown in Figure 5-3 is a straight bar of uniform cross section which is capable of resisting axial force, bending moment about $y$ axis in the plane of its cross section and twisting moment about its centroidal axis. The bending displacements about $z$ axis are neglected and panel is considered to have infinite stiffness against the drilling degree of freedom. The local $xyz$ coordinate system coincides with the principle axis of the cross section, with the $x$-axis representing the centroidal axis of the frame element. According to engineering theory of bending and torsion of beams, the axial displacements, the torsional displacements and the bending displacements in $xz$ plane are

independent of each other. Therefore these three cases will be considered separately in formulating the finite element equations.

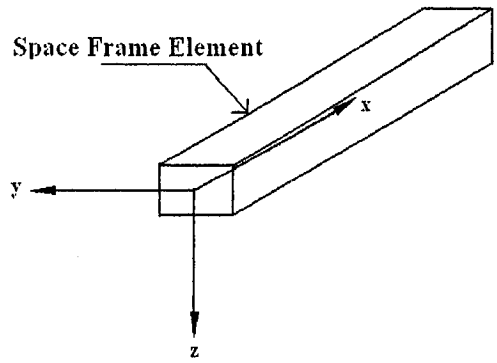


**Figure 5-3** The space frame element

*Axial Displacements*

A space frame element has two axial nodal displacements $u_1$ and $u_2$ as shown in Figure 5-4.

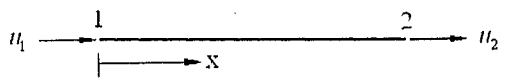


**Figure 5-4** Axial degrees of freedom of the space frame element

The equilibrium and flexibility matrices for these displacements are generated in section 2.8.1, and can be obtained from Eqs. (2-80) and (2-81), respectively as:

$$[B_e]_T = \begin{bmatrix} -1 \\ 1 \end{bmatrix} \tag{5-8}$$

$$[G_e]_T = \begin{bmatrix} \frac{L}{AE} \end{bmatrix} \tag{5-9}$$

The geometric stiffness for these displacements is null matrix.

*Torsional Displacements*

A space frame element has two torsional degrees of freedoms $\theta_{x1}$ and $\theta_{x2}$ as shown in Figure 5-5.

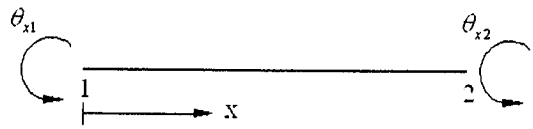


**Figure 5-5** Torsional degrees of freedom of the space frame element

A linear variation for the torsional displacements is assumed, and the displacement field is interpolated as:

$$\theta_x = N_{1t}\theta_{x1} + N_{2t}\theta_{x2} \tag{5-10}$$

where shape functions are:

$$N_{1t} = 1 - \frac{x}{\mathrm{L}} \quad \text{and} \quad N_{2t} = \frac{x}{\mathrm{L}} \tag{5-11}$$

The torsional displacement induces only shear stresses in the element, which can be interpolated as:

$$\tau_{xy} = \frac{z}{J} F_t \tag{5-12}$$

where $F_t$ is the internal torsional force in the element, $z$ is the distance from the centroidal axis and $J$ is the polar moment of inertia.

Substituting Eqs. (5-10) and (5-12) into Eq. (2-20) yields the equilibrium matrix as:

$$[B_e]_{Tr} = \begin{bmatrix} -1 \\ 1 \end{bmatrix} \tag{5-13}$$

Substituting Eq. (5-12) into Eq. (2-26) yields the flexibility matrix as:

$$[G_e]_{Tr} = \left[\frac{\mathrm{L}}{SJ}\right] \tag{5-14}$$

where $S$ is the shear modulus of the frame material. The geometric stiffness matrix for torsional displacements is also null matrix.

*Bending Displacement in $xz$ plane*

The space frame element have four nodal bending degrees of freedom in the $xz$ plane as shown in Figure 5-6, transverse displacements $w_1$ and $w_2$, and rotational displacements $\theta_{y1}$ and $\theta_{y2}$.

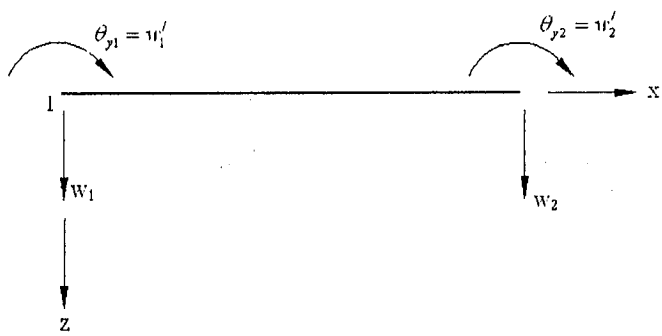


**Figure 5-6** Bending degrees of freedoms in $xz$ plane

The equilibrium and the flexibility matrices associated with these degrees of freedom are formulated in the section 2.8.2, and can be obtained from Eqs. (2-88) and (2-89) as:

$$[B_e]_b = \begin{bmatrix} 0 & 1 \\ -1 & 0 \\ 0 & -1 \\ 1 & \mathrm{L} \end{bmatrix} \tag{5-15}$$

$$[G_e]_b = \begin{bmatrix} \frac{L}{I_y} & \frac{L^2}{2I_y} \\ \frac{L^2}{2I_y} & \frac{L^3}{3I_y} \end{bmatrix} \tag{5-16}$$

The geometric stiffness matrix for these bending displacements can be obtained from the following relation [16]:

$$[K_g]_b = \int_0^L [Z]^T P[Z] dx \tag{5-17}$$

where

$$[Z] = \left[ \frac{\partial N_1}{\partial x}, \frac{\partial N_2}{\partial x}, \frac{\partial N_3}{\partial x}, \frac{\partial N_4}{\partial x} \right] \tag{5-18}$$

$P$ is the axial compressive load, and $N_1$, $N_2$, $N_3$ and $N_4$ can be obtained from Eq.(2-83). The axial compressive load $P$ can be approximately written in term of panel loading $n_x$ as [65]:

$$P = \frac{A_{st}}{A_{sk}} b_s n_x \tag{5-19}$$

where $A_{st}$ and $A_{sk}$ are the cross sectional area of the stiffener and the skin, respectively and $b_s$ is the width of the panel. The geometric stiffness matrix obtained after closed form integration of Eq. (5-17) can be written as:

$$[K_g]_b = \left( \frac{P}{30L} \right) \begin{bmatrix} 36 & 3L & -36 & 3L \\ 3L & 4L^2 & -3L & -L^2 \\ -36 & -3L & 36 & -3L \\ 3L & -L^2 & -3L & 4L^2 \end{bmatrix} \tag{5-20}$$

*The Finial Equilibrium, Flexibility, and Geometric Stiffness Matrices*

The final equilibrium, flexibility and geometric stiffness matrices of the frame element are obtained by superimposition of the matrices obtained from three independent deformation states. The final equilibrium matrix, assembled from Eqs. (5-8), (5-13) and (5-15) is:

$$[B_e]_{SF} = \begin{bmatrix} -1 & 0 & 0 & 0 \\ 0 & 0 & 0 & 1 \\ 0 & -1 & 0 & 0 \\ 0 & 0 & -1 & 0 \\ 1 & 0 & 0 & 0 \\ 0 & 0 & 0 & -1 \\ 0 & 1 & 0 & 0 \\ 0 & 0 & 1 & \mathrm{L} \end{bmatrix} \tag{5-21}$$

Similarly the finial flexibility matrix, assembled from Eqs. (5-9), (5-14) and (5-16) is:

$$[G_e]_{SF} = \begin{bmatrix} \dfrac{\mathrm{L}}{AE_s} & 0 & 0 & 0 \\ 0 & \dfrac{\mathrm{L}}{SJ} & 0 & 0 \\ 0 & 0 & \dfrac{\mathrm{L}}{EI_y} & \dfrac{\mathrm{L}^2}{2EI_y} \\ 0 & 0 & \dfrac{\mathrm{L}^2}{2EI_y} & \dfrac{\mathrm{L}^3}{3EI_y} \end{bmatrix} \tag{5-22}$$

The finial geometric stiffness matrix for the frame element includes only terms corresponding to the bending deformation, since those for the axial and the torsional displacements are null matrix and from Eq. (5-20) can be extended as:

$$[K_g]_{SF} = \left(\frac{P}{30L}\right)\begin{bmatrix} 0 & 0 & 0 & 0 & 0 & 0 & 0 & 0 \\ 0 & 36 & 0 & 3L & 0 & -36 & 0 & 3L \\ 0 & 0 & 0 & 0 & 0 & 0 & 0 & 0 \\ 0 & 3L & 0 & 4L^2 & 0 & -3L & 0 & -L^2 \\ 0 & 0 & 0 & 0 & 0 & 0 & 0 & 0 \\ 0 & -36 & 0 & -3L & 0 & 36 & 0 & -3L \\ 0 & 0 & 0 & 0 & 0 & 0 & 0 & 0 \\ 0 & 3L & 0 & -L^2 & 0 & -3L & 0 & 4L^2 \end{bmatrix} \quad (5\text{-}23)$$

### 5.2.3 Panel Stiffener Interaction

The compatibility between the panel and the stiffener is considered by combining these at the common node at the point of their intersection. If the panel is descritized into $(n_m \times n_m)$ mesh, then there will be $(n_m + 1)$ common node where frame elements can be placed as shown in Figure 5-7.

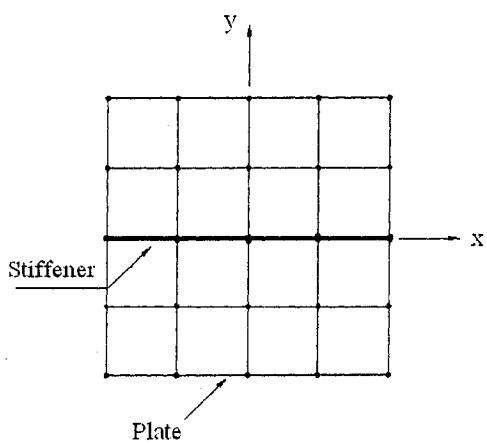


**Figure 5-7** The FE modeling of stiffened panel

The additional displacement [67] resulting from the eccentricity $e$ of the middle surface of the panel and the centroids of the stiffener is taken into account in deriving the finial

equilibrium and the geometric stiffness matrices of the stiffened panel. The rotations $\theta_{yk}$ at the panel node $k$ will produce displacement at the stiffener node $o$ as shown in Figure 5-8.

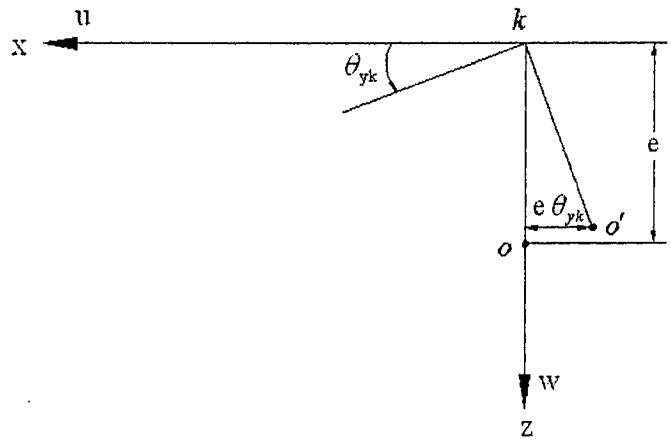


**Figure 5-8** The displacements on plane (x, z)

The displacement vector $\{q_o\}$ at the stiffener node $o$ and $\{q_k\}$ at the plate node $k$ can be written as:

$$\{q_o\}=\begin{Bmatrix} u_o \\ w_o \\ \theta_{xo} \\ \theta_{yo} \end{Bmatrix}, \quad \{q_k\}=\begin{Bmatrix} u_k \\ w_k \\ \theta_{xk} \\ \theta_{yk} \end{Bmatrix} \tag{5-24}$$

The $\{q_o\}$ can be associated with $\{q_k\}$ by the following relation:

$$\{q_o\}=[T]\{q_k\} \tag{5-25}$$

where $[T]$ is the transformation matrix and is of the form:

$$[T]=\begin{bmatrix} 1 & 0 & 0 & -e \\ 0 & 1 & 0 & 0 \\ 0 & 0 & 1 & 0 \\ 0 & 0 & 0 & 1 \end{bmatrix} \tag{5-26}$$

The equilibrium and geometric stiffness matrices for the space frame element generated at node *o* can be transformed to node *k* by the following relation:

$$[B_e]_k = [T]^T [B_e]_o \tag{5-27}$$

$$[K_g]_k = [T]^T [K_g]_o [T] \tag{5-28}$$

$[B_e]_o$ and $[B_e]_k$ are the element equilibrium matrices of the stiffener at node o and *k*, respectively. $[K_g]_o$ and $[K_g]_k$ are the geometric stiffness matrix of the stiffener at node o and *k*, respectively. The equilibrium and geometric stiffness matrices transformed at node *k* are assembled with those of the panel element to obtain the final equilibrium and the geometric stiffness matrices of the stiffened panel. The flexibility matrix of stiffener is same at node *o* and *k*, and therefore assembled directly with the panel flexibility matrix.

## 5.3. Convergence and Validation

The accuracy of the solution obtained is of paramount importance in the choice of analysis formulation. Numerical studies have been conducted for the elastic buckling analysis of the plate and the stiffened panels to validate the developed FE formulation based on force methodology. The problems are solved for which analytical solutions are available. The results for the buckling analysis are also compared with those obtained using the DM. Finally, convergence study for the buckling analysis of stiffened panels is carried out in order to estimate the order of the mesh size to be necessary for numerical solution.

### 5.3.1 Buckling Analysis of Square Plate

The FE elastic buckling analysis of the plate simply supported along all edges and subjected to uniform in plane loading is performed using the IFM. The dimensions and material properties of the plate are shown in Figure 5-9.

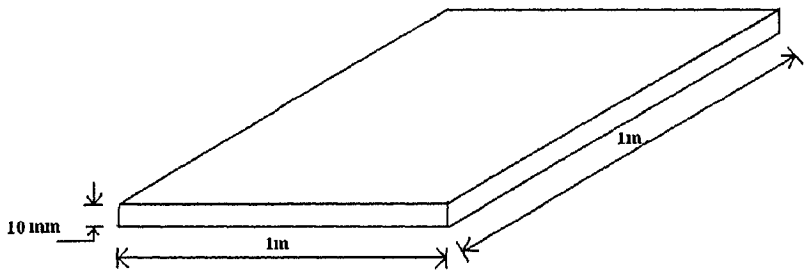


$Modulus\ of\ Elasticity = 200\,\text{GPa}$, $Poisson\ ratio = 0.3$

**Figure 5-9** The simply supported square plate

The analysis is performed with the IFM shell element. The problem is also analyzed with 4-node Kirchhoff's DM element having displacement interpolation similar to that of the IFM plate element and ANSYS Elastic 4node63 shell element [68]. The exact solution for the critical buckling load of the simply supported square plate subjected to uniform uniaxial loading is given by Timoshenko [37]:

$$\text{Critical Buckling Load } N_c = \frac{k\pi D}{b_s^{\,2} t_s} \tag{5-29}$$

where $D = \dfrac{E t_s^{\,3}}{12(1-\nu^2)}$ is the flexural rigidity of the plate, $k$ is the buckling parameter, $b_s$ is the width of plate and $t_s$ is thickness.

The value of $k$ obtained analytically for this problem is 4. The buckling load parameter obtained from all the formulations are presented in Table 5-1. The results show that the

IFM give sufficient accuracy of less than one percent error using only 25 elements, on the other hand ANSYS required 64 elements in order to achieve similar accuracy. The DM, with using highest number of 144 elements, still shows 1.8 percentage errors. The IFM converges very rapidly to the exact solution and show excellent accuracy even for coarse mesh.

**Table 5-1** Critical buckling load for simply supported square plate subjected to uniform uniaxial compressive loading

| No. of Elements | IFM | | ANSYS | | DM | |
|---|---|---|---|---|---|---|
| | Buckling Parameter ($k$) | $k$ (num) / $k$ (anal) | Buckling Parameter ($k$) | $k$ (num) / $k$ (anal) | Buckling Parameter ($k$) | $k$ (num) / $k$ (anal) |
| 4 | 3.751 | 0.938 | 3.748 | 0.937 | 4.406 | 1.102 |
| 9 | 3.892 | 0.973 | 3.82 | 0.955 | 4.249 | 1.062 |
| 16 | 3.942 | 0.986 | 3.88 | 0.970 | 4.173 | 1.043 |
| 25 | 3.966 | 0.991 | 3.916 | 0.979 | 4.134 | 1.033 |
| 36 | 3.978 | 0.994 | 3.94 | 0.985 | 4.112 | 1.028 |
| 49 | 3.985 | 0.996 | 3.956 | 0.989 | 4.098 | 1.024 |
| 64 | 3.989 | 0.997 | 3.964 | 0.991 | 4.089 | 1.022 |
| 81 | 3.992 | 0.998 | 3.972 | 0.993 | 4.083 | 1.020 |
| 100 | 3.994 | 0.998 | 3.976 | 0.994 | 4.078 | 1.019 |
| 121 | 3.996 | 0.998 | 3.98 | 0.995 | 4.075 | 1.019 |
| 144 | 3.997 | 0.999 | 3.98 | 0.995 | 4.072 | 1.018 |

A convergence study of the critical buckling load is performed and the results are shown graphically in Figure 5-10, the results obtained from the IFM are presented with those obtained from the analytical solution, the DM Kirchhoff's element and ANSYS 4-node shell element. As Figure 5-10 shows fast convergence is achieved when the IFM element is used, whereas the DM element led to a very slow convergence. The IFM and ANSYS elements converge from lower side of the analytical solution, whereas the DM element converges from the upper side. The DM shows the least accuracy as compared to other

formulations. The IFM basic 4-node element even shows superior accuracy than that of much advanced ANSYS shell element.

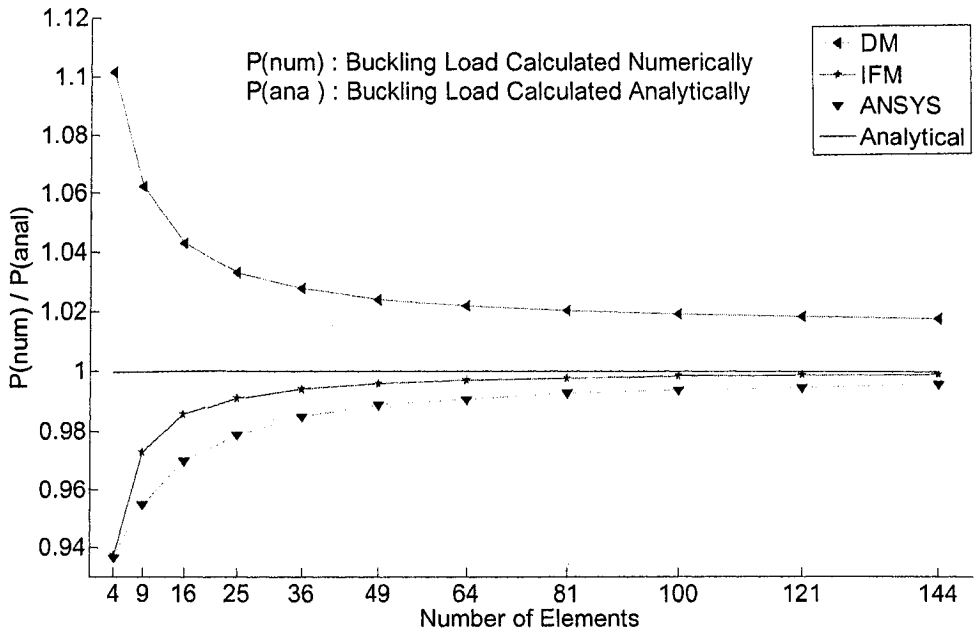


**Figure 5-10** Convergence curves for the critical buckling load of square plate

## 5.3.2 Buckling Analysis of Stiffened Panels

The simply supported square plate with one central stiffener as shown in Figure 5-11 is analyzed in the present case by varying the stiffener parameters.

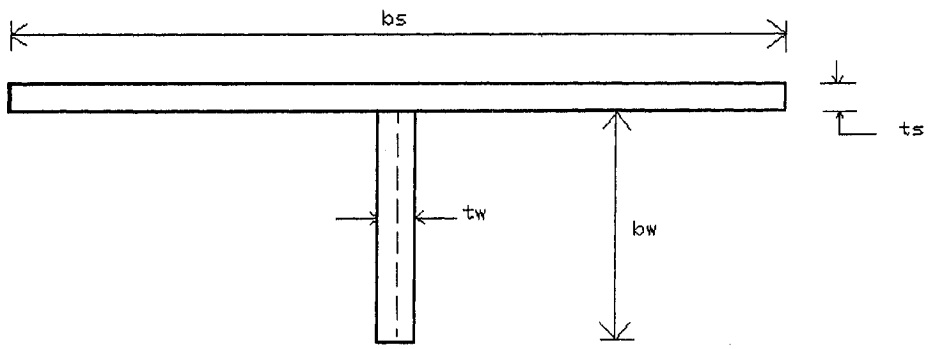


**Figure 5-11** Cross section of stiffened panel

The stiffener is placed eccentrically and the panel is subjected to uniform in plane loading along the $x$-axis. The results of the analysis are compared with those obtained analytically by Timoshenko [37]. The exact value for the critical stress can be evaluated from the following formula [37]:

$$\sigma_{cr} = k\frac{\pi^2 D}{b_s^2 t_s} \tag{5-30}$$

where $k$ is the buckling parameter and its value can obtained from tables given in Ref.[37], and $D, b_s$ and $t_s$ are the flexural rigidity, width and thickness of the plate, respectively. It should be noted here that energy of twist of the stiffener, which occurs during buckling, is neglected in Timoshenko formulation, therefore the actual value of the critical stress can be more than that given by Eq. (5-30). In order to compare the results with Timoshenko formulation, the problem is first analyzed without considering the torsional rigidity of the stiffener (IFM1). The results thus obtained are compared with Timoshenko formulation and the convergence study is performed. The analysis is also performed with considering the torsional rigidity of the stiffener (IFM2), and the effect of torsional rigidity of the stiffener on the buckling load is investigated. The two stiffeners of different sizes having same panel size and loading are analyzed in the following section.

*Stiffener 1*

The dimension of the plate and stiffener taken are:

$$b_s = 1m, L_P = 1m, t_s = 10mm, t_w = 15, b_w = 30mm. \tag{5-31}$$

The value of $k$ obtained is 7.8025. The results of the analysis obtained using the IFM1 and the IFM2 with increasing number of elements are presented in Table 5-2.

**Table 5-2** The buckling parameter ($k$) for stiffener1 with different number of elements

| Elements | IFM1 | IFM2 |
|---|---|---|
| 4×4 | 7.29 | 7.29 |
| 6×6 | 7.60 | 7.60 |
| 8×8 | 7.719 | 7.719 |
| 10×10 | 7.768 | 7.768 |
| 12×12 | 7.789 | 7.789 |

A convergence study is carried out for the buckling load. It is seen that the IFM converge to the accurate results very rapidly and generate very accurate results even for the coarse FE mesh. The IFM converge to 1% error for $(8\times8)$ FE mesh, and error reduces to 0.184 % for $(12\times12)$ mesh size. The convergence study shows that mesh size of $(8\times8)$ elements is sufficient enough to get reasonable accurate result. It can be seen that the critical buckling load obtained from IFM1 and IFM2 are same, therefore the torsional stiffness of the stiffener have no effect on the critical buckling load of the considered stiffened panel.

*Stiffener 2*

Now the stiffened panel is analyzed with large size of the stiffener. The dimensions of the stiffened panel are:

$$b_s = 1m, L_P = 1m, t_s = 10mm, t_w = 15, b_w = 60mm \tag{5-32}$$

The value of $k$ obtained analytically is 16. The results obtained using the IFM1 and the IFM2 are presented in Table 5-3. The IFM results show superior accuracy and convergence is very fast. It can be seen that the IFM produce sufficient accuracy with the mesh size of the $(8\times8)$ elements. It can be realized that the critical buckling load obtained from the IFM2 is higher than the IFM1. Therefore, in this case, the torsional rigidity of the stiffener noticeably affects the critical buckling load. It can be concluded that the

effect of the torsional rigidity of the stiffener on the buckling load depends on the size of stiffened panel, and the effect increases with increase in the size of the stiffener.

**Table 5-3** Buckling parameter ($k$)

| Elements | IFM1 | IFM2 |
|---|---|---|
| 4×4 | 15 | 16.585 |
| 6×6 | 15.554 | 17.061 |
| 8×8 | 15.753 | 17.234 |
| 10×10 | 15.846 | 17.315 |
| 12×12 | 15.896 | 17.359 |

The effect of torsional rigidity on the buckling load of the stiffened panel is presented graphically in Figure 5-12. It can be seen that IFM2 curve is offset from the IFM1 curve by certain distance, which is the measure of the effect of the torsional rigidity of the stiffener.

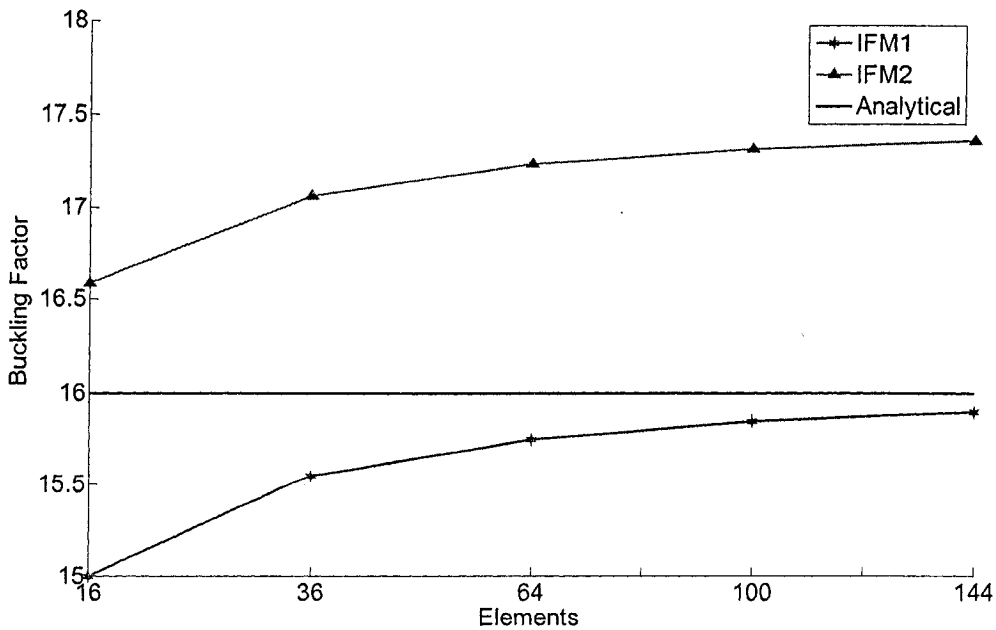


**Figure 5-12** Convergence curve for the buckling load of the stiffened panel

As the convergence study for both of these problems shows that mesh size of $(8\times8)$ elements is sufficient enough to get reasonable order of accuracy, the analysis in subsequent optimization problems is carried out with $(8\times8)$ mesh size.

## 5.4 Optimization of Stiffened Panel

Stiffened panels generally consist of large panel with equally spaced similar stiffeners attached to it. The entire width of the panel can be divided into repeating unit, having similar configuration as shown in Figure 5-13. A repeating unit includes the cross section of stiffener plus the panel skin of width equal to spacing between stiffeners. The optimization problem is reduced to only one repeating unit and the appropriate boundary conditions are applied along the longitudinal side of the stiffener to simulate the continuity of the panel. The single module model gives a good approximation to the local skin buckling mode if there are more than three or four equally spaced stringers in the panel. The boundary conditions along the length of the panel are applied such that the panel is assumed to be buckled longitudinally. All the nodes on the longitudinal axis are restrained from rotation along the longitudinal axis to approximate the continuity of the panel.

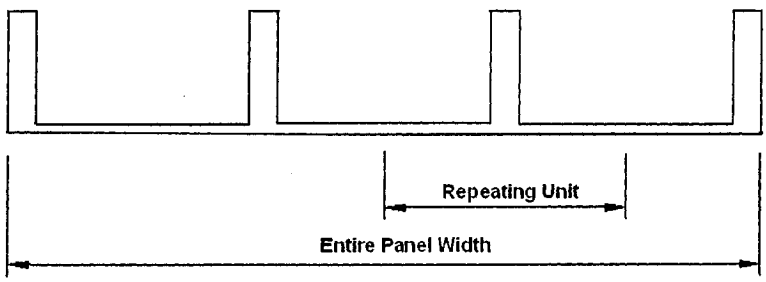


**Figure 5-13** Repeating unit of the entire panel

The objective of the optimization problem is to minimize the mass of the stiffened panel while guarding against the buckling failure. The mass of the stiffened panel can be written as:

$$M = (A_{sk} + A_{st})\rho L_P \tag{5-33}$$

where $\rho$ is the mass density and $L_P$ is the length of the panel. The length of the panel and mass density are always known, therefore objective function can be reduced to minimize the cross sectional area of the stiffened panel:

$$\text{Objective Function} = (A_{sk} + A_{st}) \tag{5-34}$$

Normalized buckling constraints may be described in standard form as:

$$g_{nc} = -\frac{N_c}{\overline{N}_c} + 1 \leq 0 \tag{5-35}$$

where $N_c$ and $\overline{N}_c$ are the critical buckling load and its associated allowable, respectively. An optimization algorithm has been developed in which the IFM as analyzer has been combined with SQP technique as optimizer. The design sensitivity analysis of the buckling load with respect to thickness of the plate and dimensions of the stiffener is performed analytically and integrated with the optimization algorithm.

## 5.5 Sensitivity Analysis of Stiffened Panels

The linear buckling analysis problem is the eigen value problem. The formulation to calculate the sensitivity of the eigen value is provided in section 3.6.3. From Eq. (3-64), the sensitivity analysis equation for the buckling analysis can be written as:

$$\frac{d\mu}{dDV_j} = \frac{\{V_L\}^T \left( \frac{d[S]}{dDV_j} - \mu \frac{d[S_b]}{dDV_j} \right) \{V_R\}}{\{V_L\}^T [S_b] \{V_R\}} \tag{5-36}$$

where $\{V_L\}$ and $\{V_R\}$ are left and right eigen vectors, respectively and $DV_j$ is the $j$th design variable. The derivative of the system matrix $[S]$ of the IFM can be written as:

$$\frac{d[S]}{dDV_j} = \begin{bmatrix} [0] \\ [C][\overline{G}] \end{bmatrix} \tag{5-37}$$

where

$$[\overline{G}] = \frac{d[G]}{dDV_j} \tag{5-38}$$

From Eq. (2-74), the IFM stability matrix can be written as:

$$[S_b] = \begin{bmatrix} [K_g][J][G] \\ [0] \end{bmatrix} \tag{5-39}$$

Taking derivative of the Eq. (5-39) with respect to $DV_j$ yields:

$$\frac{d[S_b]}{dDV_j} = \begin{bmatrix} \frac{d[K_g]}{dDV_j}[J][G] + [K_g]\frac{d[J]}{dDV_j}[G] + [K_g][J]\left[\frac{d[G]}{dDV_j}\right] \\ [0]_{(r \times n)} \end{bmatrix} \tag{5-40}$$

It can be observed from Eqs.(5-36), (5-37) and (5-40) that to find the sensitivity of the buckling load, the derivatives of the geometric stiffness and the flexibility matrix with respect to design variables are required to be calculated. It is noted that derivative of $[J]$ can be obtained from Eq. (3-66).

Since a stiffened panel is being dealt with, the design variables come from both panel and stiffener. In the present study, the length and breadth of the panel are kept constant, however the thickness of the panel is considered as the design variable. The design variables for the stiffener depend on the shape of stiffener, these are height and thickness of the stiffener for the unflange stiffened panel, and additionally width and thickness of the flange for the J-type stiffener. In the following section analytical expression for the design sensitivity of the buckling load with respect to thickness of the plate and the stiffener parameters are derived.

### 5.5.1 Sensitivity with Respect to Plate Thickness

The overall flexibility and geometric stiffness matrices of the stiffened panel are assembled from the element matrices of the plate and the stringer. Further, the plate element matrices are combination of matrices from the bending and the membrane deformation states. Therefore the derivatives of all of these matrices are required to calculate the sensitivity of linear buckling load with respect to design variables.

The finial geometric stiffness matrix of the stiffened panel is combination of the geometric stiffness matrix of the panel and the stiffener. The panel geometric stiffness matrix is independent of the thickness of the panel, so its derivative can be written as:

$$\frac{d\lfloor K_g \rfloor_P}{dt_s} = 0 \tag{5-41}$$

Stiffener geometric stiffness matrix depends on the compressive load applied on the edge of stiffener, which depends on the plate thickness. From Eq. (5-23), the derivative of the

geometric stiffness matrix of the stiffener with respect to plate thickness can be written as:

$$\frac{d[K_g]_{SF}}{dt_s} = \frac{dP}{dt_s}\frac{1}{30L}\begin{bmatrix} 0 & 0 & 0 & 0 & 0 & 0 & 0 & 0 \\ 0 & 36 & 0 & 3L & 0 & -36 & 0 & 3L \\ 0 & 0 & 0 & 0 & 0 & 0 & 0 & 0 \\ 0 & 3L & 0 & 4L^2 & 0 & -3L & 0 & -L^2 \\ 0 & 0 & 0 & 0 & 0 & 0 & 0 & 0 \\ 0 & -36 & 0 & -3L & 0 & 36 & 0 & -3L \\ 0 & 0 & 0 & 0 & 0 & 0 & 0 & 0 \\ 0 & 3L & 0 & -L^2 & 0 & -3L & 0 & 4L^2 \end{bmatrix} \tag{5-42}$$

where

$$\frac{dP}{dt_s} = \frac{-1}{t_s^2}P \tag{5-43}$$

The derivative of flexibility matrix $\frac{d[G]}{dt_s}$ is assembly of the derivative of shell flexibility matrix $\frac{d[G]_S}{dt_s}$ and the derivative of stiffener flexibility matrix $\frac{d[G]_{SF}}{dt_s}$. The $\frac{d[G]_S}{dt_s}$ is further combination of the derivative of membrane flexibility matrix $\frac{d[G]_M}{dt_s}$ and the derivative of bending flexibility matrix $\frac{d[G]_P}{dt_s}$. These matrices are evaluated from Eqs. (2-111), (2-104) and (5-22) as:

$$\frac{d[G]_P}{dt_s} = \frac{-3}{t_s}[G]_P \tag{5-44}$$

$$\frac{d[G]_M}{dt_s} = \frac{-1}{t_s}[G]_M \tag{5-45}$$

$$\frac{d[G]_{SF}}{dt_s} = 0 \tag{5-46}$$

### 5.5.2 Sensitivity With Respect To Stiffener Parameters

The general expressions for sensitivity analysis with respect to $j$th stiffener parameter $SP_j$ are formulated. As discussed previously, to find the sensitivity with respect to $SP_j$, the $\frac{d[G]}{dSP_j}$ and $\frac{d[K_g]}{dSP_j}$ are required to be evaluated. The panel geometric stiffness matrix is independent of the stiffener parameter; therefore its derivative with respect to $SP_j$ is zero:

$$\frac{d[K_g]_S}{dSP_j} = 0 \tag{5-47}$$

From Eq. (5-23), the derivative of the geometric stiffness matrix of the stiffener is:

$$\frac{d[K_g]_{SF}}{dSP_j} = \frac{dP}{dSP_j}\frac{1}{30L}\begin{bmatrix} 0 & 0 & 0 & 0 & 0 & 0 & 0 & 0 \\ 0 & 36 & 0 & 3L & 0 & -36 & 0 & 3L \\ 0 & 0 & 0 & 0 & 0 & 0 & 0 & 0 \\ 0 & 3L & 0 & 4L^2 & 0 & -3L & 0 & -L^2 \\ 0 & 0 & 0 & 0 & 0 & 0 & 0 & 0 \\ 0 & -36 & 0 & -3L & 0 & 36 & 0 & -3L \\ 0 & 0 & 0 & 0 & 0 & 0 & 0 & 0 \\ 0 & 3L & 0 & -L^2 & 0 & -3L & 0 & 4L^2 \end{bmatrix} \tag{5-48}$$

where $$\frac{dP}{dSP_j} = \frac{dA_{st}}{dSP_j} b_s n_x \tag{5-49}$$

The flexibility matrix of the plate element is also independent of the stringer parameters, so its derivative with respect to $SP_j$ is:

$$\frac{d[G]_P}{dSP_j} = 0, \quad \frac{d[G]_M}{dSP_j} = 0 \tag{5-50}$$

From Eq. (5-22), the derivative of the flexibility matrix of the stringer with respect to $SP_j$ is:

$$\frac{d[G]_{SF}}{dSP_j} = \begin{bmatrix} -\frac{L}{A_{st}^2}\frac{dA_{st}}{dSP_j} & 0 & 0 & 0 \\ 0 & -\frac{E_s L}{G_s J^2}\frac{dJ}{dSP_j} & 0 & 0 \\ 0 & 0 & -\frac{L}{I_y^2}\frac{dI_y}{dSP_j} & -\frac{L^2}{2I_y^2}\frac{dI_y}{dSP_j} \\ 0 & 0 & -\frac{L^2}{2I_y^2}\frac{dI_y}{dSP_j} & -\frac{L^3}{3I_y^2}\frac{dI_y}{dSP_j} \end{bmatrix} \quad (5\text{-}51)$$

## 5.6 Illustrative Optimization Examples

A design optimization algorithm is developed in which the IFM as analysis module is combined with the SQP as optimization module to optimize the dimension of the stiffened panel. The finite element sensitivity analysis has been used to evaluate the required gradient in SQP algorithm. The stiffeners are attached symmetrically to the panel, and length of the panel and the number of stiffeners are assumed to be known. The panel is subjected to uniform compression loading and guarded against the elastic buckling. The design variables are the thickness of panel and dimensions of the stringer. The optimum dimension of both flange and unflange stiffener subjected to same uniform compression loading, are calculated. The problem is also solved using the IFM(NG), and results are compared with those obtained using the IFM(AG). It should be noted that for both optimization problems stopping tolerance of 0.001 is considered for objective function, constraints and search direction.

## 5.6.2 Design of Unflanged Stiffened Panel

The unflange stiffener as shown in Figure 5-14 is simplest type of stiffener and used for low cost fabrication. It has low structural efficiency, but easy to machine. The design variables are the thickness of the plate, and height and thickness of the stiffener.

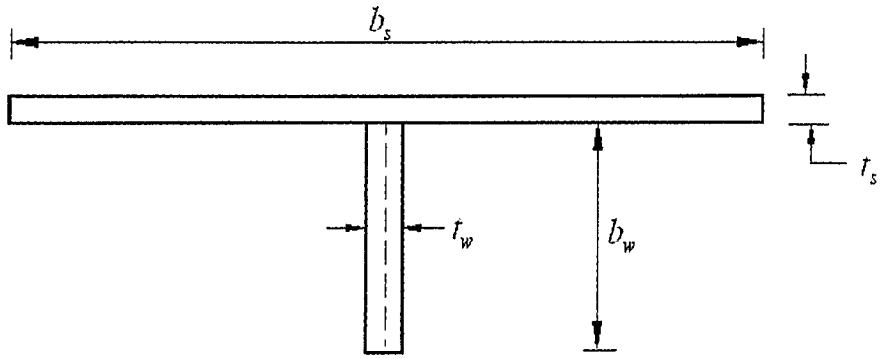


**Figure 5-14** Unflange stiffened panel

The objective function of the problem is to minimize the cross sectional area of the stiffened panel.

Area of cross section of the stiffener $A_{st} = b_w t_w$ (5-52)

Area of cross section of panel $A_{sp} = b_s t_s$ (5-53)

Objective Function $= b_s t_s + b_w t_w$ (5-54)

The other parameters are:

The distance of the centroidal axis from the lower surface of skin $h = \frac{b_w}{2}$ (5-55)

Second moment of area of the stiffener about the centroidal axis $I_y = \frac{t_w b_w^3}{12}$ (5-56)

The length of the panel is 0.57631m, and it is designed for uniform compressive loading of 1.5513 MN/m. As discussed previously, only one repeating unit of the entire panel will be optimized to reduce the computational cost. The width of the repeating unit is 0.123952m. The lower limits on the thickness of the plate, height of the stringer and thickness of the stringer are 20mm, 10cm and 20mm, respectively. As an initial design for the optimization algorithm, the thickness of the plate, height of the stiffener and thickness of the stiffener are set as 40mm, 70cm and 50mm, respectively.

**Table 5-4** Comparison of the gradient at the initial design point for the unflange stiffened panel

| | IFM(NG) (Default Step Size) | IFM(NG) (Accurate Step Size) | IFM(AG) |
|---|---|---|---|
| Height of stiffener(cm) | 0.0274 | 0.0113 | 0.0113 |
| Thickness of stiffener(mm) | 0.4753 | 0.4753 | 0.4753 |
| Thickness of plate(mm) | 7.7242 | 7.6249 | 7.6248 |

Before starting the optimization algorithm, the accuracy of the analytically sensitivity analysis is compared with numerically sensitivity analysis obtained from the MATLAB optimization toolbox at the initial design and it has been demonstrated that how the change in step size affect the accuracy of the gradient calculation. The step size taken by MATLAB toolbox default setting varies between 0.1 and 1E-8. The analytically calculated gradients and numerically calculated gradient by default setting are shown in Table 5.4. It can be seen that numerical gradient obtained from MATLAB differ from the analytical calculated gradient, and the maximum discrepancy is in the gradient with respect to height of the stiffener. The reason for the discrepancy in gradient is the incorrect step size taken by the MATLAB toolbox and discrepancy in gradient with

respect to the height of the stiffener, is maximum because of its large value as compared to other parameters. The numerically gradient is compared by varying the step size setting in MATLAB toolbox to obtained best setting, for which discrepancy is minimum. The numerical gradient using this step size setting is shown the Table 5.4. Therefore, it can be concluded that numerical technique is not reliable tool for gradient calculation and choosing best step size is challenging task in some cases.

**Table 5-5** Optimized dimensions of the unflanged stiffened panel

| | Thickness of plate(cm) | Height of the stiffener(cm) | Thickness of the stiffener(cm) | Stiffened panel cross section area($cm^2$) | Number of Iterations |
|---|---|---|---|---|---|
| IFM(AG) | 0.4114 | 5.5134 | 0.2 | 6.2025 | 7 |
| IFM(NG) | 0.4115 | 5.5107 | 0.2 | 6.2028 | 10 |

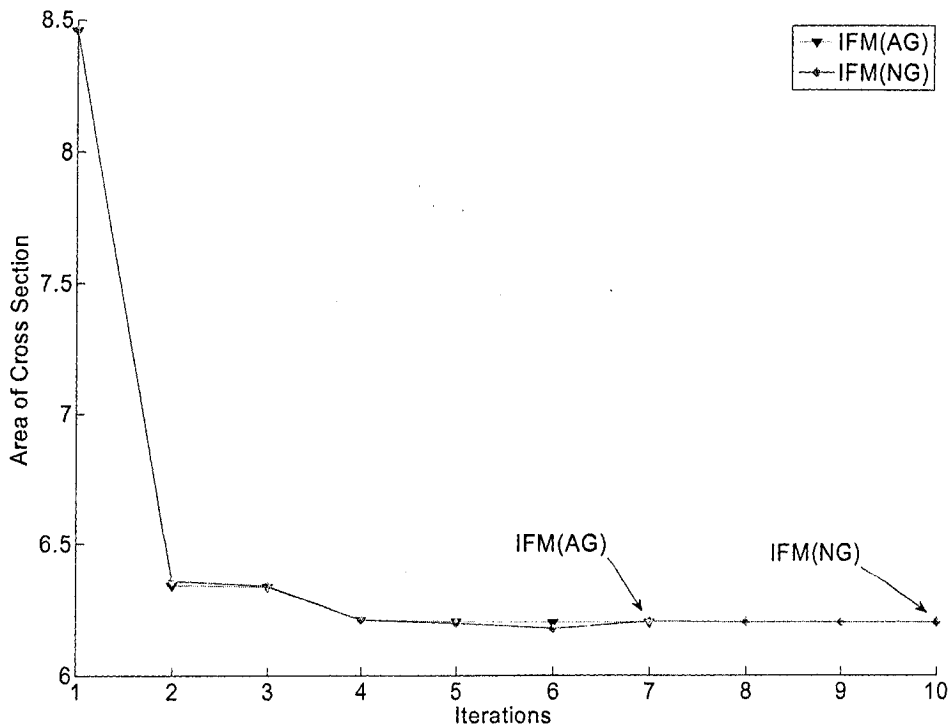


**Figure 5-15** Plot of objective function versus iteration number

The optimization of the stiffened panel is performed with both analytically calculated gradient and numerical calculated gradient. The optimum dimensions of the stiffened panel are presented in Table 5-5. A minimum cross sectional area of 6.2025 $cm^2$ is obtained. Although the IFM(AG) and the IFM(NG) converge to almost same optimum values, but the IFM(NG) take more number of iterations to converge. The number of iterations taken with analytical gradient are 7, on the other hand with the numerical gradient are 10. The plots of objective function versus number of iterations for both formulations are shown in Figure 5-15. The IFM(AG) takes much less number of iterations, and time required to calculate the gradient is also very less than the numerical gradient.

### 5.6.2 Design of J-Type Stiffener

The J-type stringer as shown in Figure 5-16 is designed. The J-type stringer provides higher structural efficiency than unflanged stiffener, but requires complicated machining. The design variables are thickness of the plate $t_s$, height of the stringer $b_w$, width of the stringer $t_w$, length of the flange $b_f$ and the thickness of the flange $t_f$.

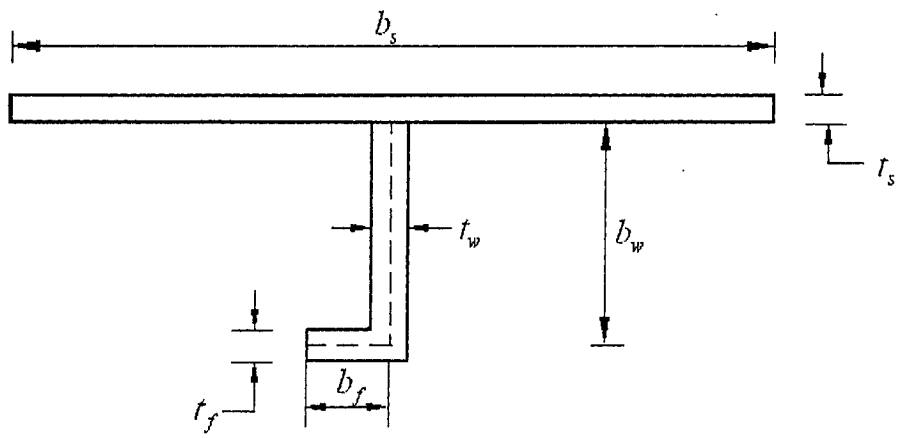


**Figure 5-16** Design parameters of the J-type stiffened panel

The objective function is to minimize cross sectional area of the stiffened panel.

Area of cross section of the stringer $A_{st} = b_w t_w + b_f t_f$ (5-57)

Area of cross section of plate $A_{sp} = b_s t_s$ (5-58)

Objective Function = $b_s t_s + b_w t_w + b_f t_f$ (5-59)

The other parameters are:

The distance of the centroidal axis from the surface of skin:

$$h = \frac{0.5 t_w b_w^2 + b_f t_f (b_w + 0.5 t_f)}{A_{st}} \tag{5-60}$$

Second moment of area of the stiffener about the centroidal axis:

$$I_y = \frac{t_w b_w^3}{12} + b_w t_w \left( h - \frac{b_w}{2} \right)^2 + \frac{b_f t_f^3}{12} + b_f t_f (b_w - h)^2 \tag{5-61}$$

The J-type stiffened panel as shown in Figure 5-16, is one of the repeating units of the entire panel. The length of the panel, width of the repeating unit, critical buckling load and boundary conditions are same as specified in previous problem. In addition to the buckling constraint, the constraints on the dimensions of the flange are applied such that width of flange is greater than 0.327 times the height of the stiffener and thickness of flange is greater than or equal to thickness of the stiffener. The initial design for the height of the stiffener, thickness of the stiffener, thickness of the plate, width of the flange and thickness of the flange are set as 50cm, 30mm, 20mm, 20cm and 40mm, respectively. The height of the stiffener, thickness of the stiffener and thickness of plate are limited to minimum value of 10cm, 20mm and 20mm, respectively.

Similar to the previous problem, the analytical and numerical gradients of the buckling constraint are compared, before the start of the optimization algorithm. The analytically

calculated gradient and numerically calculated gradient using both default step size and best step size are shown in Table 5-6. It can be observed that numerically calculated gradients using default step size differ significantly from the analytically calculated gradients. Therefore, the best step size is searched, for which discrepancy with respect to analytically calculated gradient, is minimum and optimization is performed using this step size.

**Table 5-6** Comparison of the gradient at the starting design for J-type stiffened panel

| | IFM(NG) (Default Step Size) | IFM(NG) (Accurate Step Size) | IFM(AG) |
|---|---|---|---|
| Height of stiffener(cm) | -0.0031 | 0.0007 | 0.0007 |
| Thickness of stiffener(cm) | 0.0406 | 0.0364 | 0.0364 |
| Thickness of plate(cm) | 2.0361 | 2.0632 | 2.0623 |
| Width of the flange(cm) | 0.0036 | 0.0017 | 0.0017 |
| Thickness of flange(cm) | 0.0314 | 0.0259 | 0.0259 |

**Table 5-7** Optimum Design of J-Type Stiffened Panel

| | Thickness of plate (cm) | Height of the stiffener (cm) | Thickness of the stiffener (cm) | Width of Flange (cm) | Thickness of Flange (cm) | Stiffened panel cross section area($cm^2$) | Number of Iterations |
|---|---|---|---|---|---|---|---|
| IFM(AG) | 0.4114 | 4.3956 | 0.2 | 1.4374 | 0.2 | 6.2656 | 8 |
| IFM(NG) | 0.4114 | 4.3926 | 0.2 | 1.4426 | 0.2 | 6.2661 | 12 |

The optimized dimensions of stiffened panel obtained using both analytical and numerical gradients are given in Table 5.7. An optimized area of cross section of 6.2656 $cm^2$ is obtained using the IFM(AG), and 6.2661 $cm^2$ is obtained using the IFM(NG). The numbers of iterations taken by the IFM(AG) and the IFM(NG) are 8 and 12, respectively.

The inaccuracy in sensitivity calculation by the numerical method, change the path of the optimization algorithm and results in more number of iterations. It has been noted that calculation of gradient by analytical method decreases the computational time significantly and make the optimization algorithm faster.

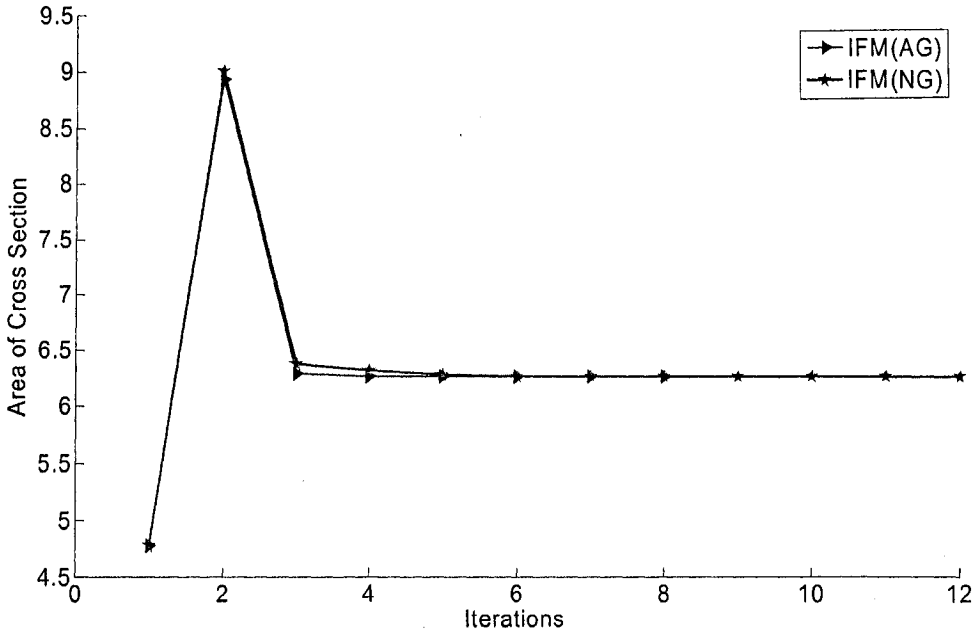


**Figure 5-17** Plot of objective function versus number of iterations

The convergence of the optimization algorithms with number of iteration are shown in Figure 5-17. It can be observed that at the beginning both the optimization algorithms follow the same path, but after a few number of iterations it differ somewhat. Therefore small differences in the gradient calculation change the path of the optimization algorithm and results in more number of iterations with numerical gradient.

Therefore it can be concluded that the IFM combined with SQP algorithm and analytical sensitivity analysis, is excellent tool for optimizing the dimensions of stiffened panel

subjected to uniform compression loading, and can be used in number of application in civil, naval and aerospace industries.

Chapter 6

# CONCLUSION AND FUTURE WORK

## 6.1 Conclusion

Many different topics in the field of structural analysis, design sensitivity analysis, optimization and design optimization of stiffened panels are covered in this thesis. A short summary and conclusion of the work are presented in the following.

### 6.1.1 Structural Analysis

The equations of the IFM are amenable to computer application and can be easily automated. The extensive numerical analysis is performed to investigate the efficiency of the IFM. The results of the analysis are compared with those obtained from the DM. It is realized from these examples that the IFM yields accurate results for both stresses and displacements even for very coarse meshes. The DM requires much finer mesh to acquire the same accuracy. The IFM converge to exact solution rapidly and show superior accuracy. Moreover, it has been observed that the results of the IFM are not much sensitive to the choice of the stress and displacement field.

### 6.1.2 Design Sensitivity Analysis

The numerical and analytical techniques for the design sensitivity analysis are introduced and consequences of using numerical techniques are described. The discrete approach which is computationally efficient and easy to implement, is used to evaluate the analytical sensitivity. The design sensitivity analysis has been implemented for the

discrete structures using the IFM. The closed form derivatives of the various finite element matrices that are required in direct method are evaluated. The sensitivity analysis equations are formulated for the stress, displacement and eigen value constraints. The efficiency and accuracy of the analytical sensitivity analysis is compared with the numerical sensitivity analysis. It has been observed that the analytical sensitivity analysis procedure is very efficient and accurate as compared to the numerical sensitivity analysis, and required less number of iterations to converge to the optimal solution. The accuracy of the numerical sensitivity analysis highly depends on the step size. The small error in the calculation of gradient by numerical method changes the path of the optimization algorithm and results in large numbers of iterations and premature convergence. Further, it has been observed in some cases that for the optimization problems subjected to frequency constraints, the IFM(AG) produce even better design as compared to the IFM(NG).

### 6.1.3 Structural Optimization

The design optimization using the IFM is investigated for the small and large scale size optimization problems. A size optimization algorithm has been developed in which the IFM as analyzer has been combined with SQP technique as an optimizer. The analytical design sensitivity analysis is integrated with optimization algorithm to provide the gradient information to the SQP. The structures are designed for the stress, displacement and frequency constraints. The problems are also investigated with the DM as analyzer and the comparison is performed. It has been observed that the IFM and the DM produce almost same optimum results for the structural optimization problems subjected to stress

and displacement constraints, but the required computational time for the IFM is significantly less than the DM. The numerical tests presented demonstrate the computational advantages of the IFM for stress and displacement constraints, which become more pronounced in large-scale optimization problems. Further, it has been observed that the computational efficiency of the IFM increases with increase in numbers of active stress constraints in the problem.

It has been observed that for the large scale structural optimization problems subjected to frequency constraints have many local minima's, the IFM and the DM can produce different optimum results. It is seen from the investigations done in this thesis that the IFM results are better than the DM. The IFM has been found more expensive for the frequencies constrained problems due to presence of null rows in the IFM mass matrix. The computational time of the IFM has been reduced by calculating the gradients by analytical methods. Finally, it is concluded that the path of the optimization algorithm depends on the analysis procedure, and the small difference in the response from the analysis procedure can change the optimization path.

### 6.1.4 Design Optimization of Stiffened panel

The IFM finite element formulation is developed for the elastic buckling analysis of eccentrically stiffened panels. The validity of the FE models has been established by extensive numerical analysis. It has been observed that the IFM has superior accuracy with respect to the DM and ANSYS, and generate sufficient accurate results even for coarse finite element mesh. Further, the convergence study for the buckling analysis of

stiffened panel is performed and it is concluded that mesh size of $(8\times8)$ elements is sufficient enough to get reasonable accuracy. The effect of torsional rigidity of the stiffener on the elastic buckling load is also investigated, and it is observed that the effect of torsional rigidity depends on the size of the stiffener. The critical buckling load increases with increase in the size of the stiffener.

A design optimization methodology has been developed to optimize the dimension of the stiffened panel while guarding against the elastic buckling, by combining the FE buckling analysis based on the IFM with the SQP. The analytical expressions for the design sensitivity of the buckling load with respect to the plate and the stiffener dimensions are formulated. The sensitivity analysis is integrated with the optimization algorithm to provide the gradient information to SQP gradient based optimization algorithm. The optimization algorithm is used to optimize the unflange and the flange stiffened panel subjected to practical uniform compression loading.

## 6.2 Recommendations

This thesis provides the basic understanding of the IFM and its applications in the field of structural optimization. The methodologies developed and presented in this investigation have been successfully applied to a significant class of structures subject to stress, displacement, frequency and stability constraints. The application of the IFM in the field of structural analysis and optimization is still in initial stage and a significant work is necessary to extend IFM for more practical problems. Some suggestions for the possible future work are given below:

- The indirect approach to formulate the compatibility equation in the IFM is implemented for simple finite elements. It becomes difficult to automate this approach for complex structures. Therefore, automating the technique for complex structure is still a challenging task.
- The finite element library developed for the IFM is limited to very basics elements and future work is required to extend it for more advanced elements.
- The eigen value analysis in the IFM is computational expensive due to the presence of null rows in the matrices. Therefore, efforts are required to develop more efficient free vibration and stability analysis in the IFM.
- The most of the work in the IFM is limited to linear analysis. The IFM methodology should be extended to nonlinear analysis.
- Most of the investigations are related to static, free vibration and stability analysis. The IFM should be investigated for dynamic loading.
- The IFM is successfully used for size optimization problems, future work can be done on using the IFM for shape optimization problems.

# REFRENCES


1. Maxwell, C., "Scientific Papers," *Vol.*2, 1869, pp.175-177.
2. Michell , A .G. M., "The Limits of Economy of Material in Frame Structures," Philosophical Magazine, Series 6, *Vol.*8, No.47, Nov1904, pp589-595
3. Shanley, F.R. ,*Weight Strength Analysis of Aircraft Structures*, Mc-Graw Hill Book Co., Inc., New York, N.Y.,1952.
4. Dantzig, G.B., "Note on Klein's Direct Use of External Principles in Solving Certain Problems Involving Inequalities," Journal of the Operations Research Society of America, *Vol.4*, pp.247-249, 1956.
5. Heyman, J., "Plastic Design of Beams and Frames for Minimum Material Consumption.", Quarterly of Applied Mathematics, *Vol.*8, pp.373-381, 1951.
6. Schmit, L.A., "Structural Design by Systematic Synthesis," Proceeding, 2nd Conference on Electronic Computation, ASCE, New York, pp.105-122, 1960.
7. Sander, G., and Flury, C., "A Mixed Method in Structural Optimization," International Journal for Numerical Methods in Engineering, *Vol.*13, pp.385-404, 1978.
8. Frind, E.O., and Wright, P.M., "Gradient Methods in Optimum Structural Design," Journal of the Structural Division, ASCE, *Vol.*101, pp.939-956, 1975.
9. Pappas, M., "Improved Methods for Large-Scale Structural Synthesis," AIAA Journal,*Vol.*19,pp.1227-1233,1981

10. Miura, H., and Schmit, L.A., "Second Order Approximation of Natural Frequency Constraints in Structural Synthesis," International Journal for Numerical Methods in Engineering, *Vol.*13, pp. 337-351, 1978.

11. Schmit, L.A. and Thornton, W.A., "Synthesis of an Airfoil at Supersonic Mach Number," NASA CR-144, 1965.

12. Love, A.E.H., *A Treatise on the Mathematical Theory of Elasticity*, Dover, New York, 1944.

13. S. Timoshenko, *History of Strength of Material*, McGraw-Hill, New York, 1953.

14. Przemieniecki, J.S., *Theory of Matrix Structural Analysis*, John Wiley, New York, 1979.

15. Robinson, J., *Integrated Theory Finite Element Methods*, John Wiley, New York, 1973.

16. Cook, R. D. et al, *Concepts and Applications of Finite Element Analysis*, Wiley, New York, 1989.

17. Kaneko , I., Lawo , M. and Thierauf , G., "On computational procedures for the force method," International Journal of Numerical Method in Engineering,*Vol.*18,pp.1469-1495,1982

18. Patnaik S. N., Berke, L., and Gallagher, R. H., "Integrated Force Method versus Displacement Method for Finite Element Analysis," Computers and Structures, *Vol.* 38, pp. 377-407, 1991.

19. Patnaik, S.N., "Integrated force method versus standard force method," International Journal of Computers and Structures, *Vol.*22, pp.151-163, 1986.

20. Kaljevic, I., Patnaik, S. N and Hopkins, D.A. "Developments of finite elements for two dimensional structural analysis using the integrated force method," Computers and Structures, *Vol.* 59, No. 4, pp. 691-706, 1996.

21. Kaljevic, I., Patnaik, S.N. and Hopkins, D.A., "Three dimensional structural analysis by the integrated force method .Computers and Structures, *Vol.*58, pp.869-886.

22. Patnaik, S. N., Berke, L., and Gallagher, R.H., "Compatibility conditions of structural mechanics for finite element analysis," AIAA Journal, *Vol.* 29, pp. 820-829, 1991.

23. Patnaik, S. N and Joseph, K.T., "Compatibility condition from Deformation Displacement Relation" *AIAA Journ*al, *Vol.* 23, pp. 1291-1293, 1985.

24. Nagabhusanam, J. and Patnaik, S. N., "General purpose program to generate compatibility matrix for the integrated force method". AIAA Journal, *Vol.* 28, pp. 1838-1842, 1985.

25. Patnaik, S. N. and Yadagiri, S., "Frequency analysis of structure by integrated force method, "Journal of Sound and Vibration*" Vol.* 83, pp. 93-109, 1982.

26. Patnaik, S.N., "Behavior of truss with stress and displacement constraints," Computers and Structures, 1986, *Vol.*22, pp. 619-623

27. Sedaghati, R and Esmailzadeh, E., "Optimum design of Structures with stress and displacement using force method," International Journal of Mechanical Science, *Vol.* 45, pp. 1369-1389, 2003.

28. Sedaghati, R, Suleman ,A. and Tabarrok , B., "Structural optimization with frequency constraints using finite element force method," AIAA Journal ,*Vol.*40,2002

29. Patnaik, S.N., "Analytical initial design for optimization by the integrated force method," Computer and Structures, 1989, *Vol.*33, pp.265-268.

30. Patnaik, S.N., Guptill, J.D. and Berke, L., "Singularity in structural optimization," International Journal of Numerical Method in Engineering *Vol.*36, pp.931-944, 1993.

31. Patnaik, S.N., Gendy, A.S., Berke, L. and Hopkins, D.A., "Modified fully utilized (MFUD) method for stress and displacement constraints," NASA TM-4743, 1997.

32. Choi, K.K. and Kim, N.H., *Structural sensitivity analysis and optimization*, Springer, New York, 2005.

33. Patnaik, S.N., and Gallagher, R.H. "Gradients of behavior constraints and reanalysis via the integrated force method," International Journal of Numerical Method in Engineering, *Vol.* 23, pp. 2205-2212, 1986.

34. Patnaik, S.N., Hopkins, D.A. and Coroneos, R., "Structural optimization with approximate sensitivities," Computer and Structures, *Vol.*58, pp.407-418, 1996.

35. Pian , T.H.H. , "A Historical note about hybrid elements," International Journal of Numerical method in Engineering,*Vol.*1,pp. 3-28,1969.

36. Troitsky, M.S., *Stiffened Plates, Buckling, Stability and Vibration*, Elsevier, Amsterdam, 1976.

37. Bryan, G.H., "On the stability of a plate under thrust in its own plane, with applications to the buckling of the sides of a ship," Proceeding of London Mathematical Society., *Vol.*-22, p.p. 54-67, 1891.

38. Timosheno, S.P., Gere, J.M., *Theory of Elastic Stability*, McGraw-Hill, New York, 1961.

39. Seide , P., "The effect of longitudinal stiffener located on one side of a plate on the compressive buckling stress of the plate stiffener combination," NASA,TN 2873,1953

40. Cox, H.L. and Riddel, J.R., "Buckling of a longitudinally stiffened flat panel," Aeronautical Quarterly, *Vol* 1, pp. 225-244, 1949.

41. Dawe, D.J., "Application of the discrete element method to the buckling analysis rectangular plate under arbitrary membrane loading," Aeronautical Quarterly, *Vol*-20, pp.114-128, 1969.

42. Shastry, B.P., Rao, G.V. and Reddy, M.N., "Stability of stiffened plate using high precision finite elements." Nuclear Engineering Design, *Vol*-36, pp. 91-95, 1976.

43. Mizusawa, T., Kajita, T., Naruoka, M., "Buckling of skew plate structure using B-spline functions." International Journal of Numerical Method in Engineering," *Vol.*-15, p.p.87-96, 1980.

44. Razzaque ,A. and Mathers , M.D., "Buckling analysis of stiffened plates and shells," Proceeding of recent Advances in Engineering Mechanics and their impact on Civil Engineering Practice," ASCE, Engineering Mechanical Division, Purdue, p.p.-1083-1086, 1983.

45. Pian, T.H.H and Tong, P. "A variational principal and convergence of finite-element based on assumed stress distribution" International Journal of Solids and Structures. *Vol.* 5,463-472, 1969.

46. Pian, T.H.H and Cheng D. "On suppression of zero energy deformation modes" International Journal of Numerical Method in Engineering, *Vol.* 19, pp. 1741-1752, 19.

47. Spilker, R.L. and Singh,S.P., "Three dimensional hybrid-stress isoparametric quadratic displacement elements," International Journal of Numerical Method in Engineering, *Vol.*18, pp. 445-465, 1982.

48. Golub, G.H., and Van Loan, *Matrix Computations*, third edition, the Johns Hopkins Press, Baltimore, 1996.

49. Timoshenko. S. and Woinowsky-Krieger, W., *Theory of Plates and Shells*, McGraw-Hill, New York, 1959.

50. Arora, J.S., *Introduction to optimum design*, McGraw-Hill, New York, 1989.

51. Haftka,T.H. and Zafar,G., *Elements of structural optimization*, Kluwer-Academic Publishers, third edition,1992.

52. Schittkowski K.,Zillober C., and Zotemantel R., "Numerical comparison of non-linear algorithms for structural optimization, Structural Optimization, Vol.-7,pp. 1-19,1994

53. Arora J.S., "Computational design optimization: A review and future directions, Structural Safety, Vol.-7, pp.131-148, 1990.

54. Thanedar P.B.,Arora J.S.,Tseng C.H.,Lim O.K. and Park G.J., "Performance of some SQP methods on structural optimization problems, International Journal of Numerical Method in Engineering ,Vol.-23,pp.2187-2203,1986.

55. Powell, M.J.D., "Algorithms for Nonlinear Constraints that use Lagrangian functions," Mathematical Programming, Vol. 14,pp. 224-248,1978.

56. Powell, M.J.D., "A Fast algorithm for nonlinearly constrained optimization calculations," Proceedings of the Dundee Conference on Numerical Analysis,Lecture Notes in Mathematics, Vol.630,pp. 144-157,Berlin,1978.

57. Haftka, R.T.,Adelman , H.M., "Recent Developments in Structural Sensitivity Analysis." Structural Optimization, Vol. 1,1989,pp. 137-151.

58. Keulen,F.V.,Haftka,R.T. and Kim,N.H. , "Review of options for Structural Design Sensitivity Analysis.Part1:Linear System." ,Computer Methods in Applied Mechanics and Engineering.,Vol.194,pp.3213-3243,2005.

59. Choi, K.K. and Twu, S.L., "On Equivalence of Continuum and Discrete Methods of Shape Sensitivity Analysis." AIAA Journal, Vol.27, pp.1418-1424, 1988.

60. Coleman, T., Branch, M.A. and Grace, A., Optimization toolbox-for use with Matlab, The Math Works Inc., User's Guide, Version 2,1999.

61. AISC, "Specification for the design, fabrication and erection of structural steel for building, American Institute of Steel Construction, Chicago, IL, USA, 1978 .

62. Fleury,C., and Schmit,L.A.Jr., "Dual Methods and Approximation Concepts in Structural Synthesis," NASA CR-32226,December 1980.

63. Khan M.R., "Optimality Criterion Technique Applied to Frame Having General Cross-Sectional Relationships", AIAA Journal, Vol.-22, pp.669-676, 1984.

64. McGee O.G. and Phan K.F., "A Robust Optimality Criteria Procedure for Cross-Sectional Optimization of Frame Structures with Multiple Frequency Limits," Computers &Structures, Vol.-38, pp.485-500, 1989.

65. Abdo M., Piperni P. and Kafyeke F., "Conceptual design of stringer stiffened compression panels," 16th Aerospace Structures and Material Symposium, Montréal, April 2003.

66. Paik J. K. et. al. "On Advanced Ultimate Limit State Design of Ship Stiffened Panels and Grillages," 2001SNAME annual meeting,2001.

67. Guo, Meiwen and Harik, I.E. "Stability of Eccentrically Stiffened Plates" Thin-Walled Structures, Vol.-14, pp. 1-20, 1992.

68. ANSYS Reference Manual. ANSYS company, 2005.

69. Vandeplaats Research & Development, "Visual DOC Refrence Manuals," Colorado, 2004.